SYNTHESIS, STRUCTURE, AND PHOTOPHYSICAL PROPERTIES OF DONOR-ACCEPTOR PURINES

By

ROSLYN SUSANNE BUTLER

A DISSERTATION PRESENTED TO THE GRADUATE SCHOOL
OF THE UNIVERSITY OF FLORIDA IN PARTIAL FULFILLMENT
OF THE REQUIREMENTS FOR THE DEGREE OF
DOCTOR OF PHILOSOPHY

UNIVERSITY OF FLORIDA

2007

© 2007 Roslyn Susanne Butler

For Mom, Carolyn Adwell

ACKNOWLEDGMENTS

I would like to thank my mom, Carolyn Adwell, for her unwavering love, support, and encouragement. I would also like to thank my dad, Jewell Butler, who has always let me know how proud he is of me and has always encouraged me in all of my pursuits. When I was young, they both instilled in me the importance of a good education. Without that I would not be where I am today. I would like to thank my entire family, they have always loyally helped me in any way possible and for that I am extremely grateful. Special thanks go to Dr. Andrew Lampkins who has become an important person in my life. He has been a wonderful colleague and friend. I would also like to thank Dixie, Dexter, and Cali Butler (my three pugs) who have continuously been by my side and have given me unconditional love. I do not know what I would have done without them. I cannot leave out little Newman, the chihuahua; I cannot wait to add him to my pack of dogs.

I would like to thank my advisor, Prof. Ron Castellano, who has scientifically guided and motivated me to achieve more than I ever thought I could. He is a wonderful scientist, person, and friend. I am very proud to say I come from his research group, and I am excited about the future of his research.

I would also like to thank Dr. Robert Holman, my research advisor at Western Kentucky University, and Dr. Spiro Alexandratos, my REU advisor at University of Tennessee. They both sparked my interest in organic chemistry and inspired me to further my scientific pursuits.

I would like to thank former and present members of the Castellano group. I would also like to thank collaborators, Prof. John Reynolds, Dr. Khalil Abboud, Prof. Kirk Schanze, Dr. Katsu Ogawa, Dr. Garry Cunningham, and Aubrey Dyer, for their scientific expertise and assistance with my work.

Finally, I would like to thank my committee members: Prof. Ken Wagener, Prof. Nicole Horenstein, Prof. Lisa McElwee-White, and Prof. Joanna Long for their scientific advice and wisdom.

TABLE OF CONTENTS

page

LIST OF TABLES

LIST OF FIGURES

Abstract of Dissertation Presented to the Graduate School
of the University of Florida in Partial Fulfillment of the
Requirements for the Degree of Doctor of Philosophy

SYNTHESIS, STRUCTURE, AND PHOTOPHYSICAL PROPERTIES OF DONOR-ACCEPTOR PURINES

By

Roslyn Susanne Butler

August 2007

Chair: Ronald Castellano
Major: Chemistry

Donor-π-acceptor (D-A) molecules have photophysical, electronic, and optoelectronic properties that make them suitable as sensors, wires, and fluorophores. Here the syntheses and properties of the first D-A systems based on purines are reported. Results show that simple chemical modifications to the heterocycle significantly improve its inherent optical properties (even beyond 2-aminopurine); the resulting fluorophores are candidates as both biological probes and optoelectronic device components. The molecular recognition functionality of purines, multiple nitrogen atoms capable of hydrogen bonding and an extended aromatic surface for π-stacking, can potentially be exploited to control molecular association and ordering.

C(2) and C(6) donor substituted purines are brominated at C(8) and then transformed via a palladium(0)-catalyzed cyanation reaction to their corresponding nitriles. Conversion of the nitriles to methyl esters comes by treatment with acidic methanol. The C(8) acceptor groups dramatically increase the fluorescence quantum yields (Φ_F) of the purines (versus a hydrogen in the C(8) position) in organic solvents to in many cases near unity (representing, for one derivative, a Φ_F enhancement of $> 2500\%$ in methylene chloride). Absorption (λ_{max} 310–365 nm), emission (λ_{max} 360–465 nm), and fluorescence lifetime data (8 ns $\geq \tau_F \geq$ 0.5 ns) were

collected for 12 D-A purines in four organic solvents and even water (for the 2-aminopurine analogues). Four of the purines could be studied in the solid state by X-ray crystallography. Theoretical calculations (DFT and ZINDO/CI) determined the absorption spectra, HOMO (–6.5 to –5.5 eV) and LUMO (–2.5 to –1.5 eV) energies, and the ground and excited state dipoles. The calculated orbital energies are in good agreement with solution-phase cyclic voltammetry data and the calculated excited state dipoles agree well with results from a Lippert-Mataga treatment of the solvent-dependent emission spectra. One D-A purine was successfully tested as the emissive layer in an organic light emitting diode (OLED). Amide bonds can be formed at the purine C(8) position (via an intermediate carboxylic acid) toward use of the molecules as heterocyclic amino acids. The amides show high quantum yields ($\Phi_F > 0.85$) in all organic solvents and well-defined conformations in the solid state.

CHAPTER 1
INTRODUCTION TO DONOR-ACCEPTOR SYSTEMS AND DONOR-ACCEPTOR PURINES

Conjugated Systems

All molecules undergo an electronic process as they absorb energy (photons at different wavelengths of light). This process is expressed by equation 1.1, where ΔE is the energy absorbed, h is Planck's constant, c is the speed of light, and λ is the wavelength of light.[1]

$$\Delta E = hc/\lambda \tag{1.1}$$

The absorbed energy (ΔE) increases the energy of a conjugated system by promoting an electron from the molecule's highest occupied molecular orbital (HOMO) to its lowest unoccupied molecular orbital (LUMO) resulting in molecular excitation. For conjugated molecules as conjugation length is increased the energy gap between the HOMO and LUMO is decreased enabling longer wavelengths (lower energy photons) to promote electrons to the LUMO. If this gap is lowered enough, absorption enters the visible range (400–800 nm) and can be detected by the human eye as color. If these electronic transitions are promoted by photons between 200 nm and 800 nm, the electronic absorption transitions that occur can be monitored using ultraviolet and visible (UV/vis) spectroscopy. A UV/vis spectrometer determines the absorption using the Beer-Lambert law (equation 1.2).[1]

$$A = \log I_0/I = \varepsilon lc \tag{1.2}$$

The absorption is A, I_0 is the intensity of light entering the sample, I is the intensity of the light exiting the sample, l is the pathlength of the sample cell, and c is the concentration (mol/L) of the sample. The molar extinction coefficient (ε) is the experimentally determined efficiency of absorption that is unique for each molecule. As conjugated systems become more complex, the

number of electronic transitions that can occur upon their interaction with light increases and UV/vis spectra can become quite complicated as multiple absorption bands begin to overlap.[1]

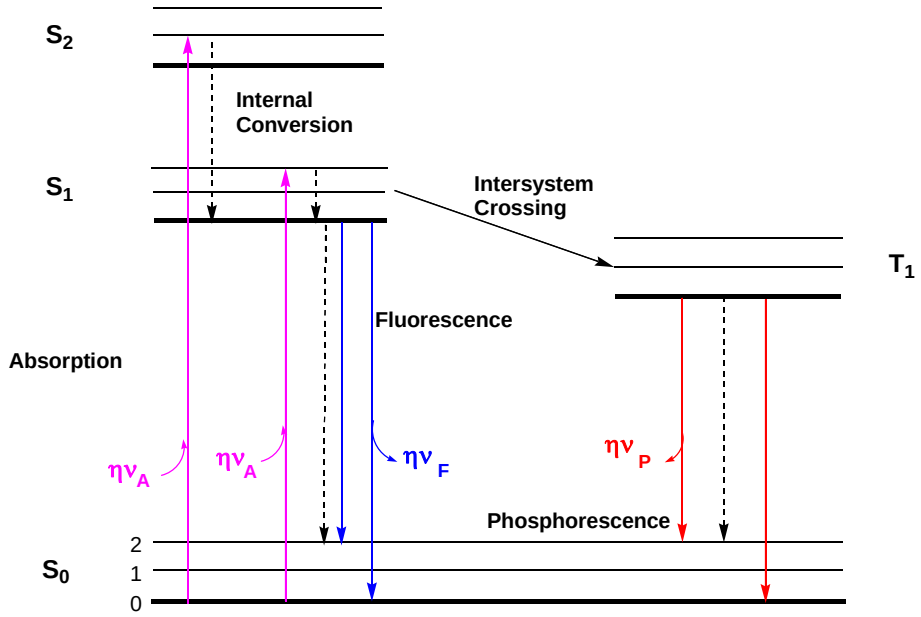

Figure 1-1. Jablonski diagram showing radiative and nonradiative electronic transitions.

The release of absorbed energy can take place through nonradiative (heat generating) or radiative (light emitting) processes as shown in the simplified Jablonski diagram in figure 1-1.[2] Nonradiative processes include relaxation, intersystem crossing, and internal conversion. Radiative processes include fluorescence (emission from the excited singlet state, S_1) and phosphorescence (emission from the excited triplet state, T_1) and are almost always initiated from the lowest excited state (S_1 and T_1).[2] The term luminescence is used for light emitting processes when the source of the emission is undetermined or contains both fluorescence and phosphorescence. Time resolved data can determine the source of a molecule's luminescence through emission rates which are typically between 1 and 10 ns for fluorescence and on the order of milliseconds to minutes for phosphorescence. A molecule's luminescence is typically reported as an emission spectrum that shows the wavelength of light the molecule emits

(emission maximum) and its intensity. Once the energy is released, the molecule is structurally unchanged from the original species.[2]

Absorption and emission spectra provide additional quantitative information related to a molecule's structure and to its potential applications. The Stokes shift, for example, is determined as the difference between the absorption and emission maximum for a given molecule in a given environment. Large variations in Stokes shift due to solvent polarity can indicate that a fluorophore will be a useful biological probe. The quantum yield (of fluorescence or luminescence) is a defining parameter of a luminophore and is defined as the total number of photons emitted relative to the number of photons absorbed (highest value, $\Phi_F = 1$); this value gives insight into how a conjugated system will perform in an electronic device or as a probe. Implications of large Stokes shifts and quantum yields in the context of fluorophore design will be discussed more thoroughly in Chapter 3.[3]

Fluorescence spectroscopy is a powerful research technique for probing the dynamics of biomolecules (e.g. conformational changes upon binding). Proteins and DNA are often studied by analyzing the changes in their fluorescence spectra under different conditions. Fluorescence spectroscopy also identifies organic molecules suitable for use in optoelectronic devices, and helps characterize optoelectronic devices such as organic light emitting diodes.[2]

Donor-π-Acceptor Systems

Conjugated systems can be functionalized with electron donor and electron acceptor groups to create donor-π-acceptor (D-π-A or D-A) systems (Figure 1-2).[4] D-π-A systems can consist of small molecules, oligomers, or polymers. The oligomers and polymers can be either linear or star-shaped.[4] The electron donor and electron acceptor create a push-pull delocalization

mediated by the π-spacer, the "flow" of π-electrons is often represented by simple valence bond theory and a zwitterionic resonance form (Figure 1-2).[4]

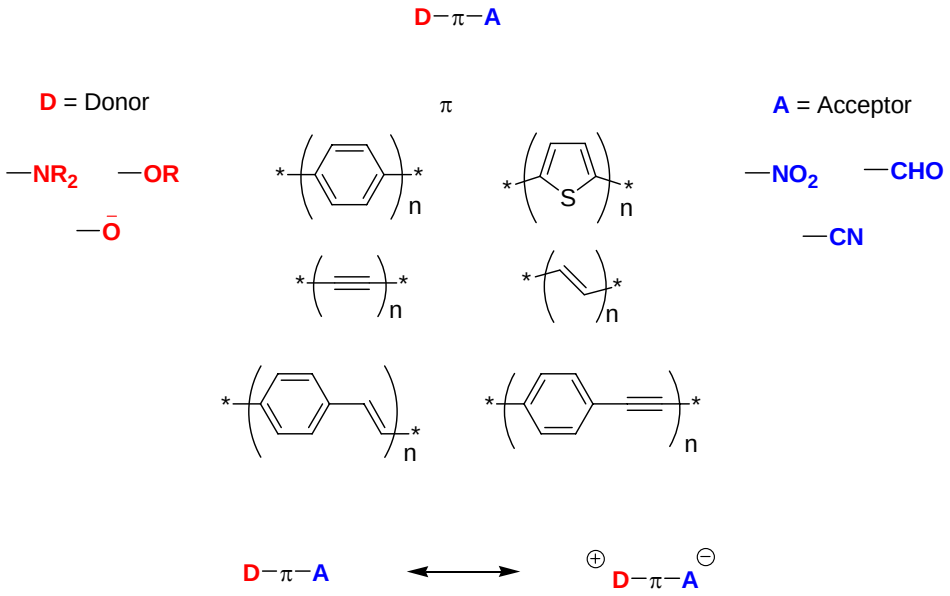

Figure 1-2. Traditional building blocks for some D-π-A systems and the resulting zwitterionic resonance generally used to describe their electronic structure.

The magnitude of this push-pull effect is related to the strength (e.g. the ionization energy of an amine substituent) and placement of the donor and acceptor groups, to the nature of the conjugated system to which they are introduced, and to the environment in which the system is placed. This molecular design can result in molecules with outstanding electrical, optical, and optoelectronic properties. The nonlinear optical (NLO) properties associated with donor-π-acceptor systems have emerged among the most important for optical data storage, data processing, and data transfer.[5]

Additional applications for D-A molecules include use in electronic devices such as field-effect transistors,[6] organic light emitting diodes,[7] and solar cells.[8] Field-effect transistors are a type of transistor that relies on an electric field to control the conductivity of a channel in a

semiconductor material. Field-effect transistors in complementary symmetry metal oxide semiconductors are the basis for modern digital integrated circuits that are responsible for the function of microprocessors. Organic light emitting diodes are semiconductors that emit light from an electroluminescent layer consisting of a film of organic compounds (discussed more thoroughly in Chapter 3). This technology is used for creating displays that can have manufacturing and energy requirement advantages over plasma and liquid crystal displays. Solar cells or photovoltaic cells are devices that convert light energy into electrical energy.

A critical and challenging issue for creating electronic devices from organic D-A molecules is the control of molecular organization when incorporating these systems into a device.[8] A noncentrosymmetric ordering of D-A molecules is required for organic materials used for second order nonlinear optics and in optoelectronic devices. This is why many devices fabricated from materials based on D-A molecules with excellent photophysical properties fail to perform well or at all. A large number of D-A molecules form π-stacked centrosymmetric (antiparallel) dimers due to electrostatic intermolecular interactions arising from their large ground state dipole moments. The centrosymmetric face-to-face stacked dimer generally quenches fluorescence by causing two exciton states to arise where only transition to the higher energy state is allowed; this can be observed experimentally as a blue-shifted absorption band (when compared to absorption for the single molecule). Rapid internal conversion to the lower energy exciton state decreases the transition probability for a radiative process to the ground state and the fluorescence is "quenched". The use of additional noncovalent interactions to control supramolecular structure could be advantageous for constructing devices.

Supramolecular Control of Donor-π-Acceptor Systems

Organizational hierarchy and self-assembly through molecular recognition are the focuses of supramolecular chemistry, so it is only fitting that incorporating aspects of molecular recognition into a D-π-A molecule could improve control over its orientation in a device, thereby improving the performance of the device.[9] Experimental time scale disintegration and reassembly of reversible supramolecular interactions also allows optimization of noncovalent interactions between monomers resulting in annealing and self-healing of structural defects. Two of the most common noncovalent intermolecular interactions employed in supramolecular chemistry are π-π and hydrogen bonding interactions.[8] Logically, π-interactions are going to occur in D-π-A systems, and due to their highly specific and directional nature hydrogen bonds are ideal for creating controlled supramolecular assemblies.[8]

Nature elegantly demonstrates how π-stacking and hydrogen bonding can create highly ordered structures with phenomenal function.[10] Self-assembly of the nucleic acids, to form double- (or multiple-) stranded DNA and RNA, is a quintessential example. At the heart of nucleic acid assembly and function are the pyrimidine and purine nucleobases.

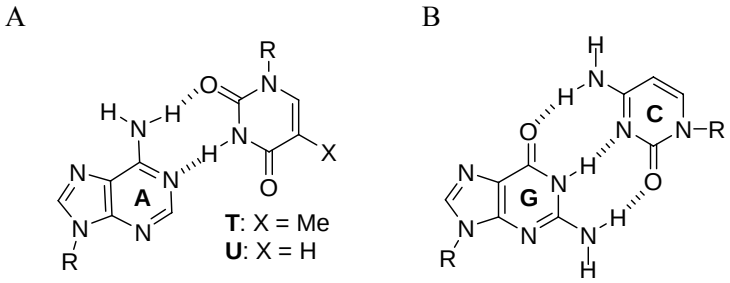

Figure 1-3. Selective hydrogen bonding between natural nucleobases. A) Two-point hydrogen bonding between adenine (A) and either thymine (T) or uracil (U). B) Triple hydrogen bonding between guanine (G) and cytosine (C).

The pyrimidines thymine (T), cytosine (C), and uracil (U) selectively base pair through multiple hydrogen bonds with the purine nucleobases adenine (A) and guanine (G). Supramolecular structures of nucleic acids are further stabilized by π-stacking and hydrophobic interactions.[11]

The purines base pair through their Watson-Crick hydrogen bonding site (Figure 1-3A,B); further assembly via the Hoogsteen site is possible and leads to the formation of 2:1 aggregates (Figure 1-4). Access to such well-defined patterns has made the pyrimidine and purine cores attractive building blocks for creating highly controlled supramolecular structures.[11]

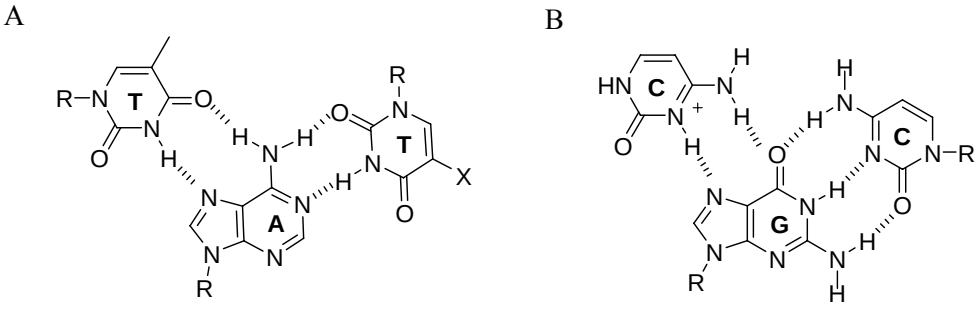

Figure 1-4. Aggregates (2:1) formed through the Watson-Crick and Hoogsteen hydrogen bonding sites. A) adenine (A) and thymine(T). B) guanine (G) and cytosine (C).

Meijer and Sijbesma have utilized the pyrimidine core to create a urea-functionalized pyrimidine (ureidopyrimidinone) unit capable of self-dimerization through four hydrogen bonds which results in the formation of a supramolecular polymer (Figure 1-5).[12-14] Such polymers offer the promise of merging the desirable materials properties of conventional covalent polymers with the self-healing behavior typical of reversibly-formed assemblies.[15-18] Pyrimidines have been used in a number of other interesting supramolecular systems; however, from here on the focus will shift to supramolecular structures created by compounds containing the purine core.[11]

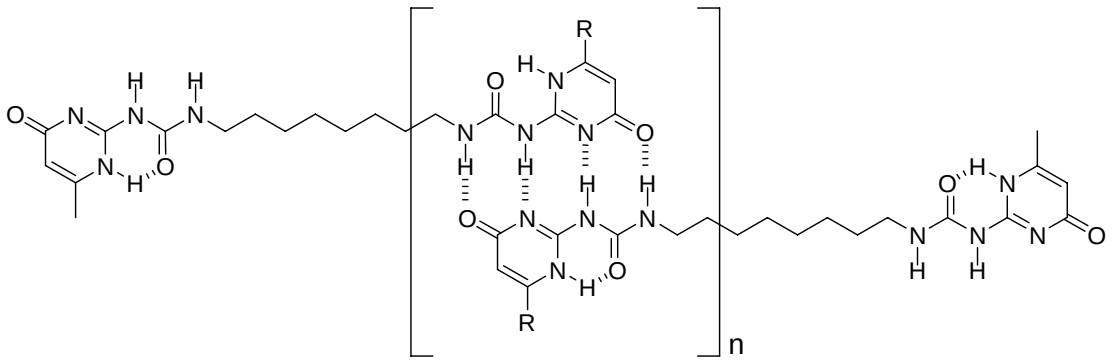

Figure 1-5. Quadruple hydrogen bonding in the ureidopyrimidinone supramolecular polymers of Meijer and Sijbesma.[16]

Purines as Conjugated Materials

Purines as heterocyclic aromatics have plenty of synthetic and supramolecular potential.[11] The planar extended aromatic core can engage in π-interactions. The four nitrogen atoms offer opportunity for hydrogen bonding and metal binding interactions while the nitrogens in the 7 and 9 positions can be functionalized (See Figure 1-6 for numbering). Carbons in the 2, 6, and 8 positions can be functionalized by addition of substituents through standard reactions that involve cationic, anionic, or radical intermediates. The conjugation of the system offers the opportunity to use it for photophysical and electronic applications. Sources of purine core precursors would not necessarily have to rely on traditional petroleum feed stocks if a method could be devised to extract and purify purine compounds from a biological source.

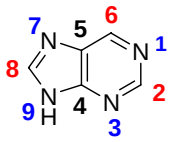

Figure 1-6. Conventional numbering of the purine core.

The modification of purine nucleobases in order to enhance their optical properties for biological applications has a rich history. Natural nucleobases are essentially non-fluorescent (Φ_F = 0.0001) making the study of nucleic acids by fluorescence spectroscopy basically

impossible without modification.[19] 2-Aminopurine (2-AP) is a common fluorescent nucleobase analogue of adenine (Figure 1-7A) that in water has a high fluorescence quantum yield (Φ_F = 0.68) and can establish stable Watson-Crick interactions with thymine (Figure 1-7B).[19,20] The red-shifted absorption (305 nm) of 2-AP also allows it to be selectively excited in the presence of the natural nucleobases.[20] In order to study DNA using fluorescence spectroscopy, 2-AP or other fluorescent nucleobase analogues are incorporated into a DNA strand in place of their corresponding nucleobase, requiring that they be amenable to sugar functionalization.[2]

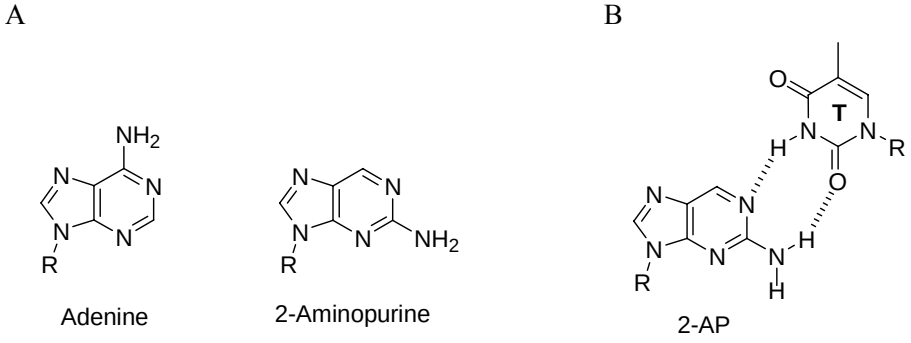

Figure 1-7. Common fluorescent nucleobase analogue 2-aminopurine. A) Adenine analogue, 2-aminopurine (2-AP). B) Watson-Crick base pairing between 2-AP and thymine.

2-AP has been used to study local interactions between nucleobases in DNA, electron transfer reactions through oligonucleotide strands,[21,22] and DNA damage due to ultraviolet radiation.[23] Recently, Turro and coworkers used 2-AP as a fluorescent base in a molecular beacon that displays an enhanced sensitivity for detecting complementary DNA.[24] When 2-AP is incorporated into oligonucleotides, its fluorescence is dramatically quenched up to 100-fold due to π-stacking interactions.[19] The quenching can take place to a lesser degree if the π-stacking of the oligonucleotide is less efficient or if the stacking is interrupted by some other interaction.[25-27] 2-AP's sensitivity to its environment can lead to observations about the dynamics of the system

that it is incorporated into; however, the reduction of fluorescence requires high concentrations of the 2-AP labeled oligonucleotide in order for the system to be studied effectively.[28]

Many researchers have prepared fluorescent nucleobase analogues through modification of natural nucleobases. Systems have been formed where the conjugation of a natural nucleobase is extended through formation of an etheno derivative,[20,29,30] or by incorporating an additional aromatic ring in between the imidazole and pyrimidine portion of the purine core (Figure 1-8A).[31] Systems have been formed by adding weak electron acceptor functionality to the C(8) position of natural purine nucleobases (Figure 1-8B). Firth and coworkers created 8-alkynylated guanosine (Figure 1-8B) and adenine (not shown).[32] Tor and coworkers found increased luminescence by incorporating a furan moiety onto the C(8) position of natural purine nucleosides.[33] Some researchers, like Kool have even shown that the base structure can be altered completely, preserving base stacking but introducing additional functionality (luminescence, enhanced metal binding, etc.) (Figure 1-8C).[34-38] All of these fluorescent analogues have exhibited increased fluorescence when compared to that of the natural nucleobases.

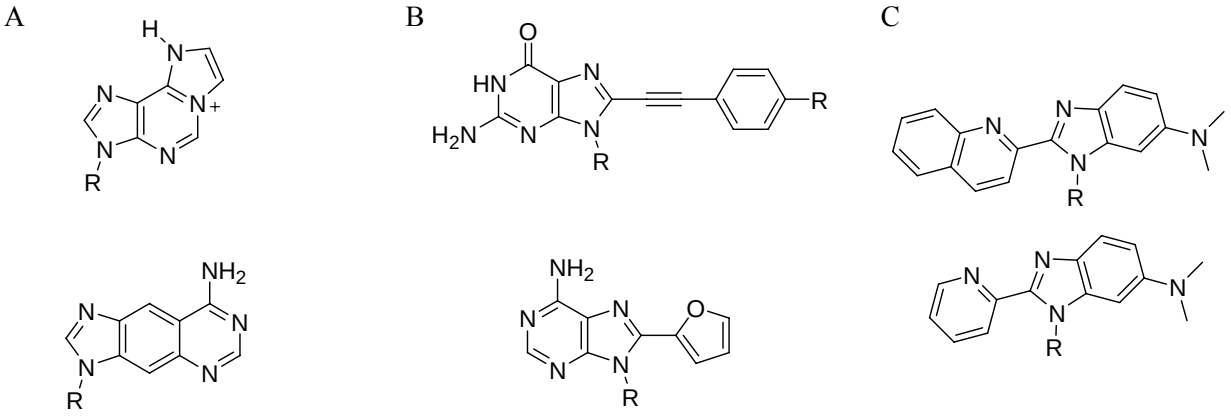

Figure 1-8. Fluorescent nucleobase analogues. A) Formed by extended conjugation. B) Formed by addition of acceptor group. C) Formed by using a complete alteration of base structure.

Nucleobases in Synthetic Functional Architectures

Remarkable examples of complex purine supramolecular structure have been achieved with guanine and guanosine derivatives, driven by hydrogen bonding. Ribbons, for example, may form with (Figure 1-9A) or without (Figure 1-9B) a net dipole [39]and the preference can be controlled by solvent interactions and/or by the nature of the R group.[39] Three-terminal devices are found to act as a field effect transistor by using polar ribbons (Figure 1-9A) to connect the drain and source terminals.[40]

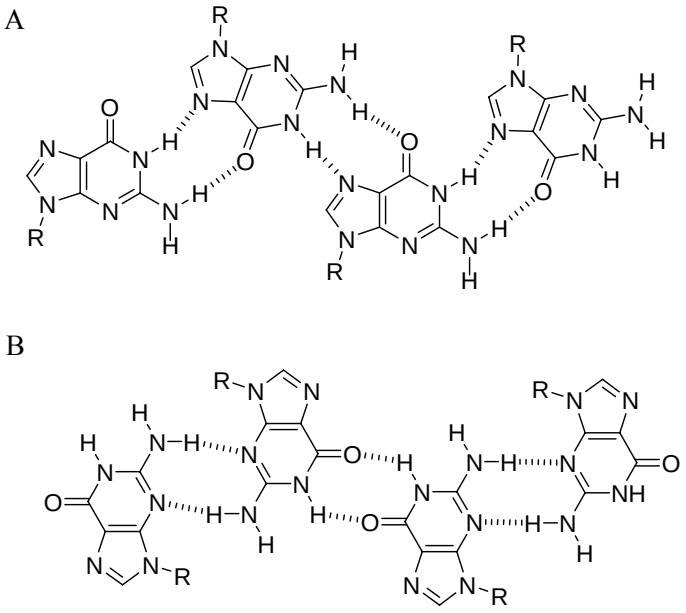

Figure 1-9. Ribbons formed by the self-assembly of guanosine derivatives. A) Ribbon that contains a net dipole. B) Ribbon that has no net dipole.

In the presence of sodium or potassium cations the guanine unit can form a self-assembled quartet structure known as the G-quartet driven by hydrogen-bonding interactions between four guanine derivatives (Figure 1-10).[41] The quartets are further stabilized by the cations that coordinate with the carbonyl oxygen of each guanine in the quartet.[42] The G-quartets can then stack with one another to form columnar nanostructures, the G-quadruplex.[43]

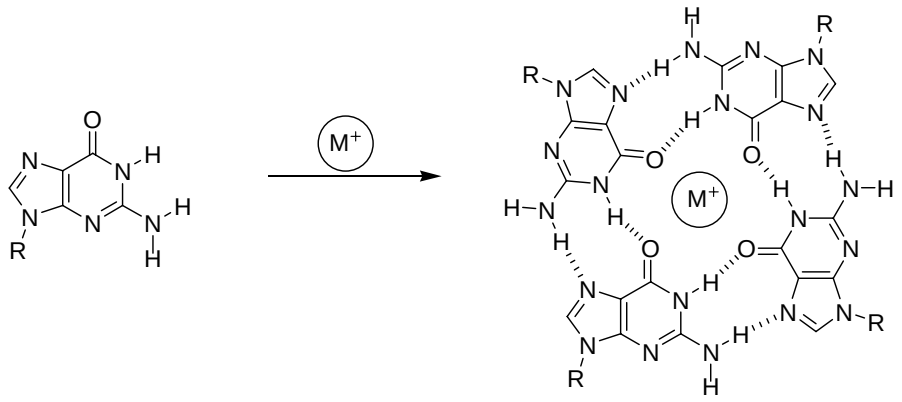

Figure 1-10. G-Quartet formed by the self-assembly of guanosine derivatives in the presence of a metal cation.

Through simple switching of the carbonyl and primary amine of guanosine, a G-pentamer is formed instead (Figure 1-11).[44] The guanine, which has a hydrogen atom in place of the R group, can lead to a hydrogen bonded network of G-quartets without the need for a cation template (Figure 1-12).[45] Addition of an oxo group to the C(8) position of a guanosine can create a self-assembled helical structure.[39] All of these examples show how simple chemical changes to the purine core can result in predictable and controllable supramolecular structures with unique functions.

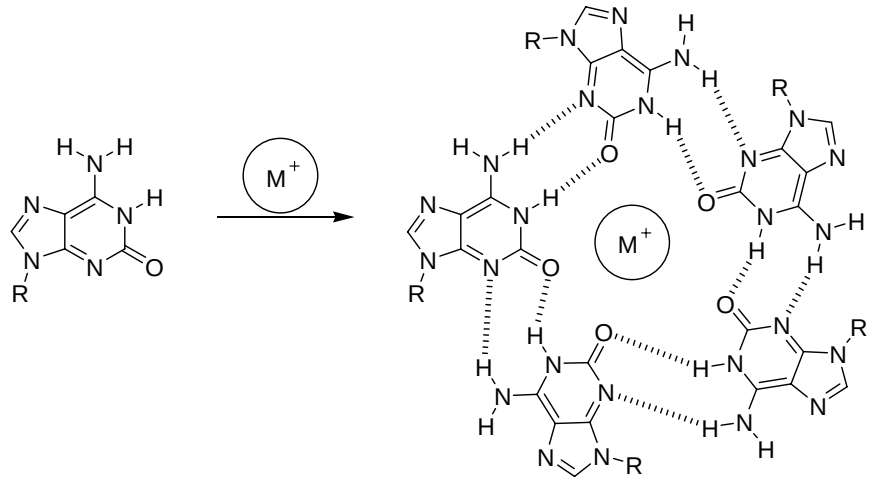

Figure 1-11. G-Pentamer formed from the self-assembly of an isomer of guanosine in the presence of a metal cation.

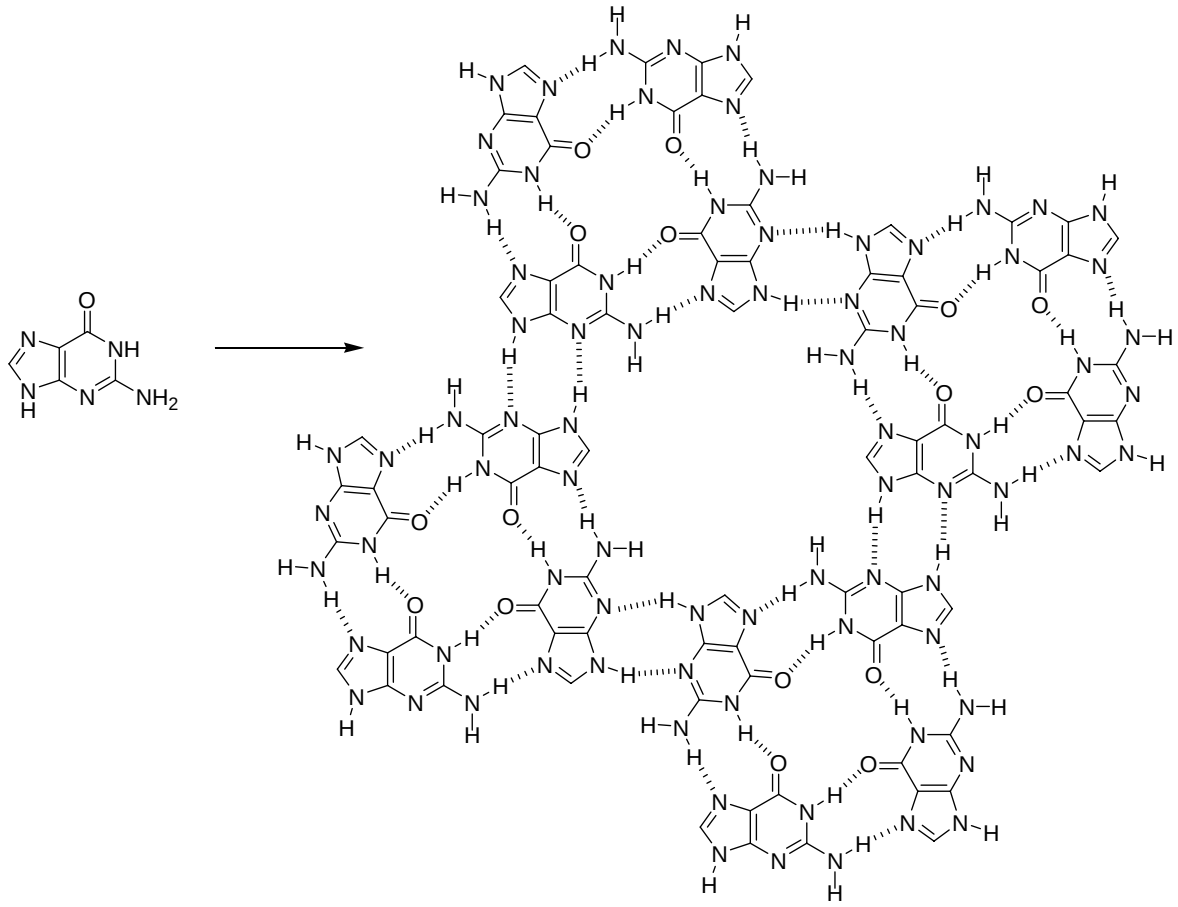

Figure 1-12. Hydrogen-bonded network formed from the guanine nucleobase.

Design of Donor-π-Acceptor Purines Based on 2-Aminopurine

We hoped to extend the traditional donor-π-acceptor concept to 2-aminopurine in order to study the fundamental changes that would result, increase the luminescence of the system, and potentially exploit the multiple noncovalent interactions available to the purine core in the context of optoelectronic materials.

The design of our D-π-A purines utilizes the purine core as the π-linker and features a relatively strong electron-accepting substituent in the C(8) position (Figure 1-13). Donor groups placed in the C(2) and C(6) positions of the purine core create the desired push-pull π-delocalization, and both donors can communicate with the acceptor in this fashion (Figure 1-14A,B).

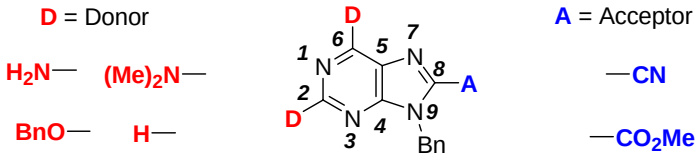

Figure 1-13. Donor-acceptor purines based on 2-aminopurine.

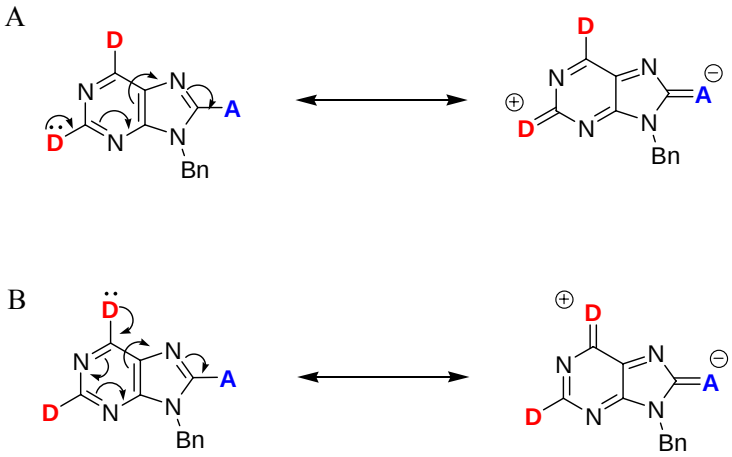

Figure 1-14. Zwitterionic resonance structures of D-A purines. A) Resonance through the C(2) position. B) Resonance through the C(6) position.

Photophysical investigation of D-π-A purines prepared in this thesis reveal the highest reported quantum yield values for simple purines with intrinsic values approaching unity. Furthmore, many of the compounds exhibit high sensitivity to their environment making them suitable for function as biological probes or nucleobase surrogates provided modification to impart water solubility. Examination of solid state crystalline structures of the D-π-A purines shows how slight changes to the donor and acceptor groups can change their packing preferences. These results are encouraging that the supramolecular structure of such purines can be tailored for use in optoelectronic devices.

CHAPTER 2
SYNTHESIS AND STRUCTURE OF NOVEL DONOR-ACCEPTOR PURINES

Introduction

Synthesis of the D-A purines starts with the biological compound guanine **2.1**, a cheap readily available starting material costing less than one dollar per gram. Using a four-step protocol (Figure 2-1) adapted from an established patented procedure[46] guanine is transformed into 2-amino-6-chloropurine (**2.4**) in 56% yield. 2-Amino-6-chloropurine (**2.4**) is otherwise a commercially available but very expensive precursor costing approximately $68 per gram. Due to the need for large quantities of **2.4**, it was more cost effective to make this molecule in-house for approximately $7 per gram (cost of materials, not labor).

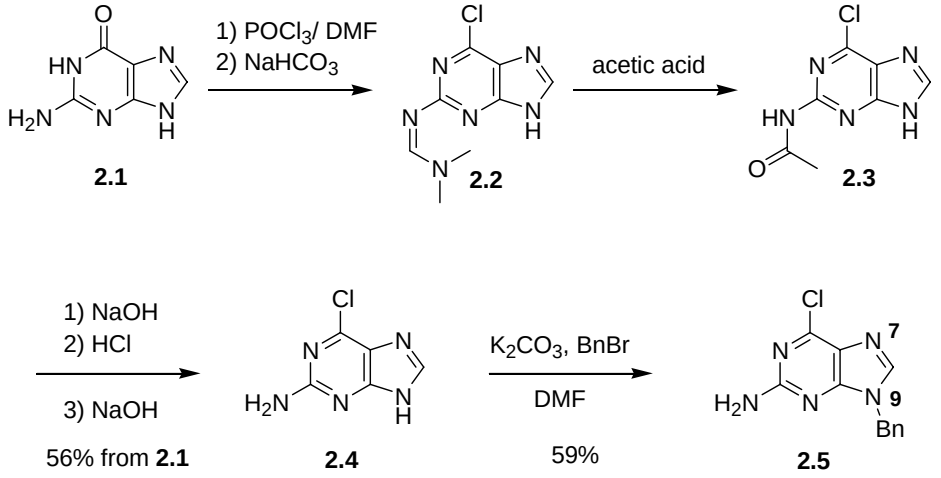

Figure 2-1. Synthesis of key synthetic intermediates 2-amino-6-chloropurine **2.4** and 2-amino-6-chloro-9-benzylpurine **2.5**.

In order to add tautomeric stability to the imidazole portion of the purine core, key intermediate **2.4** is benzylated[47] to afford 2-amino-6-chloro-9-benzylpurine (**2.5**) (Figure 2-1) and 2-amino-6-chloro-7-benzylpurine[47] (not shown). Even though both benzylated regioisomers are formed, the desired N(9) isomer is synthesized in higher yield and is easily separated from the N(7) isomer by flash chromatography or by recrystallization. The benzyl group was chosen as the N(9) alkylating group over simple alkyl groups for two reasons. Simple alkyl groups

remain in the plane of the purine ring allowing extended π-stacking to occur making the species very insoluble; the benzyl group, not being planar to the purine core, is able to frustrate long-range π-stacking and allow for more efficient solvation.[48] Second, as a robust protecting group the benzyl substituent is capable of withstanding conditions needed for functional group transformations at other positions on the purine. The benzyl group can also be removed from the purine core using Pd/C, H_2, and concentrated HCl.[47]

Chemical Manipulation of the Purine C(2) and C(6) Positions

Versatile intermediate **2.5** can be selectively modified to create a variety of C(2) and C(6) substituted purines (Figure 2-2). The C(6)-chloro substituent can be removed using catalytic hydrogenation to give the parent 2-aminopurine derivative **2.6**,[49] while nucleophilic aromatic substitution reactions like amination[50] and alcoholysis can displace the chlorine and provide compounds **2.7** and protected guanosine derivative **2.8**,[51] respectively. Transformation of the C(2) primary amine is achieved using a chloro-dediazotization[52] procedure to produce 2,6-dichloro-9-benzylpurine **2.9**. All the products formed in figure 2-2 are stable solids that can be handled easily and formed on the gram scale. These compounds do not require stringent purification and can generally be used in subsequent reactions directly after removing the solvent and drying under vacuum.

The C(2) and C(6) positions of purine compounds **2.6** and **2.9** can be transformed further into C(2) dimethylaminopurine derivatives (Figure 2-3A,B). Compound **2.9** can be heated with dimethylamine[50] in ethanol at 100 °C to give **2.10** (Figure 2-3A). The C(6) chlorine of **2.9** can also be selectively displaced with a primary amine using methanolic ammonia at 60 °C to produce **2.11**.[50] The C(2) chlorine of compound **2.11** is then transformed to a dimethylamino function[50] using dimethylamine and ethanol to form **2.12** (Figure 2-3A). 2-Amino-9-

benzylpurine (**2.6**) is placed under the same chloro-dediazotization conditions[52] used to form compound **2.9** and offers 2-chloro-9-benzylpurine (**2.13**) which can then be heated with dimethylamine and ethanol at 100 °C to produce 2-dimethylamino-9-benzylpurine (**2.14**) (Figure 2-3B).

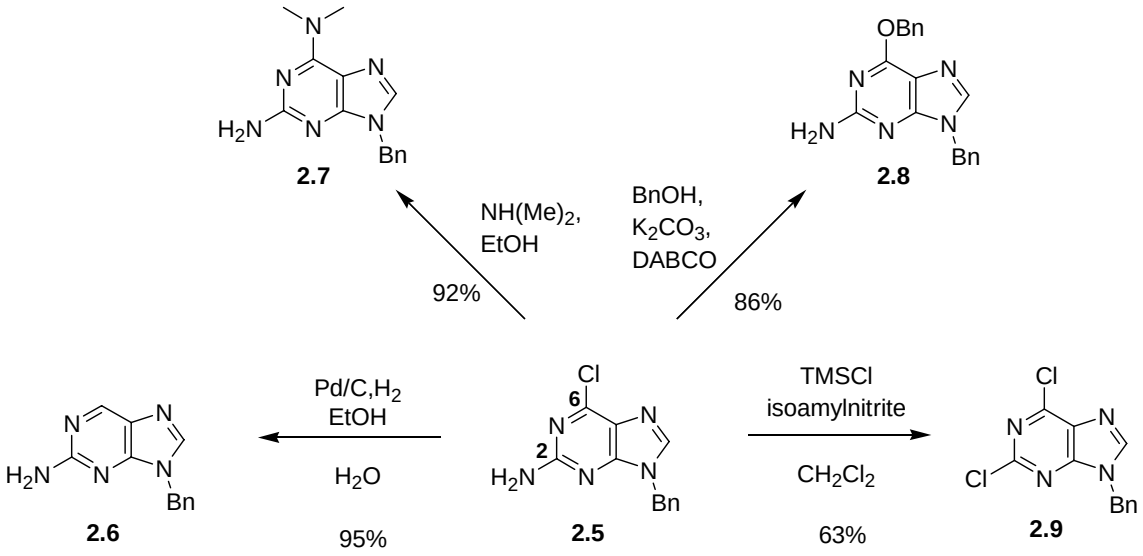

Figure 2-2. C(2) and C(6) derivatives from 2-amino-6-chloro-9-benzylpurine.

A

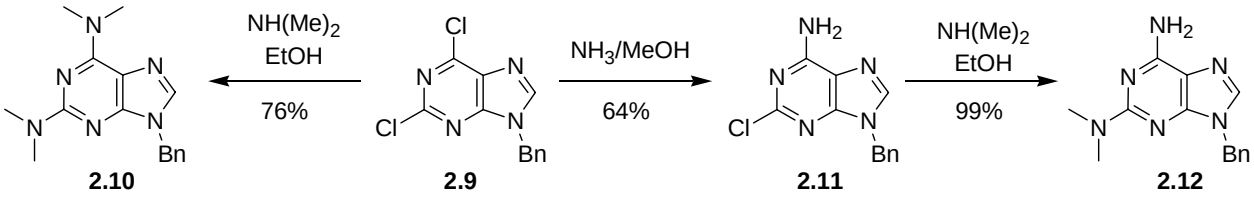

B

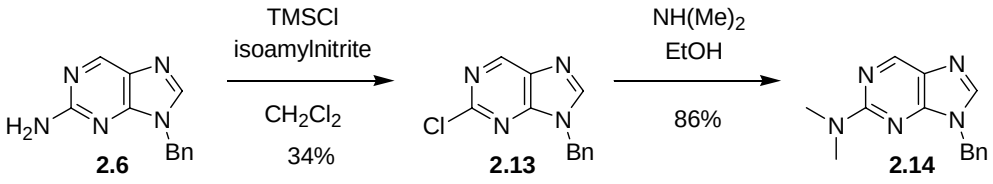

Figure 2-3. C(2) dimethylaminopurines formed from derivatives of 2-amino-6-chloro-9-benzylpurine (**2.5**).

Addition of Acceptor Groups to C(8)

Using Br_2 under ambient light, the C(8) position of compounds **2.1**−**2.6** is selectively brominated[53] in 70-90% in almost all cases (Figure 2-4), which provides a chemical handle for its further functionalization. Although also often used for purines, bromination of C(8) with NBS in THF at room temperature only rendered the unreacted starting purine and succinimide.

Formation of the C(8)-CN Purines

Several methods for creating purinecarbonitriles from precursor halopurines have been used and suffer from various disadvantages including low yields and the need for highly reactive precursor halo or pseudohalopurines such as iodopurines or sulfonylpurines. These methods include the treatment of the precursor purine with copper(I) cyanide,[54] displacement reactions involving potassium cyanide or sodium cyanide,[55] reactions with tetraethylammonium cyanide in the presence of trimethylamine,[56] and Pd-catalyzed couplings with potassium cyanide[57] and tributyltin cyanide.[58] We identified the Pd-catalyzed cross coupling method developed by Gundersen and coworkers as the most promising for our systems. In their work, C(8) purinecarbonitriles were prepared in 0-81% yield using $Pd(PPh_3)_4$, $Zn(CN)_2$,and NMP at 90 °C.[59]

Conversion of the bromides, compounds **2.6a**−**2.8a**, **2.10a**, **2.12a**, **2.14a** to the nitriles using a slightly modified Gundersen method created the first series of donor-acceptor (D-A) purines, compounds **2.6b**−**2.8b**, **2.10b**, **2.12b**, **2.14b** (Figure 2-4). The primary amine functionality and nitrogen rich nature of the purine core presented many challenges for the metal catalyzed cyanation reaction. Thorough degassing and drying of the solvent was necessary due to the sensitivity of the Pd(0) metal to oxygen. The Pd(0) metal also easily complexes to the nitrogen donor atoms of the purine requiring the use of large amounts of the catalyst (20−40%) which is significantly more than the 0.07 mmol catalyst loading used in Gundersen's method. After many inconsistent results from these reactions a literature investigation revealed that Pd

((0) and (II))-catalyzed reactions are sensitive to cyanide ions;[60] in particular, when in excess they can render the catalyst inactive[61] by forming species such as $[Pd^0(CN)_n]^{n-}$.[62] With this knowledge, consistent results were obtained by adding the catalyst to the purine and heating for approximately 30 min before slowly adding $Zn(CN)_2$/solvent mixture by syringe (over 5–6 hours).

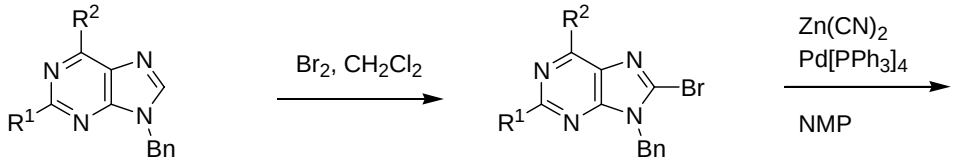

2.6 $R^1 = NH_2$, $R^2 = H$		**2.6a** $R^1 = NH_2$, $R^2 = H$	24%
2.7 $R^1 = NH_2$, $R^2 = N(Me)_2$		**2.7a** $R^1 = NH_2$, $R^2 = N(Me)_2$	78%
2.8 $R^1 = NH_2$, $R^2 = OBn$		**2.8a** $R^1 = NH_2$, $R^2 = OBn$	77%
2.10 $R^1 = N(Me)_2$, $R^2 = N(Me)_2$		**2.10a** $R^1 = N(Me)_2$, $R^2 = N(Me)_2$	89%
2.12 $R^1 = N(Me)_2$, $R^2 = NH_2$		**2.12a** $R^1 = N(Me)_2$, $R^2 = NH_2$	68%
2.14 $R^1 = N(Me)_2$, $R^2 = H$		**2.14a** $R^1 = N(Me)_2$, $R^2 = H$	80%

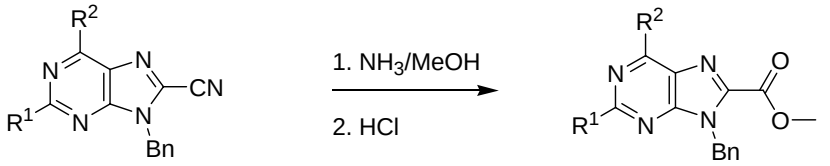

2.6b $R^1 = R^1 = NH_2$, $R^2 = H$	80%	**2.6c** $R^1 = R^1 = NH_2$, $R^2 = H$	60%
2.7b $R^1 = NH_2$, $R^2 = N(Me)_2$	91%	**2.7c** $R^1 = NH_2$, $R^2 = N(Me)_2$	86%
2.8b $R^1 = NH_2$, $R^2 = OBn$	42%	**2.8c** $R^1 = NH_2$, $R^2 = OBn$	82%
2.10b $R^1 = N(Me)_2$, $R^2 = N(Me)_2$	93%	**2.10c** $R^1 = N(Me)_2$, $R^2 = N(Me)_2$	64%
2.12b $R^1 = N(Me)_2$, $R^2 = NH_2$	77%	**2.12c** $R^1 = N(Me)_2$, $R^2 = NH_2$	75%
2.14b $R^1 = N(Me)_2$, $R^2 = H$	39%	**2.14c** $R^1 = N(Me)_2$, $R^2 = H$	71%

Figure 2-4. Functionalization of the C(8) position of the purine to form the D-A purines.

Formation of the C(8)-COOMe Purines

The second series of D-A purines, the C(8) methyl esters (**2.6c**–**2.8c**, **2.10c**, **2.12c**, **2.14c**) were subsequently synthesized by formation of the methyl imidate intermediate using known methodology that involves treating the nitrile derivatives with methanolic ammonia (Figure 2-4).[63] The methyl imidate was then readily hydrolyzed to give the C(8) methylester.[63] The C(8) methylester compounds are more soluble in acetonitrile and methanol than the C(8) cyano;

accordingly, thin layer chromatography (silica, 5% MeOH/CH_2Cl_2) indicates that they are a more polar species.

Solid State Structures

The structures of compounds **2.7b**, **2.12b**, and **2.12c** as determined in the solid state by X-ray crystallography, perfomed by Dr. Khalil Abboud, are shown in Figure 2-5. Single crystals were grown by slow evaporation of solutions of each compound in a methanol/methylene chloride mixture. Crystals for the C(8) purinecarbonitriles **2.7b** and **2.12b** formed overnight while those for the C(8) purine methylester **2.12c** formed upon slow evaporation over one week.

Molecular Level Structure

The X-ray structure of **2.7b** (Figure 2-5A) reveals the dimethylamine substituent, defined by atoms N(10), C(14), and C(15), to be planar at N(10) and with the purine core. The sum of the N(10) bond angles (e.g., C(14)-N(10)-C(15)) is 359.72°, consistent with sp^2 hybridization at nitrogen. The dimethylamine substituents on **2.12b** (Figure 2-5B) and **2.12c** (Figure 2-5C) show nearly identical geometry where the sum of the N(11) bond angles are 359.95° and 359.74°, respectively. In the case of **2.12c**, the crystal structure also shows that the nonhydrogen atoms defining the C(8) methyl ester substituent, C(14), O(15), O(16), and C(17) deviate from the mean plane defined by the purine core by no more than 0.087 Å. The N(9) benzyl substituent geometry can be defined by torsion angles α(defined by a-b-c-d) and β(defined by b-c-d-e) for **2.7b**, **2.12b**, and **2.12c** (Figure 2-5D). The values are $\alpha = -81.55$ and $\beta = 104.60$ for **2.7b**, $\alpha = 90.93$ and $\beta = -108.54$ for **2.12b**, and $\alpha = -103.10$ and $\beta = 16.64$ for **2.12c**. In all cases the benzyl group extends nearly perpendicular to the plane of the purine core (α); this is also consistent with its preferred geometry by computation. Angle β is sensitive to the intermolecular interactions involving the phenyl group in the solid state.

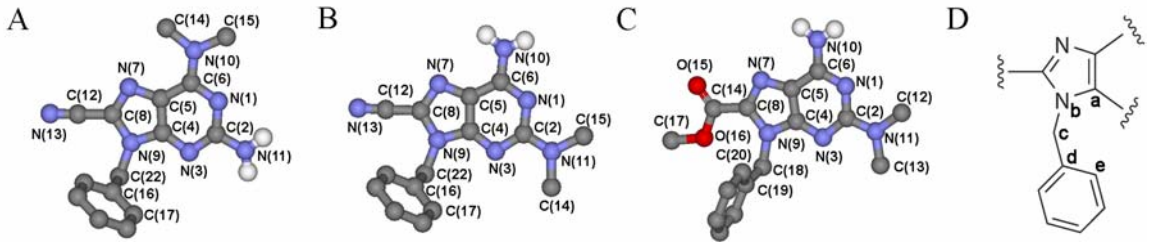

Figure 2-5. Single molecules from the crystal structure and their numbering. A) Compound **2.7b**. B) Compound **2.12b.** C) Compound **2.12c**.

Selected bond lengths derived from the crystal structure for the D-A purines and 2-aminopurine (2-AP),[64] one of just four 2-aminopurine structures available (not including those presented here),[65,66] are shown in table 2-1. Upon examination, the bond lengths between **2.7b**, **2.12b**, **2.12c**, and 2-AP deviate by little more than 0.015 Å.

Table 2-1. Selected Bond Lengths for **2.7b**, **2.12b**, **2.12c**, and 2-AP.

Bond	**2.7b**	**2.12b**	**2.12c**	**2-AP**
N(1)-C(6)	1.3411(15)	1.3292(19)	1.3407(16)	1.332(3)
N(1)-C(2)	1.3536(15)	1.3654(19)	1.3635(16)	1.365(2)
C(2)-N(3)	1.3484(15)	1.3577(18)	1.3524(16)	1.343(2)
C(2)-N(11)	1.3563(15)	1.3506(19)	1.3590(17)	1.353(3)
N(3)-C(4)	1.3446(14)	1.3323(18)	1.3402(16)	1.329(3)
C(4)-N(9)	1.3749(14)	1.3779(17)	1.3710(16)	1.368(3)
C(4)-C(5)	1.3952(16)	1.390(2)	1.3890(17)	1.400(2)
C(5)-C(6)	1.4301(16)	1.415(2)	1.4177(18)	1.381(3)
C(5)-N(7)	1.3810(14)	1.3791(18)	1.3778(16)	———
C(6)-N(10)	1.3450(15)	1.342(2)	1.3339(17)	———
N(7)-C(8)	1.3129(16)	1.3192(19)	1.3212(16)	1.318(2)
C(8)-N(9)	1.3834(14)	1.3779(19)	1.3910(15)	1.360(3)
C(8)-C(12)	1.4308(15)	1.438(2)	———	———
C(8)-C(14)	———	———	1.4895(18)	———

Bond length alternation seen in the X-ray structure of a donor-acceptor molecule has been found to be a good indication that there is charge-transfer from the donor to the acceptor in the ground state.[67] This is nicely illustrated for the cyanoethynylethenes[67,68] where bond lengths can deviate by 0.2 Å or greater between the donor and non-donor substituted derivatives.[68] The analysis shows that there may only be a very small amount of charge transfer in the ground state of the D-

A purines reported here, a result that is confirmed by electronic structure calculations (vide infra). Important to note, however, is that comparison of 2-AP to the D-A purines reported here is somewhat skewed due to the tautomeric instability that sees 13% of the N(7) tautomer found in the 2-AP crystal structure.[64]

Crystal Packing of 2.7b, 2.12b, and 2.12c

Examination of the crystal packing of all three structures reveals many of the expected noncovalent intermolecular interactions. All three purines form dimers through hydrogen bonding (Figures 2-6A, 2-8,A and 2-10A) showing typical hydrogen bonding distances[69] and all three exhibit antiparallel dipolar π-stacking (Figures 2-6B, 2-8B, 2.10B) which is a common motif for D-A molecules.[67,68,70-73] Purine **2.7b** forms a two-point hydrogen bonded dimer via the N(3) face (N(3)•••N(11) = 3.11 Å)(Figure 2-6A). Purine **2.12b,** which is the structural isomer of **2.7b**, forms a similar dimer with hydrogen bonding taking place this time from the Hoogsteen edge (N(7)•••N(10) = 3.00 Å) (Figure 2-8A). The C(8) methylester purine derivative **2.12c** also forms a dimer but does so through four hydrogen bonds (O(15)•••N(10) = 2.87 Å and N(7)•••N(10) = 3.03 Å) (Figure 2-10A). Due to strong dipolar interactions, nitriles **2.7b** and **2.12b** approach absolute antiparallel alignment of neighboring purines and short π-stacking distances of 3.32 Å for **2.7b** and 3.38 Å for **2.12b** (Figures 2-6b and 2-8b). Methylester derivative **2.12c** shows antiparallel dipolar stacking of 3.30 Å, but the molecule is slipped with respect to its neighbor such that the methylester portion of one molecule stacks with the purine core of the next (Figure 2-10B). The noncovalent intermolecular interactions revealed from these crystal structures suggest how the molecular recognition features of the nucleobases might be useful in controlling their supramolecular and solid state architectures.

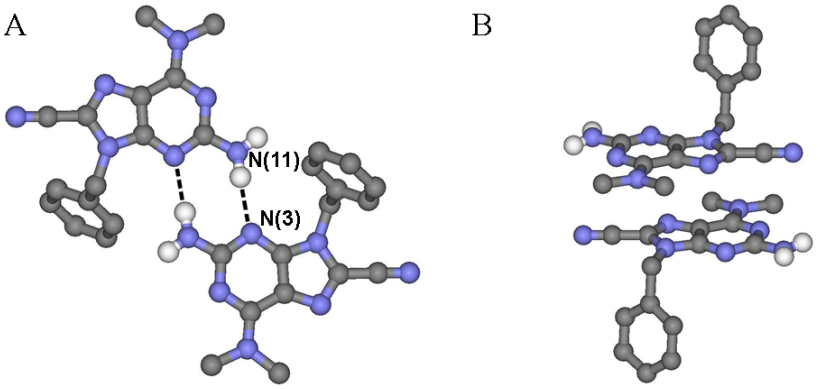

Figure 2-6. Noncovalent intermolecular interactions present in the crystal structure of **2.7b**. A) Hydrogen bonding interactions. B) π-stacking and dipolar interactions.

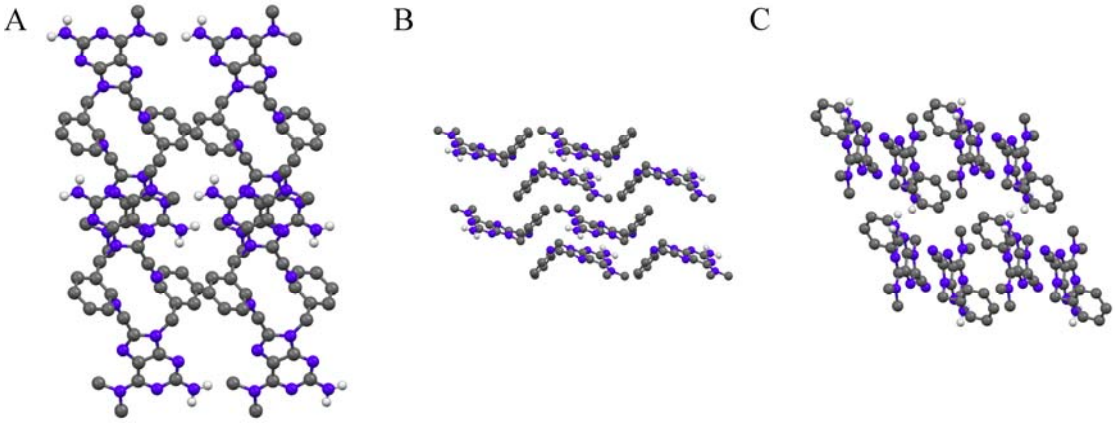

Figure 2-7. Crystal packing of **2.7b** along its three crystallographic axes. A) Axis *a*. B) Axis *b.* C) Axis *c*.

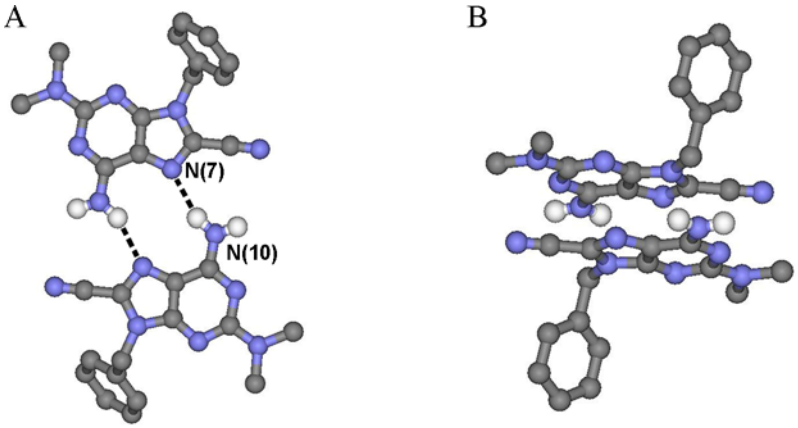

Figure 2-8. Noncovalent intermolecular interactions present in the crystal structure of **2.12b**. A) Hydrogen bonding interactions. B) π-stacking and dipolar interactions.

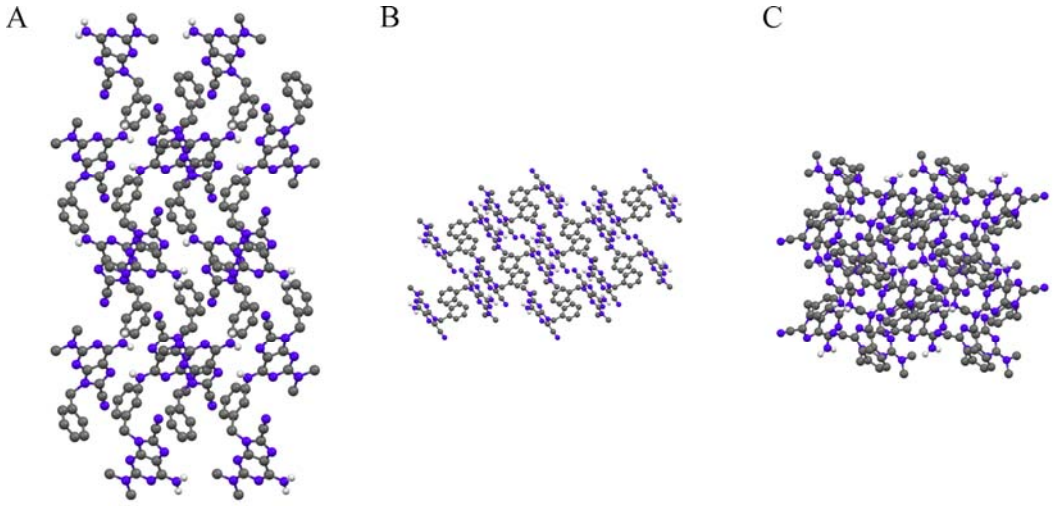

Figure 2-9. Crystal packing of **2.12b** along its three crystallographic axes. A) Axis *a*. B) Axis *b*. C) Axis *c*.

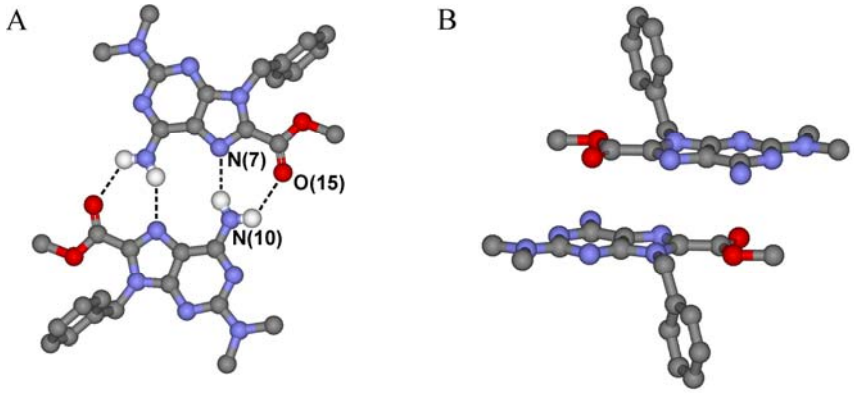

Figure 2-10. Noncovalent intermolecular interactions present in the crystal structure of **2.12c**. A) Hydrogen bonding interactions. B) π-stacking and dipolar interactions.

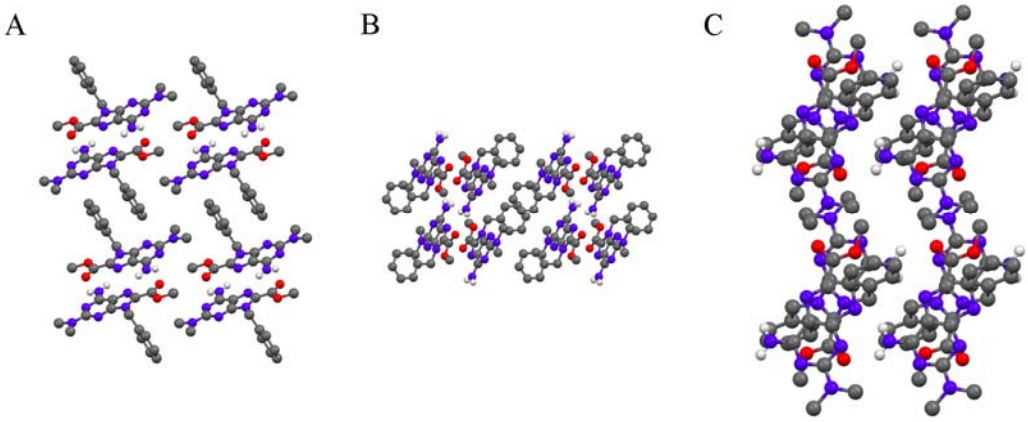

Figure 2-11. Crystal packing of **2.12c** along its three crystallographic axes. A) Axis *a*. B) Axis *b*. C) Axis *c*.

Original Synthetic Strategies

During the early stages of this research guanosine (**2.15**) was selected as the purine with which to initiate the D-A purine synthesis (Figure 2-12). Protection for the N(9) sugar hydroxy groups was necessary in order to transform the C(6) carbonyl to a chlorine; this was done by treatment with acetic anhydride using a literature procedure[74] (Figure 2-12). Subsequent conversion to the 6-chloro derivative was successful to give **2.17**[75] (Figure 2-12), however decomposition of the sugar moiety led to a low product yield of 46%. The low yield along with the lability of the N(9) sugar functionality encouraged a reexamination of the synthetic approach.

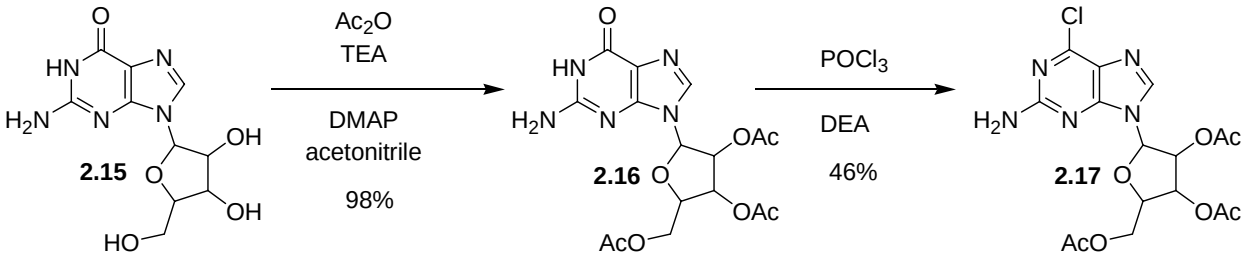

Figure 2-12. Preparation of starting material **2.17** used in an early synthetic approach to D-A purines.

The first synthetic strategy entertained for carbon-carbon bond formation on the C(8) position was deprotonation of C(8) using a strong bulky base, LTMP or LDA, followed by the addition of an electrophile (carbon dioxide, methylchloroformate, or benzylchloroformate) (Figure 2-13). This stategy was inspired by previous direct C(8) lithiation of the purine core done in the lab of Miyasaka.[76] Some of the problems encountered with Miyasaka's route included low yields of the desired product due to side product formation. Our deprotonation reactions were attempted many times and included varying the substituents on the purine, the base, equivalents of base used (1−5 equiv), temperature of the reaction (–78−50 °C), and the electrophile. The C(2) amine groups were functionalized with the Boc protecting group to see if

the free amine was complicating the reaction. Several of these reactions proved unsuccessful (Figure 2-13).

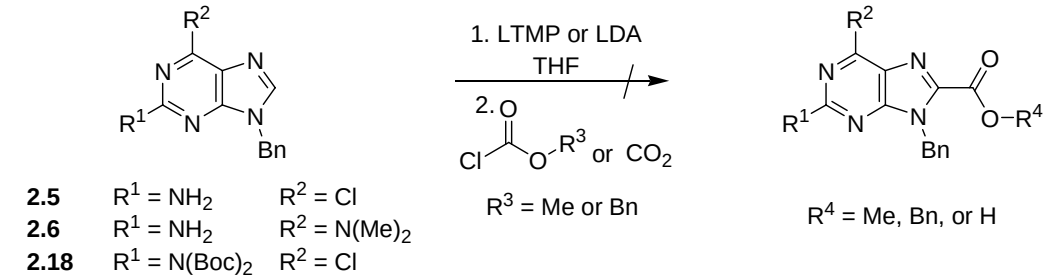

Figure 2-13. Deprotonation attempts of the C(8) position of purines.

One attempt, using 2-amino-9-benzyl purine (**2.6**), three equivalents of LDA, and one equivalent of methylchlorofomate at –78 °C successfully formed the desired product **2.6c** in 5% yield. This reaction, while encouraging, was still not sufficiently high yielding to permit continued investigation of deprotonation strategies.

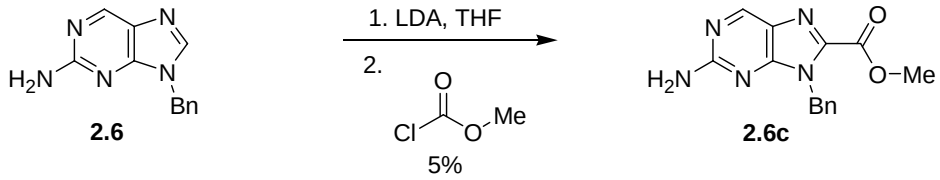

Figure 2-14. Successful C-C bond formation by C(8) deprotonation using LDA.

Lithium-halogen procedures have been used to modify the C(8) position of C(8) bromopurines[77]and were also attempted. Reacting molecules like **2.7a** with 1.2−6 equivalents of *n*-butyllithium and 2−10 equivalents of an electrophile gave no desired C(8) carbon-carbon bond formation and a complicated product mixture (Figure 2-15).

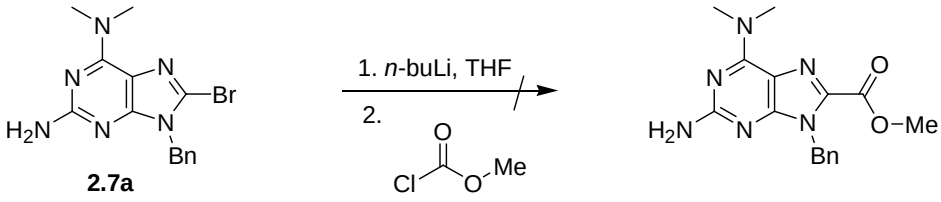

Figure 2-15. Attempted lithium-halogen exchange at the C(8) position of the purine followed by electrophile addition.

After this series of unsuccessful C(8) carbon-carbon bond formation reactions, a change of synthetic direction was necessary to effectively construct the desired C(8) modified products. It was at this time that the Pd(0)-mediated cyanation reactions discussed earlier were conceived.

Experimental Section

General. Reagents and solvents were purchased from Aldrich, Fluka, or Acros and used without further purification unless otherwise specified. THF, ether, CH_2Cl_2, and DMF were degassed in 20 L drums and passed through two sequential purification columns (activated alumina; molecular sieves for DMF) under a positive argon atmosphere. Flash chromatography (FC) was performed on Purasil SiO_2-60, 230−400 mesh from Whatman. Thin layer chromatography (TLC) was performed on SiO_2-60 F_{254} aluminum plates from EMD Chemicals with visualization by UV light or staining (e.g. $KMnO_4$). Melting points (m.p.) were determined on a Mel-temp electrothermal melting point apparatus and are uncorrected. ^1H (300 MHz) and ^{13}C NMR (75 MHz) spectra were recorded on Varian Mercury 300, Gemini 300, and VXR 300 spectrometers. Chemical shifts (δ) are given in parts per million (ppm) relative to residual protonated solvent ($CHCl_3$: δ_H 7.26 ppm, δ_C 77.00 ppm). Abbreviations used are s (singlet), d (doublet), t (triplet), q (quartet), quin (quintet), b (broad), and m (multiplet). High resolution mass spectra (HRMS) were obtained by the University of Florida Mass Spectrometry Services using a Finnigan MAT95Q Hybrid Sector spectrometer. Compound **2.1** was purchased from Aldrich. Purines **2.2**[46], **2.3**[46], **2.4**[46], **2.5**[47], **2.6**[49], and **2.8**[51] were obtained as described in the literature with some modification.

Synthesis of Compounds

General Method A (*C(8) bromination of purines; conversion of C(8)-H to C(8)-Br*). To a solution (6 mM) of starting material in CH_2Cl_2 was added bromine (33 equiv.) dropwise and the mixture was stirred at room temperature for 1 h to 24 h. The reaction was monitored by TLC to

determine when the reaction was complete. The reaction mixture was poured into 10% aqueous $Na_2S_2O_3$. The organic layer was separated and washed with brine, dried over $MgSO_4$, and concentrated under reduced pressure. The residue was purified by silica gel column chromatography (1% MeOH/CH_2Cl_2) to give the C(8) brominated product.

General Method B (*coupling of bromopurines with zinc cyanide; conversion of a to b*). To a solution (0.16 M) of C(8) bromopurine in NMP was added tetrakis(triphenylphosphine) palladium(0) (20–40 mol %), which was purified by washing with benzene and methanol. After stirring at 90 °C for 20 min a mixture of zinc cyanide (2 equiv.) suspended in NMP (0.90 mM) was added dropwise to the reaction (10 drops every 30 min for 4 h). The reaction was stirred at 90 °C overnight and then cooled and treated with aqueous ammonia (2 N, 15 mL). The mixture was extracted with ethyl acetate (3 x 100 mL). The combined organic extracts were washed with 2 N NH_4OH and brine, dried over $MgSO_4$, and concentrated under reduced pressure. The residue was purified by silica gel column chromatography (0.5% MeOH/CH_2Cl_2).

General Method C (*methanolysis of C(8) cyanopurines; conversion of b to c*). A solution of methanolic ammonia (7 N) and C(8) cyanopurine was stirred at room temperature overnight. The residue, after evaporation, was stirred in methanol while 1 N aqueous HCl was added dropwise. The solution was stirred for 2 h at room temperature, neutralized with Dowex 1 (OH^-) resin, filtered, and concentrated under reduced pressure. The crude product was purified by silica gel column chromatography (1% MeOH/CH_2Cl_2).

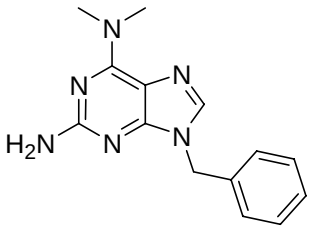

2-Amino-6-dimethylamino-9-benzylpurine (2.7). Dimethylamine (4.0 mL, 33% in abs ethanol) was added to **2.5** (1.0 g, 3.9 mmol) in abs. ethanol (40 mL) and the solution was heated to 60 °C for 20 h. The reaction mixture was evaporated to dryness and triturated with deionized H_2O. The white crystals (0.95 g, 92%) were then collected by vacuum filtration and dried under high vacuum: m.p. 170−173 °C. ^{1}H NMR (300 MHz, $CDCl_3$) δ 3.46 (s, 6H), 4.61 (s, 2H), 5.21 (s, 2H), 7.27 (m, 5H), 7.42 (s, 1H). ^{13}C NMR (75 MHz, $CDCl_3$) δ 38.22, 46.39, 114.98, 127.49, 127.93, 128.82, 135.87, 136.36, 152.91, 155.39, 159.40. HRMS calcd for $C_{14}H_{17}N_5$ $[M+H]^+$: 269.1509, found: 269.1516.

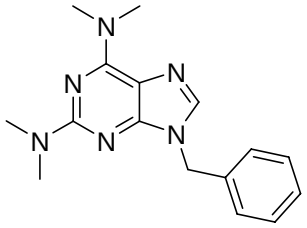

2,6-Bis(dimethylamino)-9-benzylpurine (2.10). Dimethylamine (50 mL) was added to **2.9** (2.5 g, 9.0 mmol) and the solution was heated to 100 °C for 20 h and then concentrated under reduced pressure. The crude solid was purified by silica gel column chromatography (20% EtOAc/hexanes) to afford a white solid (1.98 g, 76 %): m.p. 98–100 °C. ^{1}H NMR (300 MHz, $CDCl_3$) δ 3.17 (s, 6H), 3.46 (s, 6H), 5.22 (s, 2H), 7.30 (m, 5H), 7.40 (s, 1H). ^{13}C NMR (75 MHz, DMSO-d_6) δ 37.55, 38.19, 46.34, 113.55, 128.22, 128.44, 129.21, 137.16, 138.27, 153.40, 154.84, 159.38. HRMS calcd for $C_{16}H_{21}N_6$ $[M+H]^+$: 297.1828, found: 297.1820.

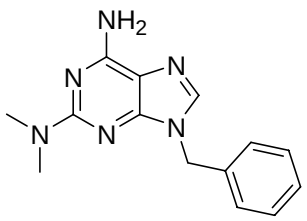

2-Dimethylamino-6-amino-9-benzylpurine (2.12). Dimethylamine (10 mL, 33% in abs ethanol) was added to **2.11** (0.30 g, 1.2 mmol) in a sealed tube. The reaction was stirred at 100

°C for 20 h, and then concentrated under reduced pressure. The crude solid was purified by silica gel column chromatography (1% MeOH/CH_2Cl_2) to afford a white solid (0.31 g, 99%): m.p. 168−171 °C. ^{1}H NMR (300 MHz, DMSO-d_6) δ 3.07 (s, 6H), 5.19 (s, 2H), 6.73 (s, 2H), 7.34 (m, 5H), 7.82 (s, 1H). ^{13}C NMR (75 MHz, DMSO-d_6) δ 37.00, 45.64, 112.39, 127.50, 127.77, 128.48, 137.35, 137.56, 151.60, 155.54, 159.48. HRMS calcd for $C_{14}H_{17}N_6$ $[M+H]^+$: 269.1509, found: 269.1515.

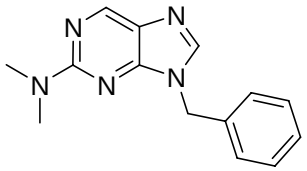

2-Dimethylamino-9-benzylpurine (2.14). Dimethylamine (4.0 mL, 33% in abs ethanol) was added to **2.13** (0.42 g, 1.7 mmol) and the solution was heated to 100 °C for 20 h and then concentrated under reduced pressure. The crude solid was purified by silica gel column chromatography (20% EtOAc/hexanes) to afford an off-white solid (0.37 g, 86%): m.p. 104–106 °C. ^{1}H NMR (300 MHz, DMSO-d_6) δ 3.15 (s, 6H), 5.30 (s, 2H), 7.34 (m, 5H), 8.22 (s, 1H), 8.68 (s, 1H). ^{13}C NMR (75 MHz, DMSO-d_6) δ 37.12, 45.71, 126.07, 127.74, 127.86, 128.63, 136.90, 142.81, 148.51, 152.85, 159.28. HRMS calcd for $C_{14}H_{15}N_5$ $[M+H]^+$: 254.1400, found: 254.1412.

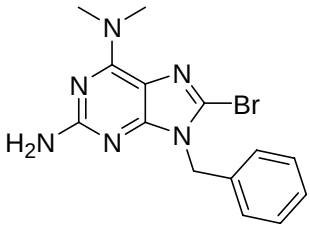

2-Amino-6-dimethylamino-8-bromo-9-benzylpurine (2.7a). Compound **2.7** (0.50 g, 1.8 mmol) was reacted under the conditions of general method **A** to yield a white solid (0.52 g, 81%): m.p. 168−169 °C. ^{1}H NMR (300 MHz, $CDCl_3$) δ 3.42 (s, 6H), 4.69 (s, 2H), 5.24 (s, 2H), 7.28 (m, 5H). ^{13}C NMR (75 MHz, $CDCl_3$) δ 38.27, 46.69, 115.54, 121.10, 127.40, 127.77,

128.63, 135.87, 154.13, 154.21, 159.19. HRMS calcd for $C_{14}H_{15}BrN_6$ $[M+H]^+$: 347.0620, found: 347.0618.

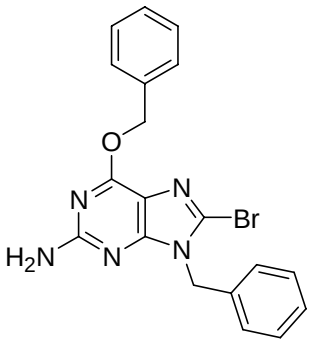

2-Amino-6-benzyloxy-8-bromo-9-benzylpurine (2.8a). Compound **2.8** (0.38 g, 0.93 mmol) was reacted under the conditions of general method **A** to yield a white solid (0.44 g, 77%): m.p. 164−166 °C. ^{1}H NMR (300 MHz, $CDCl_3$) δ 7.50 (m, 2H), 7.30 (m, 8H), 5.53 (s, 2H), 5.26 (s, 2H), 4.90 (s, 2H). ^{13}C NMR (75 MHz, $CDCl_3$) δ 47.11, 68.25, 115.85, 125.56, 127.50, 128.03, 128.07, 128.39, 128.75, 135.37, 136.20, 155.29, 159.17, 159.85. HRMS calcd for $C_{19}H_{17}BrN_6O$ $[M+H]^+$: 410.0616, found: 410.0627.

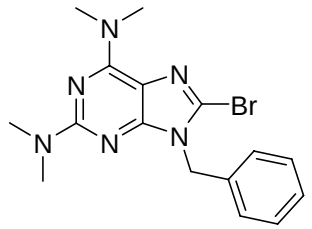

2,6-Bis(dimethylamino)-8-bromo-9-benzylpurine (2.10a). Compound **2.10** (1.5 g, 5.1 mmol) was reacted under the conditions of general method **A** to yield a white solid (1.3 g, 70 %): m.p. 130–131 °C. ^{1}H NMR (300 MHz, DMSO-d_6) δ 3.08 (s, 6H), 3.33 (bs, 6H), 5.21 (s, 2H), 7.31 (m, 5H). ^{13}C NMR (75 MHz, DMSO-d_6) δ 36.74, 37.55, 46.06, 113.20, 120.29, 127.30, 127.63, 128.61, 136.43, 152.99, 153.93, 158.43. HRMS calcd for $C_{16}H_{20}BrN_6$ $[M+H]^+$: 375.0933, found: 375.0943.

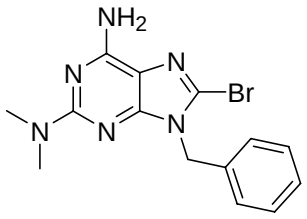

2-Dimethylamino-6-amino-8-bromo-9-benzylpurine (2.12a). Compound **2.12** (0.59 g, 2.2 mmol) was reacted under the conditions of general method **A** to yield a white solid (0.52 g, 68%): m.p. 195−197 °C. ^{1}H NMR (300 MHz, $CDCl_3$) δ 3.15 (s, 6H), 5.21 (bs, 2H), 5.23 (s, 2H), 7.29 (m, 5H). ^{13}C NMR (75 MHz, $CDCl_3$) δ 37.33, 46.11, 46.90, 113.31, 122.36, 127.90, 128.06, 128.61, 136.03, 153.87, 159.77. HRMS calcd for $C_{14}H_{16}BrN_6$ $[M+H]^+$: 347.0614, found: 347.0626.

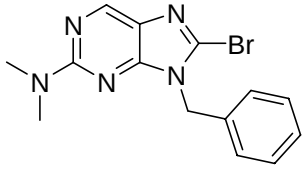

2-Dimethylamino-8-bromo-9-benzylpurine (2.14a). Compound **2.14** (0.40 g, 1.6 mmol) was reacted under the conditions of general method **A** to yield a white solid (0.42 g, 80%): m.p. 128-129 °C. ^{1}H NMR (300 MHz, $CDCl_3$) δ 3.16 (s, 6H), 5.30 (s, 2H), 7.31 (m, 5H), 8.67 (s, 1H). ^{13}C NMR (75 MHz, $CDCl_3$) δ 37.07, 46.11, 126.18, 127.41, 127.83, 128.52, 128.74, 135.88, 147.68, 153.71, 159.06. HRMS calcd for $C_{14}H_{14}BrN5$ $[M+H]^+$: 332.0506, found: 332.0517.

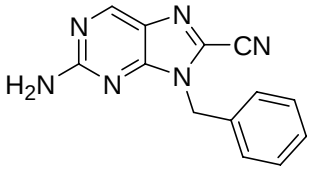

2-Amino-8-cyano-9-benzylpurine (2.6b). Compound **2.6a** (0.10 g, 0.33 mmol) was reacted under the conditions of general method **B** to yield a white solid (0.065 g, 80%): m.p. 139−142 °C. ^{1}H NMR (300 MHz, DMSO-d_6) δ 5.40 (s, 2H), 7.26 (m, 7H), 8.88 (s, 1H). ^{13}C

NMR (75 MHz, DMSO-d_6) δ 46.62, 112.17, 124.40, 126.58, 127.87, 128.87, 128.90, 129.67, 136.11. HRMS calcd for $C_{13}H_{10}N_6$ [M^+]: 250.0967, found: 250.0973.

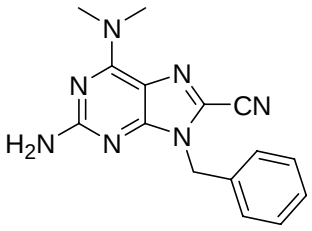

2-Amino-6-dimethylamino-8-cyano-9-benzylpurine (2.7b). Compound **2.7a** (0.20 g, 0.58 mmol) was reacted under the conditions of general method **B** to yield a white solid (0.15 g, 91%): m.p. 175−176 °C. ^{1}H NMR (300 MHz, DMSO-d_6) δ 3.40 (bs, 6H), 5.33 (s, 2H), 6.44 (s, 2H), 7.33 (m, 5H). ^{13}C NMR (75 MHz, DMSO-d_6) δ 47.56, 112.08, 114.91, 117.72, 126.90, 127.90, 128.78, 135.82, 152.77, 154.86, 161.50. HRMS calcd for $C_{15}H_{16}N_7$ [M+H]$^+$: 294.1467, found: 294.1479.

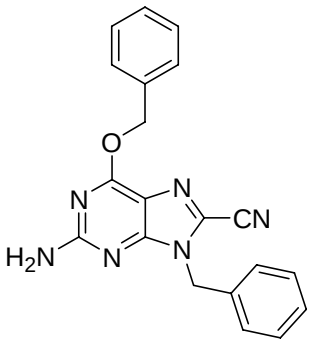

2-Amino-6-benzyloxy-8-cyano-9-benzylpurine (2.8b). Compound **2.8a** (0.30 g, 0.73 mmol) was reacted under the conditions of general method **B** to yield a white solid (0.14 g, 54%): m.p. 246−248 ° C. ^{1}H NMR (300 MHz, DMSO-d_6) δ 5.37 (s, 2H), 5.52 (s, 2H), 7.14, (s, 2H) 7.38 (m, 10H). ^{13}C NMR (75 MHz, DMSO-d_6) δ 46.22, 67.61, 111.58, 114.62, 121.17, 127.01, 128.07, 128.25, 128.42, 128.64, 128.88, 135.48, 135.89, 153.69, 161.10, 161.79. HRMS calcd for $C_{20}H_{17}N_6O$ [M+H]$^+$: 357.1464, found: 357.1432.

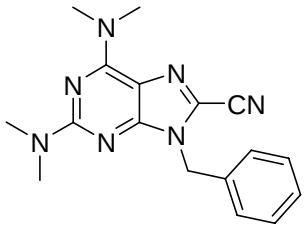

2,6-Bis(dimethylamino)-8-cyano-9-benzylpurine (2.10b). Compound **2.10a** (0.20 g, 0.53 mmol) was reacted under the conditions of general method **B** to yield a white solid (0.16 g, 93 %): m.p. 174–175 °C. ^{1}H NMR (300 MHz, $CDCl_3$) δ 3.20 (s, 6H), 3.43 (bs, 6H), 5.32 (s, 2H), 7.30 (m, 3H), 7.45 (m, 2H). ^{13}C NMR (75 MHz, DMSO-d_6) δ 35.11, 36.78, 46.03, 109.15, 112.23, 114.39, 117.79, 127.62, 128.09, 128.85, 135.95, 152.62, 154.22, 159.94. HRMS calcd for $C_{17}H_{19}N_7$ $[M+H]^+$: 322.1780, found: 322.1783.

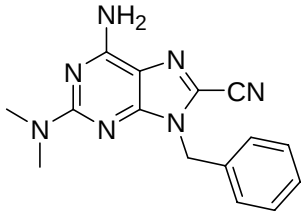

2-Dimethylamino-6-amino-8-cyano-9-benzylpurine (2.12b). Compound **2.12a** (0.10 g, 0.29 mmol) was reacted under the conditions of general method **B** to yield a white solid (85 mg, 77 %): m.p. 205−209 ° C. ^{1}H NMR (300 MHz, DMSO-d_6) δ 3.12 (s, 6H), 5.33 (s, 2H), 7.34 (m, 7H). ^{13}C NMR (75 MHz, DMSO-d_6) δ 36.90, 46.02, 112.25, 113.92, 118.50, 127.67, 128.10, 135.86, 136.00, 151.49, 156.28, 161.02. HRMS calcd for $C_{15}H_{16}N_7$ $[M+H]^+$: 294.1467, found: 294.1492.

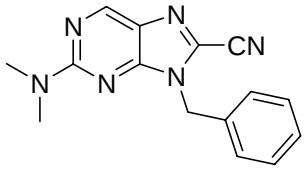

2-Dimethylamino-8-cyano-9-benzyl purine (2.14b). Compound **2.14a** (0.20 g, 0.60 mmol) was reacted under the conditions of general method **B** to yield a white solid (0.065 g, 39 %): m.p. 111–113 °C. ^{1}H NMR (300 MHz, $CDCl_3$) δ 3.30 (s, 6H), 5.41 (s, 2H), 7.35 (m, 5H)

8.83 (s, 1H). ^{13}C NMR (75 MHz, $CDCl_3$) δ 29.93, 38.01, 47.19, 111.51, 126.04, 128.76, 128.98, 129. 27, 134.78, 134.99, 151.78. HRMS calcd for $C_{15}H_{14}N_6$ $[M+H]^+$: 279.1353, found: 279.1355.

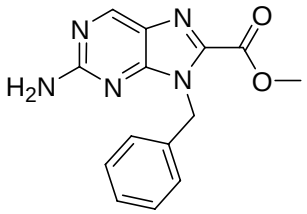

2-Amino-8-methylester-9-benzylpurine (2.6c) Compound **2.6b** (0.10 g, 0.40 mmol) was reacted under the conditions of general method **C** to yield a white solid (0.068 g, 60%): m.p. 226−228 ° C. ^{1}H NMR (300 MHz, $CDCl_3$) δ 3.97 (s, 3H), 5.27 (s, 2H), 5.74 (s, 2H), 7.29 (m, 5H), 8.84 (s, 1H). ^{13}C NMR (75 MHz, $CDCl_3$) δ 47.05, 53.22, 127.18, 127.92, 128.13, 128.87, 136.71, 151.75, 153.26, 159.86, 161.43. HRMS calcd for $C_{14}H_{13}N_5O_2$ $[M+H]^+$: 283.1069, found: 283.1086.

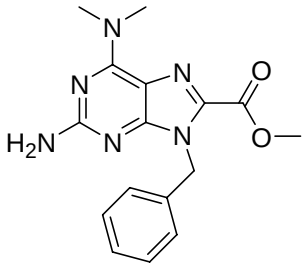

2-Amino-6-dimethylamino-8-methylester-9-benzylpurine (2.7c). Compound **2.7b** (0.062 g, 0.21 mmol) was reacted under the general method **C** to yield a white solid (0.054 g, 86%): m.p. 175−180 ° C. ^{1}H NMR (300 MHz, $CDCl_3$) δ 3.51 (bs, 6H) 3.91 (s, 3H) 4.77 (s, 2H) 5.70 (s, 2H) 7.26 (m, 5H). ^{13}C NMR (75 MHz, DMSO-d_6) δ 37.00, 46.12, 52.02, 114.23, 126.49, 127.12, 128.41, 132.89, 137.89, 137.60, 154.38, 155.46, 159.28, 161.02. HRMS calcd for $C_{16}H_{19}N_6O_2$ $[M+H]^+$: 327.1569, found: 327.1583.

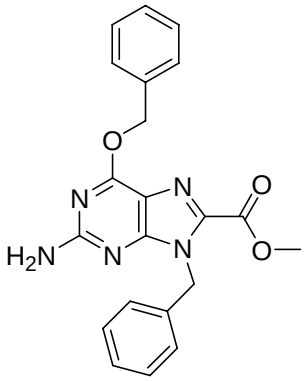

2-Amino-6-benzyloxy-8-methylester-9-benzylpurine (2.8c). Compound **2.8b** (0.037 g, 0.10 mmol) was reacted under the conditions of general method **C** to yield a white solid (0.038 g, 95%): m.p. 180−185 °C. ^{1}H NMR (300 MHz, $CDCl_3$) δ 3.90 (s, 3H), 5.03 (s, 2H), 5.53 (s, 2H), 5.70 (s, 2H), 7.31 (m, 10H). ^{13}C NMR (75 MHz, $CDCl_3$) δ 47.20, 52.64, 68.46, 115.51, 127.52, 127.69, 128.18, 128.37, 128.53, 128.65, 135.90, 136.74, 137.13, 155.26, 159.70, 160.53, 162.56. HRMS calcd for $C_{21}H_{19}N_5O_3$ $[M+H]^+$: 390.1566, found: 390.1544.

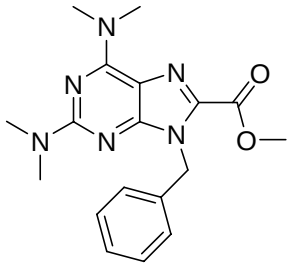

2,6-Bis(dimethylamino)-8-methylester-9-benzyl purine (2.10c). Compound **2.10b** (0.10 g, mmol) was reacted under the conditions of general method **C** to yield a white solid (0.070 g, 64 %): m.p. 147−148 ° C. ^{1}H NMR (300 MHz, $CDCl_3$) δ 3.20 (s, 6H), 3.50 (bs, 6H), 3.90 (s, 3H), 5.70 (s, 2H), 7.26 (m, 5H). ^{13}C NMR (75 MHz, DMSO-d_6) δ 36.77, 46.27, 52.05, 113.63, 127.24, 127.29, 128.40, 132.91, 137.64, 154.21, 154.77, 159.35, 159.57. HRMS calcd for $C_{18}H_{23}N_6O_2$ $[M+H]^+$: 355.1882, found: 355.1881.

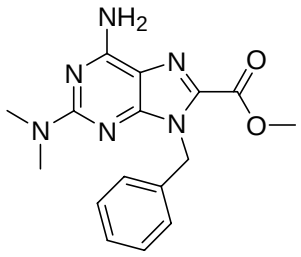

2-Dimethylamino-6-amino-8-methylester-9-benzylpurine (2.12c). Compound **2.12b** (0.10 g, 0.34 mmol) was reacted under the conditions of general method **C** to yield a white solid (0.067 g, 60%): m.p. 250−252 ° C. ^{1}H NMR (300 MHz, DMSO-d_6) δ 3.10 (s, 6H), 3.80 (s, 3H), 5.55 (s, 2H), 7.26 (m, 7H). ^{13}C NMR (75 MHz, DMSO-d_6) δ 36.91, 46.25, 51.94, 113.12, 127.30, 128.39, 133.75, 137.67, 153.04, 156.83, 159.39, 160.58. HRMS calcd For $C_{16}H_{18}N_6O_2$ [M^+]: 326.1491, found: 326.1488.

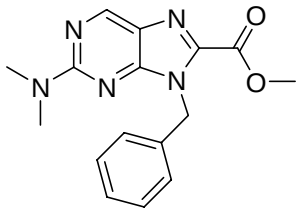

2-Dimethylamino-8-methylester-9-benzyl purine (2.14c). Compound **2.14b** (0.043 g, 0.16 mmol) was reacted under the conditions of general method **C** to yield a white solid (0.034 g, 71 %): m.p. 167–169 °C. ^{1}H NMR (300 MHz, DMSO-d_6) δ 3.21 (s, 6H), 3.87 (s, 3H), 5.64 (s, 2H), 7.28 (m, 5H), 8.92 (s, 1H). ^{13}C NMR (75 MHz, DMSO-d_6) δ 37.86, 47.05, 53.33, 125.56, 128.07, 128.23, 129.24, 137.79, 139.27, 152.69, 154.34, 160.07, 160.83. HRMS calcd for $C_{16}H_{17}N_5O_2$ [M+H]$^+$: 312.1455, found: 312.1468.

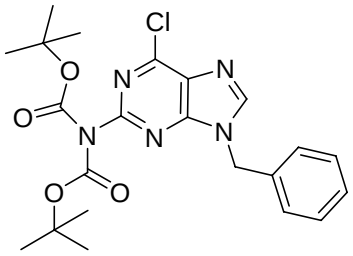

2-Di-tertbutoxycarbonlyamine-6-chloro-9-benzylpurine (2.18). Compound **2.5** (0.10 g, 0.39 mmol), $(Boc)_2O$ (0.25 g, 1.2 mmol), and DMAP (0.004 g, 0.04 mmol) were dissolved in dry THF (2 mL) and stirred at rt overnight. The solvent was removed under reduced pressure and the product was purified by flash chromatography (10% EtOAC/hexanes) to yield a white solid (0.074 g, 42%): ^{1}H NMR (300 MHz, DMSO-d_6) δ 1.31 (s, 18H) 5.53 (s, 2H) 7.32 (m, 5H) 8.94 (s, 1H).^{13}C NMR (75 MHz, DMSO-d_6) δ 27.3, 47.1, 83.3, 127.4, 128.1, 128.8, 129.4, 135.9, 149.0, 149.2, 150.0, 150.9, 152.5. HRMS calculated for $C_{22}H_{26}N_5O_4Na$ $[M+Na]^+$: 482.1566, found: 482.1573.

X-ray Crystallography

General. Data were collected at 173 K on a Siemens SMART PLATFORM equipped with a CCD area detector and a graphite monochromator utilizing MoK_α radiation (λ = 0.71073 Å). Cell parameters were refined using up to 8192 reflections. A full sphere of data (1850 frames) was collected using the ω-scan method (0.3° frame width). The first 50 frames were re-measured at the end of data collection to monitor instrument and crystal stability (maximum correction on I was < 1 %). Absorption corrections by integration were applied based on measured indexed crystal faces.

The structures were solved by the Direct Methods in *SHELXTL6*, and refined using full-matrix least squares. The non-H atoms were treated anisotropically, whereas the hydrogen atoms were calculated in ideal positions and were riding on their respective carbon atoms.

Compound 2.7b. The methyl H atoms on C(14) and C(15) are disordered and each set was refined in two parts and in a riding model with their site occupation factors fixed at 50%. A total of 208 parameters were refined in the final cycle of refinement using 4656 reflections with $I > 2\sigma(I)$ to yield R_1 and wR_2 of 3.83% and 10.27%, respectively. Refinement was done using F^2.

Compound 2.12b. A total of 207 parameters were refined in the final cycle of refinement using 3304 reflections with $I > 2\sigma(I)$ to yield R_1 and wR_2 of 4.75% and 12.0%, respectively. Refinement was done using F^2.

Compound 2.12c. The two protons on N(10) were obtained from a Difference Fourier map and refined without any constraints. A total of 227 parameters were refined in the final cycle of refinement using 2572 reflections with $I > 2\sigma(I)$ to yield R_1 and wR_2 of 3.92% and 9.82%, respectively. Refinement was done using F^2.

CHAPTER 3
PHOTOPHYSICAL AND ELECTRONIC PROPERTIES OF DONOR-ACCEPTOR PURINES

Before molecules are considered for optoelectronic devices or used as biological probes it is critical to determine their photophysical and electronic properties, stability, and behavior in the solid state and in solution.[78] Knowing the solvent-induced absorption and emission changes for a fluorophore is relevant to its potential use for reporting structural changes and intermolecular interactions within biological microenvironments.[79,80] For materials applications, the ability to tailor optical properties in the context of controlled molecular (and supramolecular) architectures is important. This chapter describes the UV/vis, fluorescence, and solvatochromism properties of the D-A purines (Figure 3-1). Cyclic voltammetry and computational data are also provided that correlates well with photophysical data. Finally, the first usage of a purine in a light emitting device is reported.

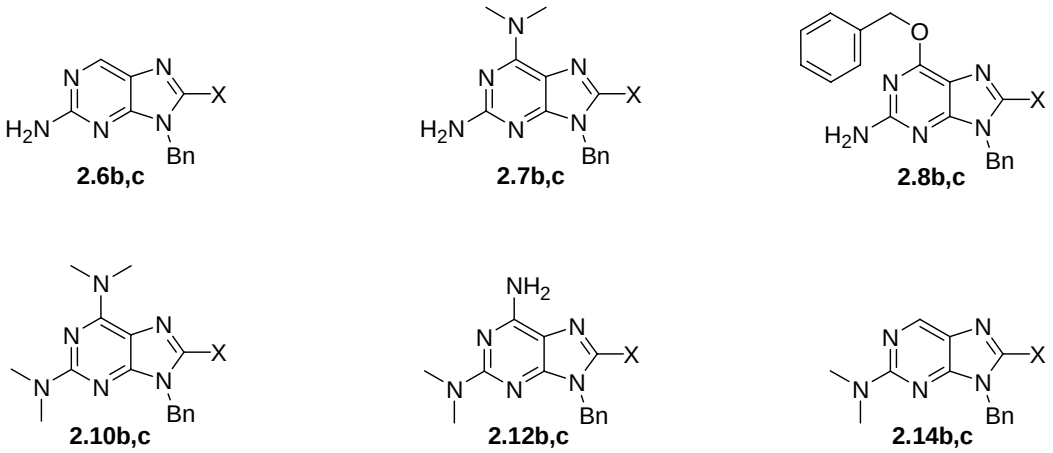

Figure 3-1. Donor-acceptor purines targeted for photophysical studies.

Interest in the photophysical properties of substituted purines and 2-aminopurine (2-AP) derivatives spans over six decades. Studies of 2-AP derivatives have been traditionally resigned to aqueous solutions[81] (vide supra) due to their poor solubility in organic solvents and their more

typical application in aqueous (biological) environments. Limited attention has been given to purines as fluorophores that might be used in or processed from organic solution. Photophysical measurements in organic solvents have been performed (although not comprehensively so) for 2-AP[19] and 2-AP derivatives such as 2-dimethylaminopurine[82] and the ethenopurines.[83] Tor's recently prepared C(8)-furano substituted purines represent new compounds for such studies (Figure 1-8B).[33] The N(9) benzyl group of the purines in Figure 3-1 makes their photophysical measurement in organic solvents possible wherefrom they can potentially be processed for materials applications. The photophysical studies discussed in this chapter show that addition of acceptor groups to the purine C(8) position appears as a general way to produce the first nucleobase derivatives that have near unity quantum yields across a range of organic solvents.[38,83-85] Upon removal of the benzyl (or similar) protecting group, the compounds should be quite suitable for applications in water. To this end, preliminary photophysical data for compounds **2.6b** and **2.6c** (with the benzyl group in place) in aqueous solution shows that they indeed maintain (and even enhance) their exceptional optical properties.

UV/vis data for C(8)-H, C(8)-CN, and C(8)-COOMe Purines in Methylene Chloride

UV/vis measurements were performed for each C(8)-H, -CN, and -COOMe purine (Tables 3-1−3-3) at 5, 10, 20, 40, and 60 μM in methylene chloride. A representative series of absorption spectra are shown for nitrile **2.7b** in figure 3-2. Examination of the UV/vis spectra reveals two significant low-energy bands whose maximum absorption wavelengths are concentration independent. By analogy to 2-AP[81] and further confirmed by computation (vide infra), the lowest energy (emitting) band is assigned to the $^1(\pi\pi^*\ L_a)$ transition, and the higher energy non-emitting band to the $^1(\pi\pi^*\ L_b)$ transition.[86]

Mason,[81] Drobnik[87,88], and Smagowicz[82] concluded early on from analysis of the absorption bands of substituted and unsubstituted purines that the long-wavelength $^1(\pi\pi^* L_a)$ absorption band is due principally to a longitudinally (along the long axis of the purine) polarized transition. Substituents on the C(2) position of the purine core, positioned at an angle 30° from this axis, therefore significantly affect its energy (and λ_{max}), as do substituents on C(8). Substituents in the C(6) position, situated transverse to the long axis, contribute less.[81] For example, adenine (C(6)-amino) and 6-dimethylaminopurine show a modest difference in λ_{max} values for their $^1(\pi\pi^* L_a)$ absorption (260 versus 275 nm in water, respectively), while the difference between 2-aminopurine and 2-dimethylaminopurine is much larger (305 versus 332 nm in water, respectively).[81] C(6) substituents do, however, more significantly affect the higher energy $^1(\pi\pi^* L_b)$ absorption band. These general trends are apparent in the long-wavelength absorption data shown for the C(8)-H purines used in this work (Table 3-1). Purines **2.6** and **2.14**, for example, bearing donors only in the C(2) position, show the most red-shifted $^1(\pi\pi^* L_a)$ absorption bands. As in Mason's work,[81] the stronger C(2)-dimethylamino donor of **2.14** extends λ_{max} to ~ 330 nm.

Data from figure 3-2 could be plotted to confirm that the optical density varies linearly with concentration (Figure 3-3). This experiment, repeated for each of the purines discussed in this work, provides some assurance that the molecules are not significantly aggregating under the solvent and concentration conditions chosen. Self-association could occur by hydrogen bonding[89] or dipolar π-stacking[67,71] for these nucleobases. Extinction coefficients, presented as log ε, could then be calculated by multiplying the slope of the line from the absorption vs. concentration plot by 10^6. Only the absorption data for the lowest energy emitting $^1(\pi\pi^* L_a)$ transition are shown in tables 3-1−3-12.

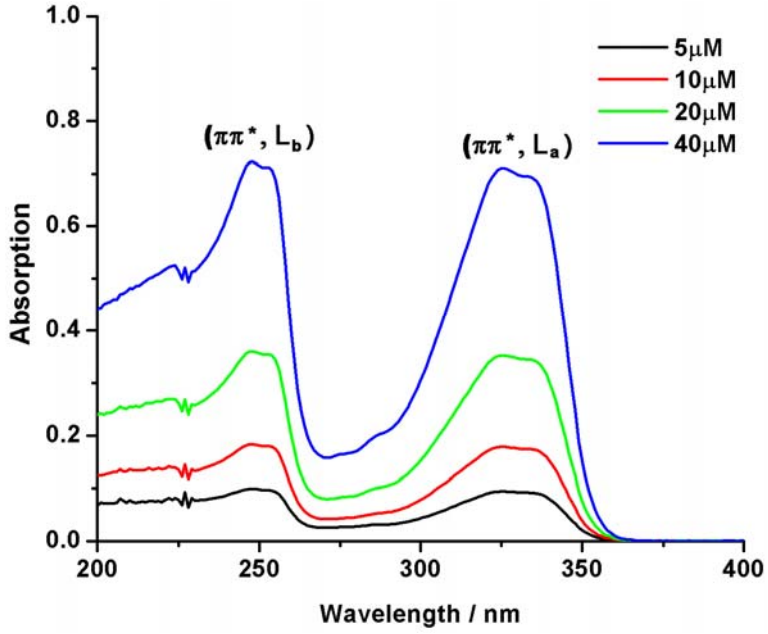

Figure 3-2. Absorption spectra for compound **2.7b** upon dilution in methylene chloride.

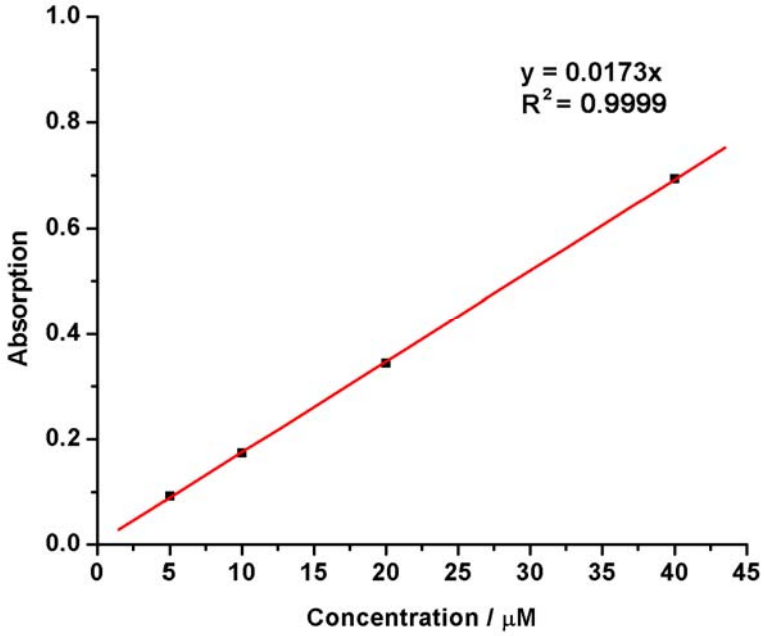

Figure 3-3. Absorption intensity at 334 nm vs. concentration for compound **2.7b**.

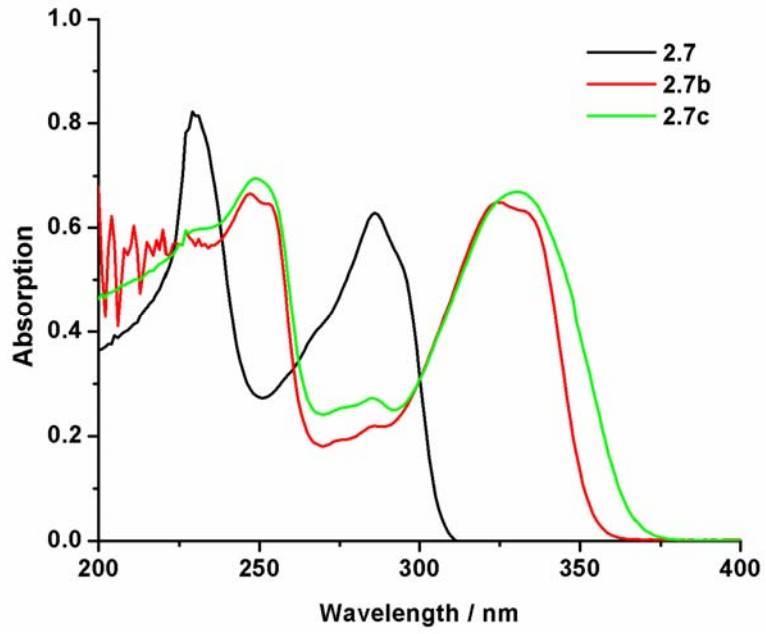

Figure 3-4. Absorption spectra for C(8)-H (**2.7**), C(8)-CN (**2.7b**), and C(8)-COOMe (**2.7c**) containing the same C(2) and C(6) substituents.

Figure 3-4 shows graphically the response of the absorption maxima of the $^1(\pi\pi^*\ L_b)$ and $^1(\pi\pi^*\ L_a)$ bands upon installing a -CN or -COOMe acceptor group in the C(8) position of **2.7**; the $^1(\pi\pi^*\ L_b)$ is red-shifted by about 20 nm while the $^1(\pi\pi^*\ L_a)$ is shifted by a larger 44 nm. These changes are consistent with an increase in conjugation length. Interestingly, the absorption maxima are comparable between the C(8)-CN and -COOMe derivatives **2.7b** and **2.7c**, a trend that exists for nearly all of the purines studied (where $\Delta\lambda_{max(CN/COOMe)} \sim 6$ nm). The bathochromic shifts observed upon C(8)-acceptor substitution are universal for the D-A purines prepared, and the largest change is ~51 nm (for the **2.10** series). Even the "parent" **2.6** series shows a red-shift of ~26 nm upon CN/COOMe introduction, a potentially useful improvement for selective excitation over 2-AP for biological applications. Finally, the extinction coefficient maxima are uniformly high for the C(8)-H, -CN, and -COOMe purines and comparable to literature values (Tables 3-1−3-12).[81,90]

Table 3-1. Absorption and Emission Properties for C(8)-H Purines in CH_2Cl_2.[a]

Purine	λ_{max}, abs/nm	log ε /M^{-1} cm^{-1}	λ_{max}, [b] em/nm	$\Delta\lambda_{max}$, em-abs/nm	Φ_F [c]
2.6	304	3.9	357	53	0.20
2.7	286	4.1	351	65	0.013
2.8	281	4.0	360	79	0.033
2.10	297	4.1	392	95	0.033
2.12	299	3.9	360	61	0.12
2.14	330	3.8	393 [d]	63	0.76

[a]All measurements performed at room temperature. [b]All experiments were performed using optical densities ≤ 0.1 at the excitation wavelength (λ_{ex} = 290 nm). [c]Fluorescence quantum yields are relative to the quantum yield of quinine sulfate in 0.5 M H_2SO_4 (Φ_F = 0.546). [d]Measurement performed at the excitation wavelength (λ_{ex} = 320 nm).

Table 3-2. Absorption and Emission Properties for C(8)-CN Purines in CH_2Cl_2.[a]

Purine	λ_{max}, abs/nm	log ε /M^{-1} cm^{-1}	λ_{max}, em/nm	$\Delta\lambda_{max}$, [b] em-abs/nm	Φ_F [c]	τ_F/ns
2.6b	326	3.2	371	45	0.20	0.5±0.2
2.7b	324	4.2	375	51	0.30	1.6±0.3
2.8b	311	4.3	355	44	0.81	3.1±0.2
2.10b	348	4.4	388	40	0.20	7.6±1.1
2.12b	336	4.1	387	51	0.97	3.2±0.3
2.14b	361	4.2	429	68	0.90	4.2±0.2

[a]All measurements performed at room temperature. [b]All experiments were performed using optical densities ≤ 0.1 at the excitation wavelength (λ_{ex} = 320 nm). [c]Fluorescence quantum yields are relative to the quantum yield of quinine sulfate in 0.5 M H_2SO_4 (Φ_F = 0.546).

Table 3-3. Absorption and Emission Properties for C(8)-COOMe Purines in CH_2Cl_2.[a]

Purine	λ_{max}, abs/nm	log ε /M^{-1} cm^{-1}	λ_{max}, [b] em/nm	$\Delta\lambda_{max}$, em-abs/nm	Φ_F [c]	τ_F/ns
2.6c	328	4.1	379	51	0.42	1.8±0.2
2.7c	330	4.2	393	63	1	3.1±0.3
2.8b	315	4.3	371	56	0.98	2.5±0.1
2.10c	348	4.3	409	61	0.90	2.7±0.3
2.12c	338	4.1	409	71	1	3.3±0.1
2.14c	362	4.1	433	71	0.81	3.4±0.2

[a]All measurements performed at room temperature. [b]All experiments were performed using optical densities ≤ 0.1 at the excitation wavelength (λ_{ex} = 320 nm). [c]Fluorescence quantum yields are relative to the quantum yield of quinine sulfate in 0.5 M H_2SO_4 (Φ_F = 0.546).

Steady State Fluorescence of C(8)-H, C(8)-CN, and C(8)-COOMe Purines in Methylene Chloride

Two different excitation wavelengths were chosen based on the $^1(\pi\pi^* L_a)$ absorption transition to examine the fluorescence of the purine derivatives. The C(8)-H derivatives, with

the exception of **2.14**, were excited at 290 nm, while the C(8)-CN, and -COOMe derivatives, and compound **2.14,** were excited at 320 nm. The shape of the excitation spectrum for compound **2.7c** is essentially the same as its $^1(\pi\pi^*$ $L_a)$ absorption band; therefore, excitation at any point of the absorption band leads to the efficient conversion into the low-lying emitting state (the fluorescence emission is independent of the excitation wavelength used as stated by Kasha's rule).[2]

Emission spectra were recorded for C(8)-H, -CN, and -COOMe purines in methylene chloride (Tables 3-1−3-3 and Figures 3-4 and 3-5). The emission data revealed significant spectral and quantum yield (Φ_F) differences as a result of C(8) substitution. The emission bands are generally red-shifted by ~ 20 nm upon addition of the C(8)-CN acceptor group, expected due to the increased conjugation length of the molecule. They are red-shifted an additional 5–20 nm upon the nitrile's transformation to the methyl ester. This is illustrated by the **2.6** series of compounds (**2.6**, **2.6b**, and **2.6c**) as the emission maximum increases from 357 nm to 371 nm with C(8) cyano addition and from 371 nm to 379 nm when transformed to the methylester. Exceptions to this trend are seen with the **2.8** and **2.10** series of purines as the emission maxima decrease 4 and 5 nm, respectively, upon C(8)-CN addition. This result is most likely due to a small amount of water or methanol contamination present in the C(8)-H compounds. General solvatochromism studies from the literature reveal that small amounts (< 1%) of polar protic solvents can cause significant increases in emission maxima due to specific solvent effects.[2] This is also consistent with solvent studies presented in this work.

Quantum Yield Measurements in Methylene Chloride

Quantum yields (Φ_F), the efficiency of absorbed photons that are emitted, were calculated (equation 3-1) from the absorbance (A) at the excitation wavelength, the area under the emission

curve (F), and the solvent refractive index (η) of solutions of purine compounds (x) and standards (s) prepared using dried and degassed solvents.

$$\Phi_{F(x)} = (A_s/A_x)(F_x/F_s)(\eta_x/\eta_s)^2 \Phi_{F(s)} \quad (3\text{-}1)$$

During the early stages of quantum yield determination, many inconsistent results were obtained. The purity and quality of both the solvent and compound were found to be extremely important. In addition to being pure, the solvents must also be dried and degassed to prevent any deviations in absorption maxima from water and to prevent quenching of fluorescence resulting from molecular oxygen. Measurements from a standard with a known quantum yield are necessary for determination of new quantum yields. The standard must be excited at the same wavelength as the unknown compound, so it must absorb in the same range as the unknown. After the evaluation of several standards, including anthracene, 2,6-diphenylanthracene, and quinine sulfate, the latter 0.5 M H_2SO_4 ($\Phi_F = 0.546$)[3] appeared to give the most consistent results. In order to verify the literature quantum yield value of quinine sulfate, a second standard was measured; typically anthracene in ethanol ($\Phi_F = 0.27$)[3], and the quantum yield of each standard was calculated using the literature value of the other standard. This was done every time quantum yields for the purine compounds were measured. The quantum yield of the standards and purines had to be measured on the same day to circumvent day-to-day variations in the fluorometer laser.

The quantum yields of the C(8)-H purines were found to vary with changes in substitution. The quantum yield of the parent 2-aminopurine derivative **2.6** in methylene chloride ($\Phi_F = 0.20$) is somewhat higher than literature values for 2-aminopurine derivatives in nonprotic solvents. For 2-amino-9-ethylpurine, a quantum yield of 0.085 in chloroform is reported,[19] and quantum yields of 0.10, 0.045, 0.12, and 0.08 are found[82] for the same compound in ethyl ether, ethyl

acetate, DMF, and acetonitrile, respectively. The 2-dimethylaminopurine derivative **2.14** was found to have a comparable quantum yield ($\Phi_F = 0.76$) to literature values measured for 2-dimethylaminopurine in similarly nonprotic ether ($\Phi_F = 0.71$), ethyl acetate ($\Phi_F = 0.64$), and DMF ($\Phi_F = 0.72$).[82]

The addition of C(8)-CN in general led to dramatic quantum yield increases. Compounds **2.7b** ($\Phi_F = 0.013 \rightarrow 0.30$), **2.8b** ($\Phi_F = 0.033 \rightarrow 0.81$), and **2.10b** ($\Phi_F = 0.033 \rightarrow 0.20$) showed quantum yields that increased an order of magnitude upon addition of the C(8) cyano group and for compounds **2.12b** and **2.14b** quantum yields increased to ≥ 0.90. Once the C(8) cyano groups were transformed to methylesters the quantum yield increased again with nearly all compounds approaching unity (Table 3-3). Tor and Greco have recently found that they could transform the virtually non-emissive nucleosides guanosine and adenosine into highly emissive variants by adding a furan to the C(8) position (C(8)-furano guanosine ($\Phi_F = 0.69$); C(8)-furano adenosine ($\Phi_F = 0.57$)).[33]

Donor substituents on the C(2) and C(6) positions of the purine contribute considerably, but not equivalently, to the observed emission properties as seen from the increase in quantum yield of 2-dimethylaminopurine vs. 2-aminopurine (vide supra). Comparison of isomeric species **2.7b** and **2.12b** (Figure 3-5) also nicely shows that introduction of the strongest donor to C(2), in this case $N(CH_3)_2$, has the most significant effect on the emission maximum. Compound **2.7b** has a quantum yield of 0.30, however upon switching the C(2) and C(6) substituents the quantum yield becomes near unity for compound **2.12b** ($\Phi_F = 0.97$). This finding is consistent with the transition dipole moment being positioned along the purine's longitudinal axis, such that C(2) substituents (oriented only 30° from this axis) more significantly affect the energy of the

emitting state. Transversely-oriented C(2) substituents are found to have a smaller effect on the emission maxima (Figure 3-4).

The C(2) and C(6) donor substituents seem to affect the quantum yields of the C(8)-CN purines differently than the C(8)-COOMe purines (Figures 3-5 and 3-6). This phenomenon could be a result of the cyano group being aligned with the long axis of the purine, allowing C(2) donor groups to influence most strongly the emission properties. The C(8)-COOMe acceptor group, however, features an off-axis geometry which allows it to borrow from both the C(2) and C(6) donors.

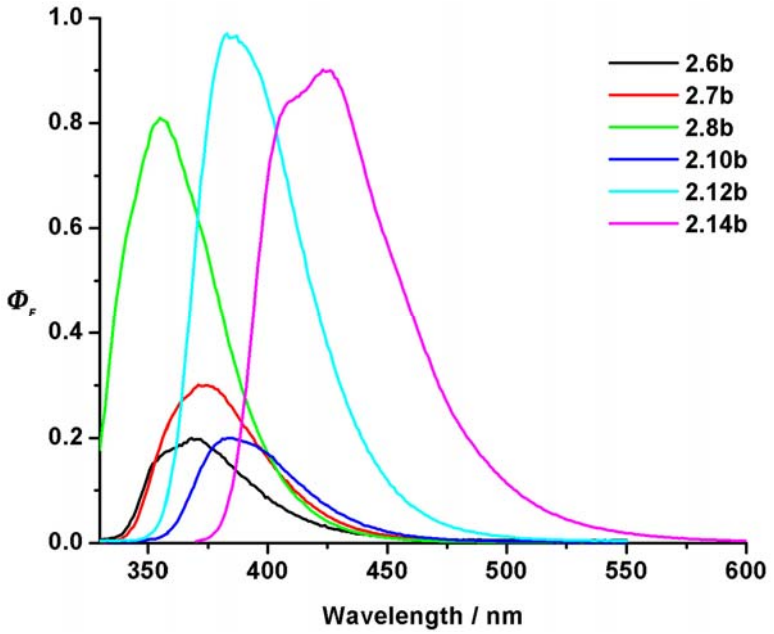

Figure 3-5. Emission spectra of C(8)-CN purines in methylene chloride.

Stokes Shifts of Purine Compounds in Methylene Chloride

The Stokes shift is the energy loss that occurs between excitation and emission of a fluorophore.[2] Stokes shift values ($\Delta\lambda$) are calculated by taking the difference of the emission maximum and the absorption maximum. These energy losses are observed for all fluorescent molecules in solution.[2] Large Stokes shifts (35–135 nm) generally indicate a significant

reordering of the surrounding solvent molecules upon excitation and accompany the existence of a charge separated excited state.[2] The Stokes shifts are typically smallest for the C(8)-CN purines, from 40–68 nm, and largest for the C(8)-H purines, 53–95 nm. The C(8)-COOMe purines fall in between with a Stokes shift range of 51–71 nm. The ground state and excited state dipoles are aligned more for the C(8)-CN purines leading to less solvent reorganization upon excitation and consequently a smaller Stokes shift. These numbers, however, show that there is no significant increase upon addition of acceptor groups to C(8) in methylene chloride (Tables 3-1–3-3).

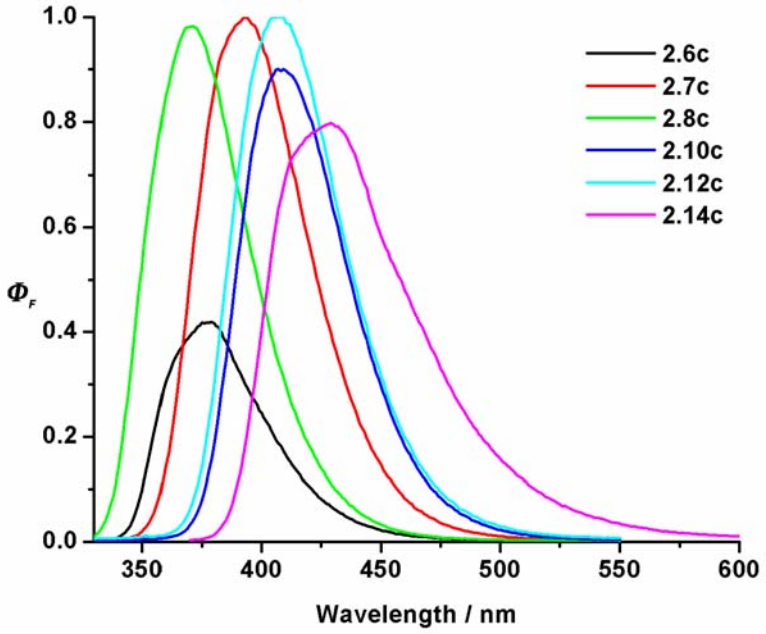

Figure 3-6. Emission spectra of C(8)-COOMe compounds in methylene chloride.

Fluorescence Lifetime Data for C(8)-CN and -COOMe in CH_2Cl_2

Fluorescence lifetime data (time-resolved fluorescence) was performed using the time domain method (pulse fluorometry). In this method the sample is excited with a pulse of light that is preferably much shorter than the decay time (τ) of the sample. The excitation pulse is first sent to the sample; the time dependent intensity is then measured. Next, the decay time is

calculated from the slope of a plot of log $I(t)$ versus t, or from the time at which the intensity (I) decreases to $1/e$ of the intensity at $t = 0$.[2]

Time resolved emission data was collected for the C(8)-CN and -COOMe D-A purines in methylene chloride. Excitation was performed for all compounds at 337 nm (all measured compounds absorbed at the wavelength) using a nitrogen laser with a pulse width of ~800 ps. This is the highest energy wavelength that can be used for this laser without passing the beam through a frequency doubler which decreases the intensity of the beam and makes the data collection more difficult and time consuming. The lifetime measurements reveal that the τ_F values correspond to the quantum yields, and the best emitters have τ_F values of ~ 3 ns. All decays could be fit, with χ^2 values close to 1, to a single exponential, and are consistent with fluorescence emission from the low-lying S_1 state. Literature values show 2-dimethyladenosine with τ_F values of 0.71 and 1.27 ns in acetonitrile and dioxane, respectively.[91] Also found in the literature are lifetime values in water for 2-aminopurine (τ_F = 11.8 ns) and 2-amino-9-methylpurine (τ_F = 11.1 ns).[90] These values are difficult to compare with the D-A purines presented in this work, because of solvent and substitution, but they do fall into a similar range.

Solvatochromism Studies for C(8)-H, -CN, and -COOMe Purines

Solvatochromism describes the influence of a 'medium' on UV/vis and fluorescence spectra. The 'medium' can be a solvent, solid, micelle, organized molecular film, even a vacuum.[92] Here we discuss the effects of solvent polarity on the absorption and emission properties of the C(8)-H, -CN, and -COOMe purines. The solvents used for this study include 1,4-dioxane, methylene chloride, acetonitrile, and methanol whose relative polarities increase in the order in which they are listed.[93] The same general emission trend observed in methylene chloride, where the C(8)-CN and C(8)-COOMe D-A purines show higher quantum yields than

the C(8)-H purines, are observed with 1-4 dioxane, acetonitrile, and methanol. Compounds **2.6b** and **2.6c** were also measured in water.

Solvent Influence on Absorption and Emission Spectra

Absorption and emission spectra were obtained for C(8)-H purines **2.1–2.6** and for the C(8)-CN (**2.1b–2.6b**) and -COOMe (**2.1c–2.6c**) purines in 1,4-dioxane, methylene chloride, acetonitrile, and methanol (Tables 3-1−3-12). The absorption maximum (λ_{max}) for each purine appears to have similar values regardless of the polarity of the solvent used; for example, the $^1(\pi\pi^*$ $L_a)$ absorption maximum for **2.7b** changes by only 8 nm across the polarity range of solvents (Figure 3-7).

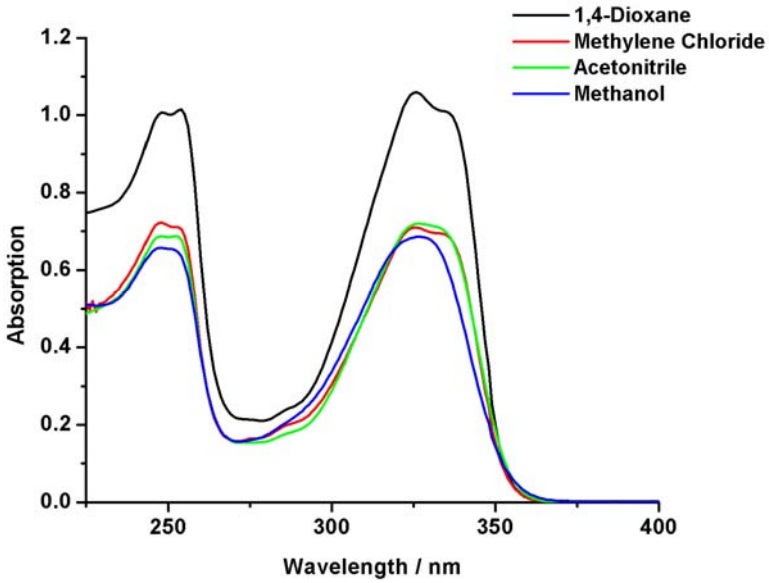

Figure 3-7. Absorption data for 40 μM solutions of compound **2.7b** in different solvents.

The insensitivity of the absorption maxima to solvent indicates that the ground state and the excited state are solvated equally in all the solvents. Again, absorption vs. concentration plots of each compound in all of the solvents verify that their optical densities vary linearly with concentration. Linearity is found even in dioxane, a solvent known to promote the association of

polar π-systems by dipolar π-stacking as seen for the merocyanine dyes developed by Würthner and coworkers.[70]

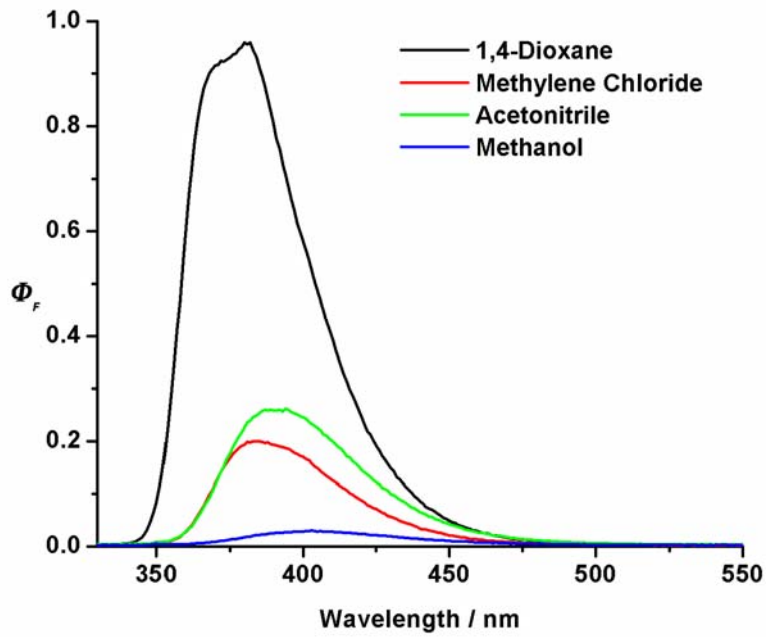

Figure 3-8. Emission spectra for **2.10b** in solvents of varying polarities.

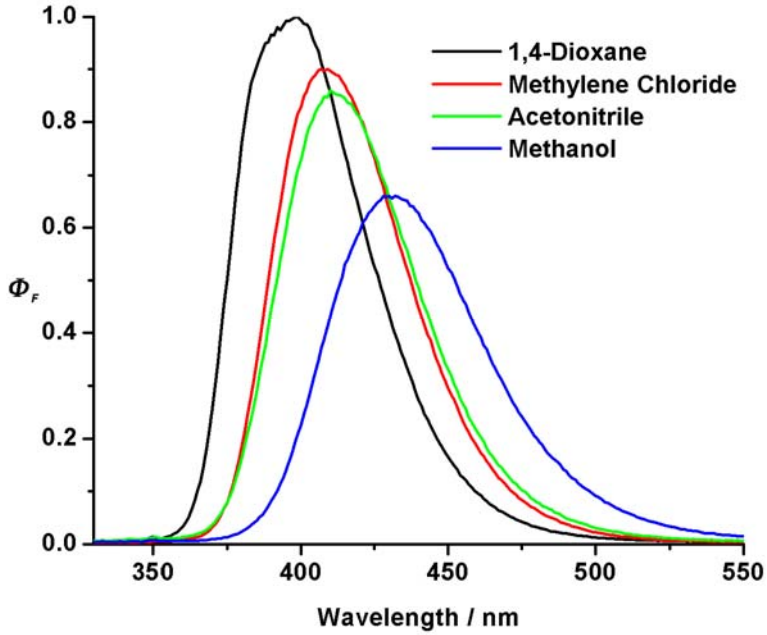

Figure 3-9. Emission spectra for **2.10c** in solvents of varying polarites.

This result is consistent with the lower ground state dipole moments calculated for the purines (~ 2–6 D) versus the merocyanine derivatives (12–19 D).[71] The log(ε) determined for each of the compounds also remains high despite the solvent used.

The expected bathochromic shifts of the emission peaks occur with increasing solvent polarity due to greater interaction of the excited state dipole with the solvent; this results in a reduction in energy of the excited state (Figures 3-8–3-11).[94] Accordingly, there is an increase of the Stokes shift for each purine as solvent polarity is increased indicating a greater degree of solvent reorganization.[2]

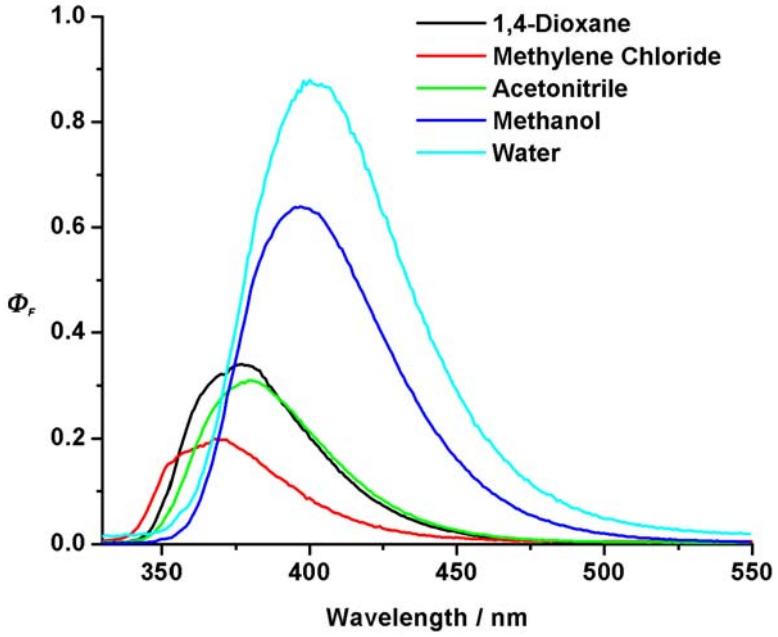

Figure 3-10. Emission spectra of **2.6b** in solvents of varying polarities.

Large bathochromic shifts are generally good for (biological) applications that involve microenvironment sensing/reporting. These changes make possible the fluorometric detection of small structural changes in biomolecules. The D-A purines presented here are more sensitive to solvent effects than the unsubstituted C(8)-H purines reported in this work and in the literature. The parent **2.6** is found to share a solvent sensitivity similar to that of 2-AP reported in the

literature. Swagowicz reported Stokes shifts for 2-AP of 51 nm in ethyl ether and 72 nm in water;[82] a 21 nm range between the lowest and highest polarity solvents studied. Similarly, a 20 nm range was found for compound **2.6** in going from 1,4-dioxane to water. Stokes shift ranges observed for compounds **2.6b** and **2.6c** are 25 nm and 40 nm, respectively, showing a slight increase in the C(8)-CN derivative and a significant increase for the C(8)-COOMe derivative.

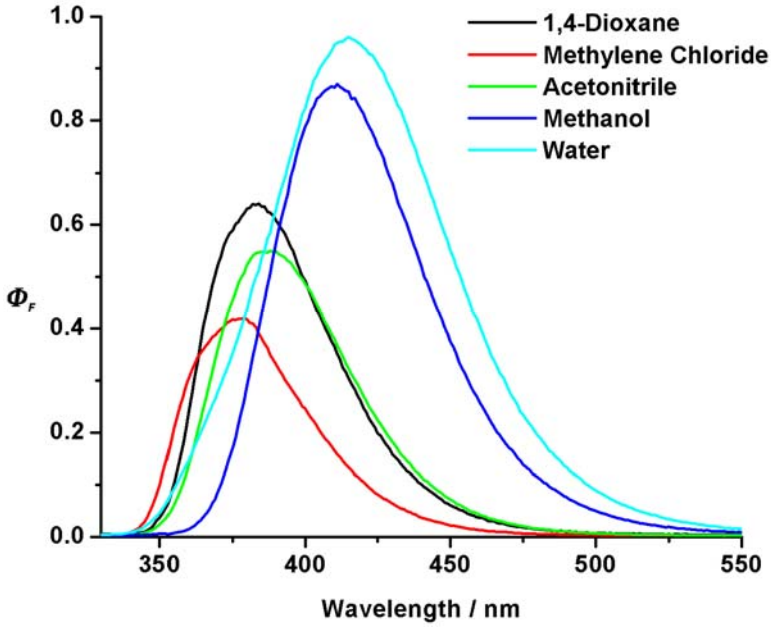

Figure 3-11. Emission spectra for **2.6c** in solvent of varying polarities.

The quantum yield values for the majority of the purine compounds decrease with increasing solvent polarity; for example, the quantum yield of **2.10b** dramatically decreases from 0.96 in 1,4-dioxane to 0.032 in methanol (Figure 3-8). Luminescence quenching in polar solvents is commonly observed for chromophores. Although the nature of this quenching is not generally understood by any one explanation, it is linked to the energy gap law that describes the rates of non-radiative deactivations.[92] The energy of the more polar excited state of the molecule is lowered through more efficient solvation as a result of the more polar solvent. This causes the radiationless transitions to become faster and/or the radiative transitions to become slower making the effective transition energy diminish with increasing solvent polarity. Protic solvents

also have the ability to quench luminescence by protonating some of the charge separated excited state molecules. Evidence of this has been seen by means of isotope exchange experiments with naphthylamine.[92] The C(8) methyl ester family of compounds shows only moderate decreases in luminescence, by comparison to C(8)-H and C(8)-CN derivatives, as solvent polarity is increased. The quantum yield values for **2.10c** are unity in 1,4-dioxane and 0.66 in methanol (Figure 3-9).

Table 3-4. Absorption and Emission Properties for C(8)-H Purines in 1,4-Dioxane.[a]

Purine	λ_{max}, abs/nm	log ε /M^{-1} cm^{-1}	λ_{max}, [b] em/nm	$\Delta\lambda_{max}$, em-abs/nm	Φ_F [c]
2.6	308	3.9	358	50	0.053
2.7	287	4.2	369	82	0.0077
2.8	283	4.1	372	89	0.012
2.10	293	4.1	367	74	0.41
2.12	293	4.0	355	62	0.085
2.14	327	3.9	391[d]	64	0.63

[a]All measurements performed at room temperature. [b]All experiments were performed using optical densities ≤ 0.1 at the excitation wavelength (λ_{ex} = 290 nm). [c]Fluorescence quantum yields are relative to the quantum yield of quinine sulfate in 0.5 M H_2SO_4 (Φ_F = 0.546). [d]Measurement performed at the excitation wavelength (λ_{ex} = 320 nm).

A few of the purine compounds (**2.6**, **2.6a**,**b**, and **2.12**) exhibit an overall enhanced luminescence as solvent polarity is increased, and for the parent series **2.6** this is dramatic (Figures 3-10 and 3-11); for example, the quantum yield of the C(8)-CN derivative **2.6b** increases from 0.34 in 1,4-dioxane to 0.88 in water.

Table 3-5. Absorption and Emission Properties for C(8)-H Purines in Acetonitrile.[a]

Purine	λ_{max}, abs/nm	log ε /M^{-1} cm^{-1}	λ_{max}, [b] em/nm	$\Delta\lambda_{max}$, em-abs/nm	Φ_F [c]
2.6	305	4.0	361	56	0.18
2.7	285	4.2	360	75	0.026
2.8	281	4.0	361	80	0.030
2.10	295	4.1	364	69	0.06
2.12	294	4.0	363	69	0.17
2.14	328	3.8	404[d]	76	0.58

[a]All measurements performed at room temperature. [b]All experiments were performed using optical densities ≤ 0.1 at the excitation wavelength (λ_{ex} = 290 nm). [c]Fluorescence quantum yields are relative to the quantum yield of quinine sulfate in 0.5 M H_2SO_4 (Φ_F = 0.546). [d]Measurement performed at the excitation wavelength (λ_{ex} = 320 nm).

Table 3-6. Absorption and Emission of C(8)-H Purines in Methanol.[a]

Purine	λ_{max}, abs/nm	log ε /M^{-1} cm^{-1}	λ_{max}, [b] em/nm	$\Delta\lambda_{max}$, em-abs/nm	Φ_F [c]
2.6	310	3.8	368	58	0.47
2.6[e]	*303*	-----	*373*	*70*	*0.91*
2.7	286	4.2	368	82	0.0006
2.8	284	4.0	370	86	0.015
2.10	295	4.2	375	80	0.018
2.12	295	4.0	368	73	0.25
2.14	330	3.8	405[d]	75	0.46

[a]All measurements performed at room temperature. [b]All experiments were performed using optical densities ≤ 0.1 at the excitation wavelength (λ_{ex} = 290 nm). [c]Fluorescence quantum yields are relative to the quantum yield of quinine sulfate in 0.5 M H_2SO_4 (Φ_F = 0.546). [d]Measurement performed at the excitation wavelength (λ_{ex} = 320 nm). [e]Measurements taken in water.

Table 3-7. Absorption and Emission of C(8)-CN Purines in 1,4-Dioxane.[a]

Purine	λ_{max}, abs/nm	log ε /M^{-1} cm^{-1}	λ_{max}, [b] em/nm	$\Delta\lambda_{max}$, em-abs/nm	Φ_F [c]
2.6b	331	4.2	381	50	0.34
2.7b	334	4.4	373	39	0.78
2.8b	313	4.3	362	49	0.73
2.10b	345	4.3	383	38	0.96
2.12b	339	4.2	382	43	0.92
2.14b	355	4.4	424	69	0.91

[a]All measurements performed at room temperature. [b]All experiments were performed using optical densities ≤ 0.1 at the excitation wavelength (λ_{ex} = 320 nm). [c]Fluorescence quantum yields are relative to the quantum yield of quinine sulfate in 0.5 M H_2SO_4 (Φ_F = 0.546).

Table 3-8. Absorption and Emission of C(8)-CN Purines in Acetonitrile.[a]

Purine	λ_{max}, abs/nm	log ε /M^{-1} cm^{-1}	λ_{max}, [b] em/nm	$\Delta\lambda_{max}$, em-abs/nm	Φ_F [c]
2.6b	330	3.2	381	51	0.31
2.7b	326	4.3	378	52	0.075
2.8b	313	4.3	366	53	0.65
2.10b	344	4.3	394	50	0.26
2.12b	338	4.3	396	58	0.55
2.14b	357	3.9	440	83	0.53

[a]All measurements performed at room temperature. [b]All experiments were performed using optical densities ≤ 0.1 at the excitation wavelength (λ_{ex} = 320 nm). [c]Fluorescence quantum yields are relative to the quantum yield of quinine sulfate in 0.5 M H_2SO_4 (Φ_F = 0.546).

There are some literature examples of amplified quantum yields and this phenomenon is believed to result from an $n \rightarrow \pi^*$ state (nonluminescent) crossing to a $\pi \rightarrow \pi^*$ state (luminescent) in a

more polar solvent medium.[92] This increase in quantum yield with increasing solvent polarity is seen with 2-AP in the literature.[82]

Table 3-9. Absorption and Emission of C(8)-CN Purines in Methanol.[a]

Purine	λ_{max}, abs/nm	log ε /M^{-1} cm^{-1}	λ_{max}, [b] em/nm	$\Delta\lambda_{max}$, em-abs/nm	Φ_F [c]
2.6b	333	3.2	398	65	0.64
2.6b[d]	*331*	*2.8*	*406*	*75*	*0.88*
2.7b	327	4.2	389	62	0.014
2.8b	318	4.1	382	64	0.14
2.10b	342	4.4	403	61	0.032
2.12b	338	4.2	410	72	0.80
2.14b	358	4.0	456	98	0.14

[a]All measurements performed at room temperature. [b]All experiments were performed using optical densities ≤ 0.1 at the excitation wavelength (λ_{ex} = 320 nm). [c]Fluorescence quantum yields are relative to the quantum yield of quinine sulfate in 0.5 M H_2SO_4 (Φ_F = 0.546).[d] Measurements taken in water.

Table 3-10. Absoption and Emission of C(8)-COOMe in 1,4-Dioxane.[a]

Purine	λ_{max}, abs/nm	log ε /M^{-1} cm^{-1}	λ_{max}, [b] em/nm	$\Delta\lambda_{max}$, em-abs/nm	Φ_F [c]
2.6c	331	4.2	386	55	0.64
2.7c	334	4.3	391	57	1
2.8c	313	4.3	376	63	0.97
2.10c	344	4.3	402	58	1
2.12c	340	4.4	399	59	1
2.14c	358	4.2	426	68	0.83

[a]All measurements performed at room temperature. [b]All experiments were performed using optical densities ≤ 0.1 at the excitation wavelength (λ_{ex} = 320 nm). [c]Fluorescence quantum yields are relative to the quantum yield of quinine sulfate in 0.5 M H_2SO_4 (Φ_F = 0.546).

Table 3-11. Absorption and Emission of C(8)-COOMe Purines in Acetonitrile.[a]

Purine	λ_{max}, abs/nm	log ε /M^{-1} cm^{-1}	λ_{max}, [b] em/nm	$\Delta\lambda_{max}$, em-abs/nm	Φ_F [c]
2.6c	330	4.3	388	58	0.55
2.7c	332	4.4	399	67	0.83
2.8c	316	4.2	382	66	0.87
2.10c	347	4.3	415	68	0.86
2.12c	342	4.1	414	72	0.75
2.14c	359	4.1	444	85	0.60

[a]All measurements performed at room temperature. [b]All experiments were performed using optical densities ≤ 0.1 at the excitation wavelength (λ_{ex} = 320 nm). [c]Fluorescence quantum yields are relative to the quantum yield of quinine sulfate in 0.5 M H_2SO_4 (Φ_F = 0.546).

Table 3-12. Absorption and Emission of C(8)-COOMe Purines in Methanol.a

Purine	λ_{max}, abs/nm	log ε /M^{-1} cm^{-1}	λ_{max}, [b] em/nm	$\Delta\lambda_{max}$, em-abs/nm	Φ_F [c]
2.6c	335	4.1	412	77	0.87
2.6c [d]	*325*	*4.1*	*420*	*95*	*0.96*
2.7c	331	4.2	420	89	0.39
2.8c	321	4.3	405	84	0.92
2.10c	347	4.2	432	85	0.66
2.12c	345	4.1	436	91	0.76
2.14c	362	4.1	466	104	0.17

[a]All measurements performed at room temperature. [b]All experiments were performed using optical densities ≤ 0.1 at the excitation wavelength (λ_{ex} = 320 nm). [c]Fluorescence quantum yields are relative to the quantum yield of quinine sulfate in 0.5 M H_2SO_4 (Φ_F = 0.546). [d]Measurements taken in water.

A Lippert-Mataga Analysis of the C(8)-H, -CN, and -COOMe Purines

The Lippert-Mataga equation (Equation 3-2) was developed to approximate the energy difference between the ground state (represented by the ground state dipole moment, μ_g)[95] and the excited state (represented by the excited state dipole moment, μ_e) of a molecule using the orientation polarizability (Δf) (Equation 3-3) of the solvent, a term derived from the solvent's refractive index (n) and dielectric constant (ε).

$$\nu_A - \nu_F = 2(\mu_e\text{-}\mu_g)^2 \Delta f/hca^3 + C \quad (3\text{-}2)$$

$$\Delta f = [(\varepsilon - 1)/(2\varepsilon + 1)] - [(n^2 - 1)/(2n^2 + 1)] \quad (3\text{-}3)$$

For the other terms in the equation that are not already defined h (= 6.626 x 10^{-34} J•s) is Plank's constant, c (= 2.998 x 10^8 m/s) is the speed of light, a represents the radius of the cavity in which the fluorophore resides (the Onsager radius), and $\nu_A - \nu_F$ is the Stokes shift (in cm^{-1}). This equation describes phenomena related to general solvent effects in which the molecular species is considered to be a dipole in a continuous medium of uniform dielectric constant and does not account for specific solvent-molecule interactions like hydrogen bonding or solute-solute interactions.[2]

A fluorophore's solvent sensitivity can be estimated by a Lippert-Mataga (Lippert) plot. Here $\nu_A - \nu_F$ is plotted against Δf for several different bulk solvents or for mixtures of solvents. A linear plot indicates the dominance of general solvent effects. The slope (k) of the line can then be used to calculate $\Delta\mu_{eg}$ (Equation 3-4).[95]

$$\Delta\mu^2_{eg} = \tfrac{1}{2}khca^3 \qquad (3\text{-}4)$$

A larger k indicates more sensitivity of the molecule to its solvent environment.

Lippert plots constructed for the purines show in general modest linearity, as given by the coefficient of determination, R^2, calculated from a least squares analysis. Graphical examples for the best fitting purines in each class are provided as Figures 3-12 through 3-14. Specific solvent effects, including hydrogen bonding[96] and preferential solvation, may contribute to nonlinearity; the response of the purines to these effects is difficult to predict.[2] The correlation coefficients do not generally improve if the methanol data is omitted, although this has been observed for other D-A fluorophores where hydrogen bonding by solvent has been implicated.[80] Worth noting also is that on average larger slopes (k) are found for the C(8)-CN and C(8)-COOMe D-A compounds, demonstrating their higher sensitivity to solvent polarity than the C(8)-H derivatives. This higher sensitivity is likely due to an enhanced charge separation for the acceptor-modified purines.[2]

Table 3-13. Lippert-Mataga Data for Selected Purines.

Purine	slope (k) cm^{-1}	R^2	$\Delta\mu_{eg}$, D	μ_g, D (theory)	μ_e, D	μ_e, D (theory)
2.6	1978	0.99	4.10	3.85	7.95	5.02
2.12b	5190	0.75	8.12	5.66	13.78	11.04
2.12c	4417	0.69	7.49	3.16	10.65	9.77

Estimating $\Delta\mu_{eg}$ from the Lippert plots is error prone in the cases of modest correlation values, nonetheless this has been done for the examples shown. Using Equation 3-4 and an estimated value for the Onsager radius for each purine (taken as 3.5 Å for **2.6** and 4.0 Å for both

2.12b and **2.12c**; the latter two are similar in structure to PRODAN that has an accepted radius of 4.2 Å),[97] $\Delta\mu_{eg}$ could be calculated. From this value and the theoretically-determined μ_g (vide infra) a value emerges for the excited state dipole, μ_e. The magnitude of μ_e correlates very well with values from computation.

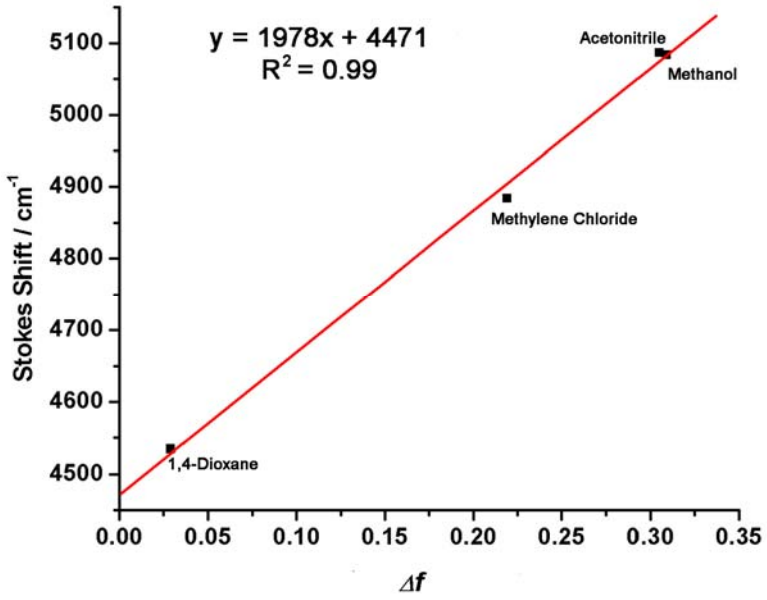

Figure 3-12. Lippert-Mataga plot for **2.6**.

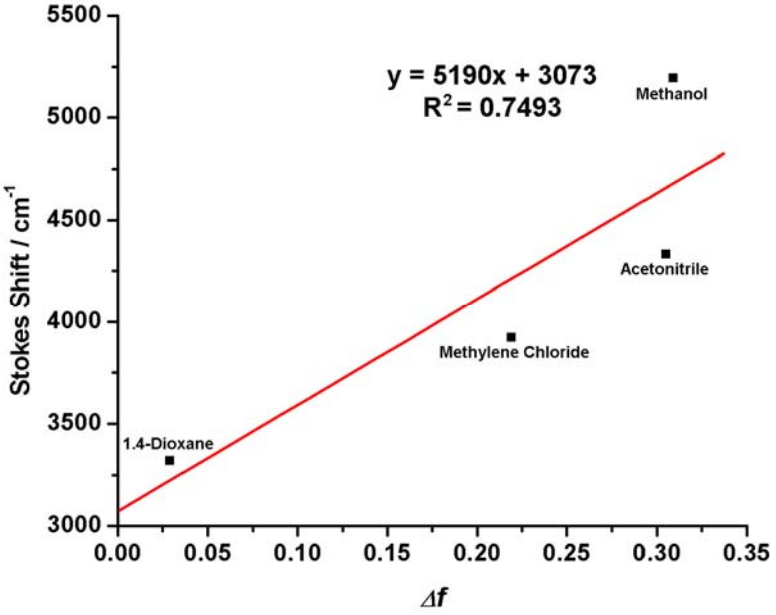

Figure 3-13. Lippert-Mataga plot for **2.12b**.

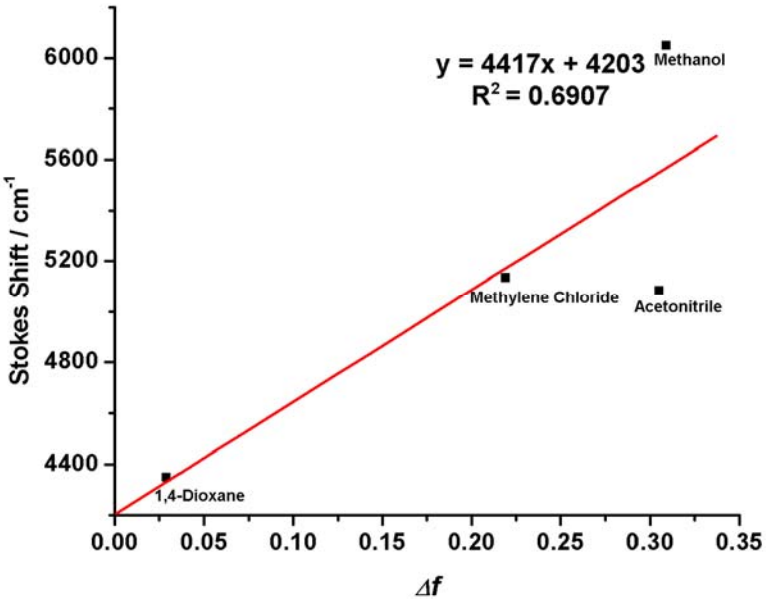

Figure 3-14. Lippert-Mataga plot for **2.12c**.

The Chemical and Photochemical Stability of C(8)-H, C(8)-CN, and -COOMe Purines

The C(8)-H, -CN, and -COOMe purines showed no decomposition by TLC analysis, ^{1}H and ^{13}C NMR, and HRMS after months of being stored neat in vials with exposure to air and ambient light. After days in solutions of 1,4-dioxane, methylene chloride, acetonitrile, and methanol with exposure to air and ambient light the purines showed no significant loss of absorption (< 1%). Evaluation of an emitting compound's absorption loss is a method sometimes used to evaluate the molecule's photostability.[98] When the D-A purines were placed in solution and exposed to 254 nm light from a hand-held UV lamp for varying time intervals, changes were observed in the absorption spectra. As shown for **2.14b** and **2.14c** (Figures 3-15 and 3-16), complete deterioration of the $^{1}(\pi\pi^{*}\ L_a)$ absorption band occurs after ~ four hours in methylene chloride and a new blue-shifted absorption band (λ_{max} = 309 nm) emerges. The $^{1}(\pi\pi^{*}\ L_b)$ absorption band is shifted to the red during the experiments. The structure of the new species that forms, possibly from direct reaction with oxygen, has not been determined.

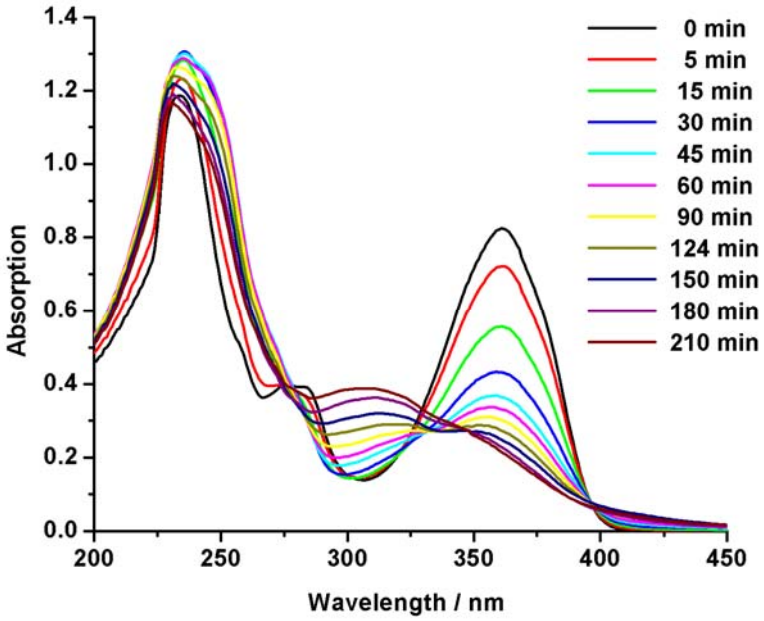

Figure 3-15. Changes observed in the absorption spectrum of a 60 μM solution of **2.14b** in methylene chloride after exposure to 254 nm ultraviolet light at varying time intervals.

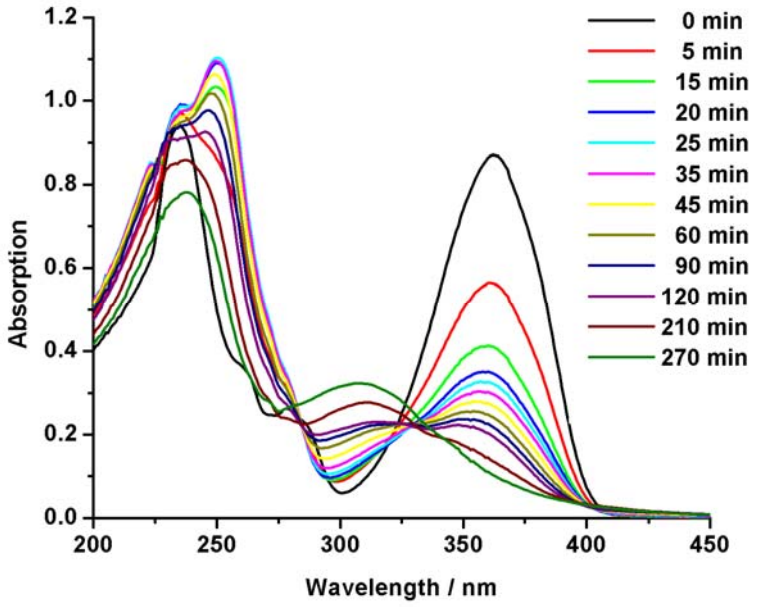

Figure 3-16. Changes observed in the absorption spectrum of a 60 μM solution of **2.14c** in methylene chloride after exposure to 254 nm ultraviolet light at varying time intervals.

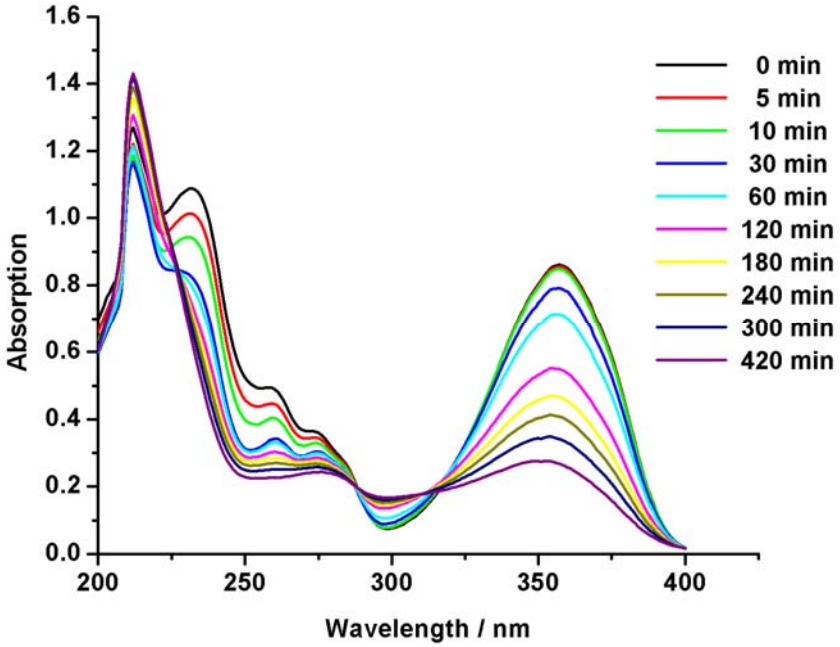

Figure 3-17. Changes observed in the absorption spectrum of a 60 μM solution of **2.14c** in 1,4-dioxane after exposure to 254 nm ultraviolet light at varying time intervals.

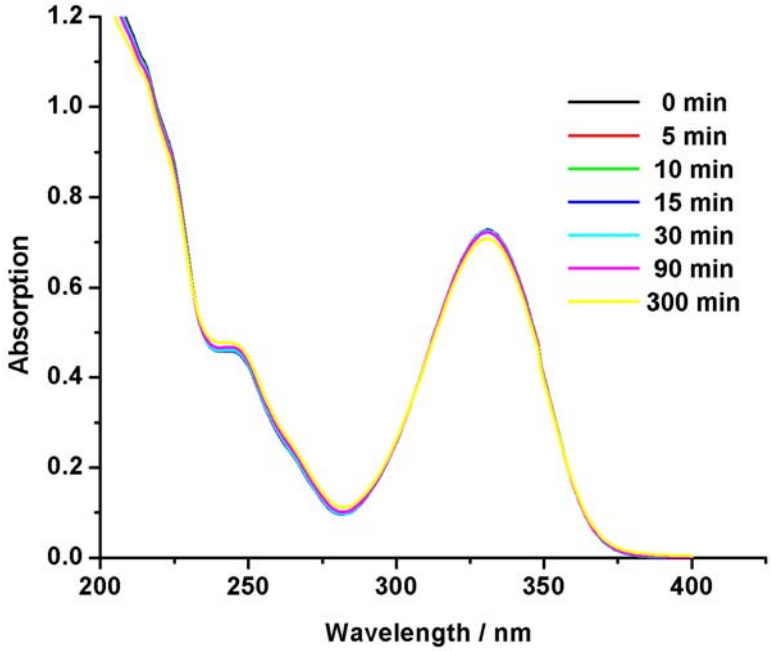

Figure 3-18. Changes observed in the absorption spectrum of a 60 μM solution of **2.6c** in water after exposure to 254 nm ultraviolet light at varying time intervals.

The rate of decomposition is somewhat slowed in 1,4-dioxane as shown for **2.14c** (Figure 3-17); in this case no significant new absorption bands are observed. Finally, the decomposition rate appears most suppressed in water as shown for **2.6c** (Figure 3-18) that loses very little of its absorption intensity after 300 min of exposure. This last result bodes well for the use of the modified purines in aqueous-based sensing applications.

Electronic Properties of the D-A Purines

Theoretical Calculations

Electronic structure calculations have become essential to chromophore design and study, particularly for establishing their potential use in optoelectronic applications. Both semiempirical and high-level DFT calculations have been used to shed additional light on the electronic nature of the D-A purines and their absorption properties. The ground state geometries, dipoles, and orbital energies have been obtained for 9-methyl-2-aminopurine (**2.6-Me**), **2.6**–**2.14b**, and **2.6**–**2.14c** from DFT calculations at the B3LYP/6-31++G** level (as implemented in Gaussian 03).[99] Other levels of theory not supplemented by diffuse functions provided similar, but somewhat less accurate values (B3LYP/6-31G**, B3LYP/6-311G**, and B3LYP/aug-cc-pVDZ). For the D-A purines, the benzyl groups have been abbreviated to methyl (Me) substituents to save computational time, and frequency calculations have been performed in all cases to assign the optimized geometries as energy minima or transition states (all except **2.12b**-Me are minima, vide infra). To demonstrate the accuracy of the calculations, Table 3-14 compares the bond lengths for 2-AP and **2-7b** (crystal structure data from Table 2-1) with their calculated 9-methyl analogues. The values are the same within ~ 0.02 Å. In most cases, the optimized geometries do show slight pyramidalization of the C(2) and C(6) amino (or dimethylamino) nitrogens. These deviations have been analyzed in terms of the wagging angle, ω, in the Experimental section.

Table 3-14. Selected Bond Lengths for **2.7b** and 2-AP from the crystal, and their 9-methyl derivatives from computation.

Bond	**2.7b**	**2.7b-Me**	**2-AP**	**2.6-Me**
N1-C6	1.3411(15)	1.346	1.332(3)	1.335
N1-C2	1.3536(15)	1.350	1.365(2)	1.358
C2-N3	1.3484(15)	1.344	1.343(2)	1.347
C2-N11	1.3563(15)	1.369	1.353(3)	1.371
N3-C4	1.3446(14)	1.335	1.329(3)	1.331
C4-N9	1.3749(14)	1.372	1.368(3)	1.374
C4-C5	1.3952(16)	1.410	1.400(2)	1.412
C5-C6	1.4301(16)	1.435	1.381(3)	1.395
C5-N7	1.3810(14)	1.374	———	———
C6-N10	1.3450(15)	1.358	———	———
N7-C8	1.3129(16)	1.321	1.318(2)	1.308
C8-N9	1.3834(14)	1.390	1.360(3)	1.390
C8-C12	1.4308(15)	1.421	———	———

Summarized in table 3-15 are the dipole and orbital energy data obtained for the D-A purines from the DFT calculations. Complementary orbital density plots of the HOMO and LUMO levels could be generated using Molden v. 4.6[100] to show graphically the electronic nature of the ground state (Figure 3-19). The orbital features are quite similar within and between the nitriles and methyl esters. The HOMO consists of delocalized p orbitals on the purine plane, with the greatest density in the N(9)-C(4)-C(5)-C(6) region consistent with what has been observed for parent 2-AP.[101] Localized p_z orbitals are seen on the exocyclic donor heteroatoms and the acceptor functionality, and there is more substantial charge separation in the HOMO for the nitriles (consistent also with their greater ground state dipole moments; average for nitriles = 5.73 D, esters = 3.96 D, **2.6-Me** = 3.85 D). The LUMO is also of π character but now largely concentrated on the acceptor substituent, the cyano group or methyl ester. Generally the density on the C(2) donor group diminishes most substantially in the LUMO; the C(6) donor orbital coefficient is only slightly affected. The energies of the HOMO and LUMO levels scale with the substituents and substitution patterns in reasonable ways. For example, **2.6b**, bearing one donor group, has the lowest HOMO and LUMO energies. Purine **2.10b**, with two

dimethylamino substituents, has the highest. In general the HOMO/LUMO values for the esters are ~ 0.3 eV higher than the nitriles; the calculated HOMO-LUMO gaps are slightly lower (~ 0.1 eV) for the esters. The results confirm that the cyano groups are stronger electron acceptors, although the optical properties also clearly depend on the geometry/structure of the electron accepting group.

Table 3-15. Electronic Structure Data for D-A Purines.[a]

Purine[b]	μ_g	HOMO calcd, *CV*[c] (eV)	LUMO calcd, *CV*[c] (eV)	ΔE calcd, *CV*[c] (eV)	ΔE optical[d] (eV)	λ_{max} L_a calcd (nm, [eV]), *f*[e]	λ_{max} L_a CH_2Cl_2 (nm)
2.6b-Me	5.45	–6.52	–2.27	4.25	3.5	328, 0.57	326
2.7b-Me	5.00	–5.88, *–5.48*	–1.68, *–2.28*	4.20, *3.20*	3.4	340, 0.60	334
2.8b-Me	6.60	–6.29	–1.87	4.42	3.6	327, 0.59	311
2.10b-Me	5.52	–5.64 *–5.34*	–1.60 *–2.11*	4.04 *3.23*	3.3	344, 0.62	348
2.12b-Me[f]	5.66	–5.75 *–5.59*	–1.68 *–2.56*	4.07 *3.03*	3.4	339, 0.61	336
2.14b-Me	6.13	–6.08	–2.14	3.94	3.1	333, 0.59	361
2.6c-Me	5.19	–6.24	–2.04	4.20	3.4	331, 0.58	328
2.7c-Me	2.43	–5.62	–1.55	4.07	3.3	349, 0.58	322
2.8c-Me	4.74	–6.03	–1.69	4.34	3.5	333, 0.59	315
2.10c-Me	2.81	–5.40	–1.48	3.92	3.2	354, 0.61	348
2.12c-Me	3.16	–5.53	–1.56	3.97	3.2	348, 0.61	338
2.14c-Me	5.42	–5.82	–1.94	3.88	3.1	338, 0.61	362

[a] See the Experimental section for computational details. [b] All benzyl groups have been replaced by methyl groups for the calculations. [c] Cyclic voltammetry data; for details, see the Experimental section. [d] Calculated as the end-absorption of the lowest energy transition in the UV-vis spectrum. [e] All correspond to one-electron HOMO (S_0) → LUMO (S_1) transitions. [f] One imaginary frequency was identified for this structure indicating a transition state. The frequency is associated with minor inversion of the C(2) amino group based on analysis of the coordinate files.

ZINDO/S CI semi-empirical calculations[102] using the optimized DFT ground state geometries reveal that the lowest energy transition is associated with promotion of an electron from the HOMO to the LUMO in all cases. Given the large calculated oscillator strength (*f*) for this transition, it is an allowed process for which the trend in energy gap (327–354 nm; 3.79–3.50 eV) correlates well with the trend in λ_{max} in CH_2Cl_2 (311–362 nm; 3.99–3.43 eV). Based on

the plots in Figure 3-19, the transition mainly involves transfer of charge from the amino group on C(2) (and the pyrimidine ring) to the C(8) acceptor group.

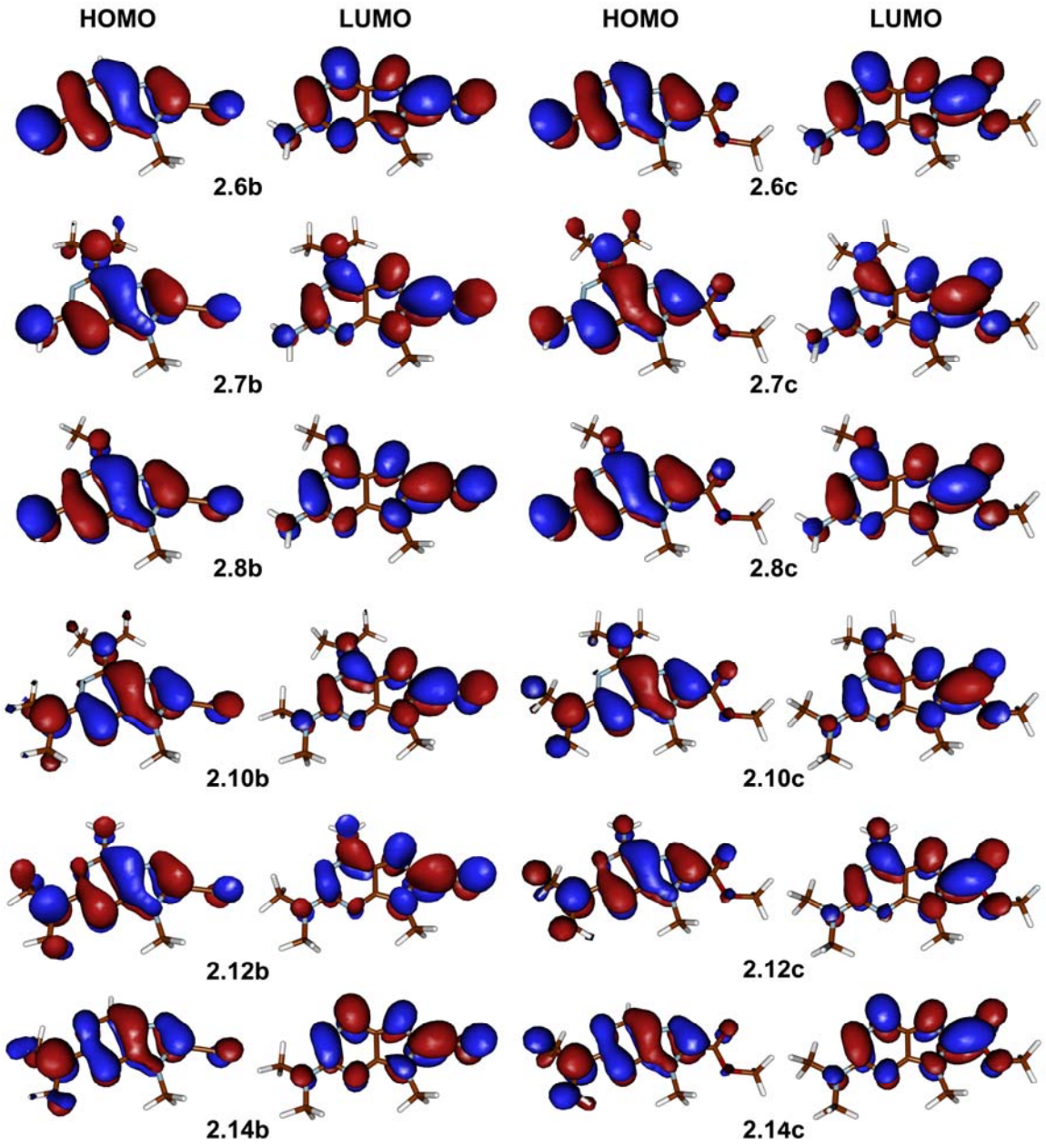

Figure 3-19. Orbital density plots (Molden v. 4.6) for D-A purines calculated from the B3LYP/6-31++G** optimized geometries.

Cyclic Voltammetry Studies

The difference between the first oxidation potential and the first reduction potential, determined by cyclic voltammetry, can be regarded as a measure for the HOMO-LUMO gap.

Electrochemical studies have been performed, in collaboration with Aubrey Dyer (in the group of Prof. John Reynolds), for purines **2.7b**, **2.10b**, and **2.12b**. Measurements (at least three independent reductive and oxidative scans) were performed using 10 mM solutions of the purines in CH_2Cl_2 with 0.2 M *n*-Bu_4NClO_4 as the supporting electrolyte; redox potentials were determined versus the ferricinium/ferrocene couple. The average HOMO and LUMO values, determined from the oxidation and reduction onsets (Table 3-15), respectively, are shown in Table 3-15. The most electron rich purine, **2.10b**, shows the highest HOMO and LUMO values. The HOMO values in general agree within 0.4 eV with the computational results and the calculated HOMO-LUMO gaps agree within 0.2 eV of the optical band gaps determined from the solution absorption spectra. Given the latter, the DFT calculations appear to largely overestimate the LUMO energies (> 0.5 eV). Nonetheless, the experiments show that the theoretically-determined HOMO energies and the optical band gap are sufficient to determine the LUMO energies for the D-A purines within ~ 0.2 eV.

Device Measurements for D-A Purine 2.7b

D-A molecules are often targets for organic light emitting diode (OLED) research due to their ability to fluoresce efficiently, transport charge, and to undergo charge transfer to an electrode.[78] Since the donor-acceptor compounds presented in this work fluoresce efficiently in solvent, their capability of performing in a device was explored with D-A purine **2.7b** in collaboration with Aubrey Dyer (in the group of Prof. John Reynolds) (Figure 3-20A). The result of this study revealed **2.7b** to be a blue emitter (Figure 3-20B). One device was fabricated by spin-coating a dispersion of PEDOT:PSS (the oxidized form of poly(ethylenedioxythiophene) and poly(styrene sulfonate)) in water onto ITO (indium-doped tin oxide) deposited on glass. This PEDOT:PSS layer (~ 15 nm) acts to smooth out the ITO layer and aids in hole injection.

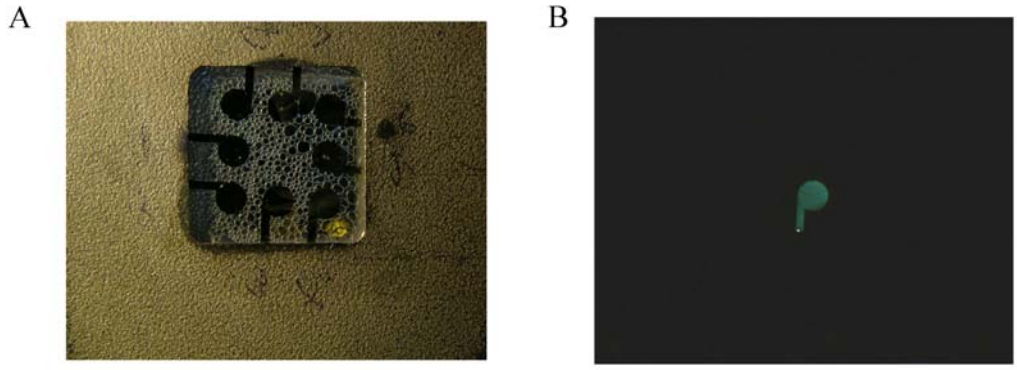

Figure 3-20. Organic light emitting diode (OLED) for **2.7b**. A) The device used to test the electroluminescence. B) Electroluminescence of **2.7b** seen in the device.

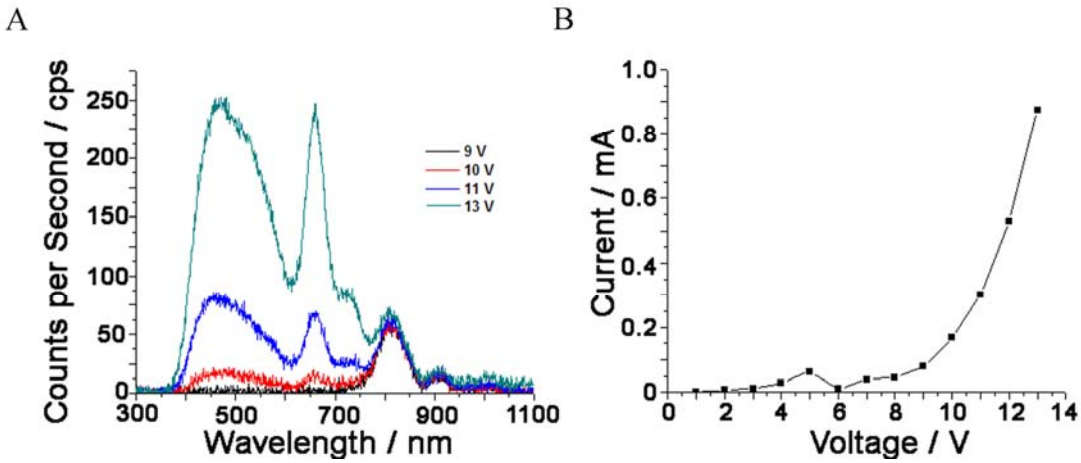

Figure 3-21. Measurements taken with the OLED device. A) Electroluminescence spectra of **2.7b**. B) Graph showing the turn-on voltage of the OLED device.

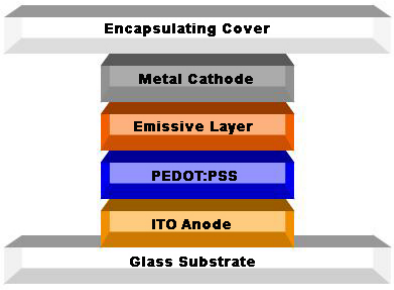

Figure 3-22. Schematic model of the OLED device using **2.7b** as the emissive layer.

The emissive layer, **2.7b**, was then spin-cast from a solution of chloroform onto the PEDOT:PSS layer. A thin layer of calcium (~ 10 nm) deposited on top of the emissive layer acts as the

cathode and finally aluminum was deposited (~ 150 nm) onto the calcium to encapsulate the device from oxygen and water.

The electroluminescence spectrum shows two peaks of interest, λ_{max} ~ 450 nm and λ_{max} ~ 650 nm (Figure 3-21A). The higher energy peak is red-shifted approximately 60 nm when compared to the most bathochromic shift (Table 3-9) found in solution for this compound. Bathochromic shifts are generally observed when comparing photophysical measurements from solution to measurements in the solid state where π-stacking interactions are more substantial.[103] The turn-on voltage for **2.7b** appears to be approximately 9 V (Figure 3-21B). This turn-on voltage appears to be slightly higher than turn-on voltages for optimized systems reported in the literature which are generally below 5 V.[104,105] Though these results are promising, the electroluminescence for this device is very weak. One reason for the poor efficiency may be that some crystallization of the compound has taken place upon substrate deposition. It is believed that vapor depositing the purine onto the substrate could give more intense electroluminescence by forming a thinner emissive layer that is less likely to crystallize. It is also possible that use of a carrier polymer (PMMA or PS) with the purines could produce better films. Further experiments in this area are currently underway.

Experimental Section

UV-Visible Data. Absorption spectra were measured for 5, 10, 20, 40, and 60 μM solutions of the purines on a Cary 100 Bio UV-Visible spectrophotometer (thermostatted at 25 °C) using dried and degassed methylene chloride (CH_2Cl_2). The absorption intensity at λ_{max} was then plotted against the concentration to confirm, by linearity, that the compounds followed Beer's law. Once confirmed, molar extinction coefficients (ε) were determined from the linear plot for each compound (where $A = \varepsilon bc$).

Fluorescence Lifetime Measurements. Fluorescence lifetime measurements were performed on a Photon Technology International, Inc. Time Master Fluorescence Lifetime system. Excitation was performed via a nitrogen laser at 337 nm (pulse width approximately 800 ps), and a quartz fiber optic was used to convey light to the sample chamber. Samples for fluorescence lifetime measurements of the C(8)-CN and C(8)-COOMe compounds were prepared by making ~ 5 μM solutions of each compound in dried and degassed methylene chloride. Each compound was excited at 337 nm and the monochromator was set to the corresponding $\lambda_{em(max)}$ for each compound. After the measurement of each compound, a scattering agent (Ludox® AM-30 colloidal silica, 30% wt. % suspension in water) was measured under the same parameters as the compound in order to find the instrument response time. The instrument response time along with the data collected for each sample was placed into the Time Master software to generate the fluorescence lifetime data.

Fluorescence Quantum Yield Measurements. Fluorescence quantum yield measurements were performed by collecting correlating absorption and steady-state emission spectra on a Perkin-Elmer Lambda 25 dual beam absorption spectrometer and a SPEX Fluoromax spectrophotometer, respectively. The unknowns and standards were prepared with dried and degassed solvent at or below a 10 μM concentration and absorbance below an intensity of 0.1.

$$\Phi_{F(x)} = (A_s/A_x)(F_x/F_s)(\eta_x/\eta_s)^2\Phi_{F(s)}$$

Φ_F is the fluorescence quantum yield, A is the absorbance at the excitation wavelength, F is the area under the emission curve, and η is the refractive index of the solvent used. Subscripts s and x refer to the standard and unknown, respectively. Quantum yields were calculated using quinine sulfate in 0.5 M H_2SO_4 ($\Phi_F = 0.546$) as the standard.[3]

Computation. Starting geometries were obtained from semi-empirical calculations using the AM1 method as implemented in HyperChem v. 7.5 for Windows (HyperCube, Inc., Gainesville, FL). The ground state geometries, dipoles, and orbital energies were then obtained from DFT calculations at the B3LYP/6-31++G** level as implemented in Gaussian 03.[99] The DFT calculations were performed on the SGI Altix system "Cobalt" through available computational time (Prof. A. Roitberg, UF) at the National Center for Supercomputing Applications (NCSA) at the University of Illinois, Urbana-Champaign. Frequency calculations were performed at the same computational level. The resultant geometries were used for ZINDO/S CI calculations[102] using HyperChem v.7.5 where the highest 20 occupied and the lowest 20 unoccupied orbitals were considered for determination of the electronic transition energies, polarizations, and oscillator strengths. The currently accepted values for the overlap weighting factors of 1.267 (s-s) and 0.585 (p-p) were used.

In many cases the amino groups of the optimized purine structures show slight pyramidalization. These deviations can be parameterized in terms of the wagging angle, ω, defined as the angle C(2 or 6)–N–centroid between R substituents (H or CH_3) (Table 3-16). An alternative way of expressing the same distortion is through the N(1)-C(2)-N(11)-R and N(3)-C(2)-N(11)-R torsion angles (that deviate from 0°). For 2-AP-Me, these values are –15.8° and 16.4°, respectively (compared with –22.8° and 23.1° from MP2/6-31G** calculations on 2-AP in the literature).[106] In general, such slight pyramidalization represents a small stability gain for the molecule in the gas phase (< 1 kcal mol^{-1}).[106]

Cyclic Voltammetry. Electrochemical measurements were performed using an EG&G PAR model 273A potentiostat/galvanostat in a three-electrode cell configuration consisting of a silver wire pseudo reference electrode calibrated with a ferrocene/ferricinium couple, platinum

button as the working electrode, and a platinum flag as the counter electrode (scan rate = 75 mV s^{-1}). For the studies, 10 mM solutions of the purines in CH_2Cl_2 containing 0.2 M *n*-Bu_4NClO_4 were prepared. All measurements were performed in a glove box and repeated in at least triplicate.

Table 3-16. Amino and Dimethylamino Group Wagging Angles (ω, in degrees) Calculated from the Optimized Geometries of the D-A Purines.

Purine	C(2)-NH_2	C(2)-$N(CH_3)_2$	C(6)-NH_2	C(6)-$N(CH_3)_2$
2.6-Me	27.4	———	———	———
2.6b-Me	16.8	———	———	———
2.7b-Me	26.2 (5.3)[a]	———	———	10.5 (17.0)[a]
2.8b-Me	21.9	———	———	———
2.10b-Me	———	15.6	———	11.2
2.12b-Me[b]	———	0.4 (2.3)[a]	0.4 (8.3)[a]	———
2.14b-Me	———	12.6	———	———
2.6c-Me	21.7	———	———	———
2.7c-Me	28.7	———	———	9.8
2.8c-Me	25.1	———	———	———
2.10c-Me	———	16.6	———	11.2
2.12c-Me	———	16.0 (5.2)[a]	2.1 (4.4)[a]	———
2.14c-Me	———	14.0	———	———

[a] Value from X-ray analysis (N(9)-benzyl). [b] One imaginary frequency was identified for this structure indicating a transition state. The frequency is associated with minor inversion of the C(2) amino group based on analysis of the coordinate files.

CHAPTER 4
USING THE DONOR-ACCEPTOR PURINE UNIT AS A FUNCTIONAL SYNTHETIC BUILDING BLOCK

Introduction

The purine core is an excellent heterocyclic building block for the construction of functional materials capable of molecular recognition, sensing, and displaying supramolecular behavior. The nitrogen-rich lining of the core gives ample opportunity for hydrogen bonding or metal binding, and the polarizable π-surface allows for efficient π-stacking interactions. This Chapter identifies general ways, through synthetic chemistry, that the donor-acceptor (D-A) purines can be further functionalized for incorporation into noncovalent supramolecular systems, or covalent oligomeric and/or polymeric architectures. Looking at the structures of the purines, there are several atomic starting points: C(2), C(6), C(8), N(7), and N(9). The most attractive way to "build" off of C(8) while potentially preserving the core's photophysical properties is to employ the acid precursor functionality (–CN or $–CO_2Me$); discussed here are ways to make the first amide bonds from this position. A second strategy worth exploring is to use the $–NH_2$ group on C(2) or C(6) as a nucleophile; early progress in this direction is presented and some of its advantages and disadvantages discussed. Finally, presented in the Future Work section are ways that N(7) and N(9) could potentially be promising functionalization points, particularly toward the incorporation of D-A purines into DNA, RNA, or PNA backbones.

A Complementary Thrust: ε-Purinyl Amino Acids

Numerous nitrogen rich heterocycles have been employed in synthetic oligopeptides.[107-109] The incorporation of heterocycles directly within the peptide's mainchain is a powerful design to realize information-rich molecules capable of specifically recognizing biological targets.[110] It did not escape us that the C(8)-CN and -COOMe functionality of the D-A purines, together with

C(2) amino functionality, affords novel ε-purinyl amino acids that can serve as scaffolds from which unique chemical architectures can be built.

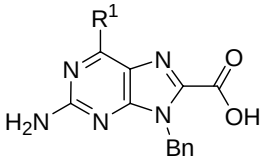

R^1 = H, NH_2, $N(Me)_2$, OBn

Figure 4-1. Novel ε-purinyl amino acids.

Homo- and heteropurinyl oligopeptides could be formed through direct covalent linkage of the ε-purinyl amino acids; the homopurinyl oligopeptide made from stringing identical molecules of ε-purinyl amino acids together in a head-to-tail fashion is shown in Figure 4-2. Simple molecular mechanics calculations with deprotected oligomers further illustrate the concept and some of its attractive features (Figures 4-3 and 4-4). The energy-minimized structure (MacroModel, Amber* force field) shows a near planar dipurinyl peptide arrangement defined by torsion angles labeled θ_1 and θ_2 (θ_1, θ_2 = 0° or 180°) (Figure 4-3). Reduced torsional degrees of freedom, enforced by favorable electrostatic interactions between –NH and C=O groups, maintain a curvature along the polar edge of the molecule as the length of the oligopeptide is extended. This curvature is expected to result in oligopeptides suitable for binding grooved biomolecular surfaces or forming predictable three-dimensional structures.

Computation shows that a three unit purinyl homopeptide fits into the minor groove of DNA and that an 18 unit purinyl homopeptide could form a covalent macrocycle with a 4.5 nm diameter that is lined with multiple binding sites. Given the interesting photophysical properties of the D-A monomers, it is expected that these architectures would present advantages in detection through increased conjugation length and/or have unique optical properties.

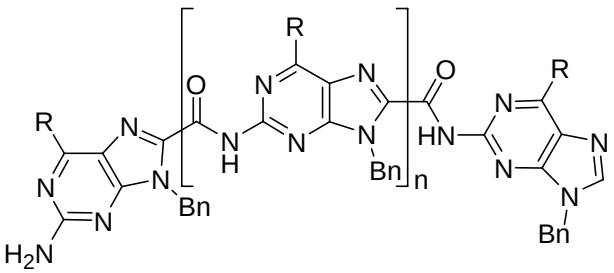

Figure 4-2. Homopurinyl oligopeptide from ε-purinyl amino acids.

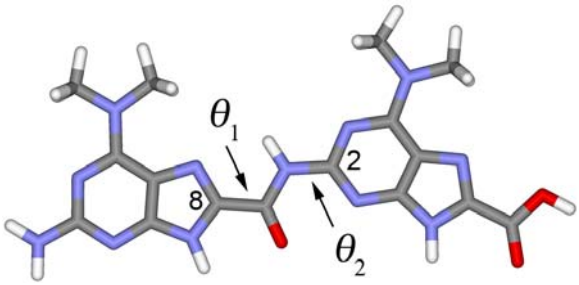

Figure 4-3. Computationally derived torsion angle preferences for a dipurinyl peptide constructed from deprotected monomer **2-7c**.

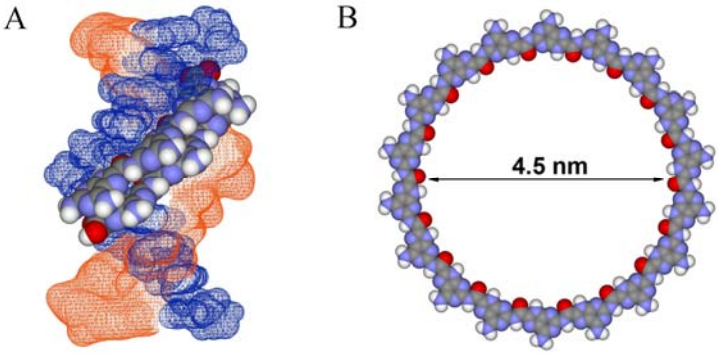

Figure 4-4. Oligopeptide curvature with potential molecular recognition and supramolecular capabilities. A) 2:1 Minor groove binding of DNA by a three unit homopurinyl peptide. B) 18 unit homopurinyl peptide forming a covalent macrocycle.

Hetero-oligopeptide structures are also conceivable and one design might incorporate both ε-purinyl amino acids and conventional α-amino acids into a peptidic main chain. The different noncovalent interactions unique to the amino acid components are expected to work cooperatively to form three-dimensional structures capable of folding and unfolding in response to environmental stimuli—a new class of foldamers could be born.[111] There is much work being

done to form synthetic, self-folding oligomers capable of biomolecule-like function.[111] An example of one hetero-oligopeptide that might serve in this capacity is shown in Figure 4-5, where ε-purine amino acids are linked by an α-amino acid tripeptide with the sequence Gly-^{D}Pro-Gly.

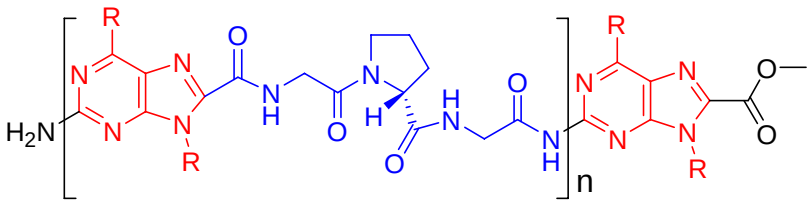

Figure 4-5. Design for a hetero-oligopeptide containing ε-purinyl amino acids linked with conventional α-amino acids.

The computationally-determined three-dimensional folded structure of such an oligomer is shown in Figure 4-6 as it comes from a Monte Carlo molecular dynamics simulation (MacroModel, Amber* force field, GB/SA water solvation treatment). The result shows a helical secondary structure as a result of the π-stacking preferences of the purines and the γ-turns enforced by hydrogen bonding within the Gly-^{D}Pro-Gly sequences. Substitution on N(9) and C(6) of the purine core could introduce other functionality and control solubility/aggregation. Finally, and importantly, the N-terminal ε-purinyl amino acid in such oligopeptide architectures could serve as a fluorescent reporter of secondary structure and conformation.

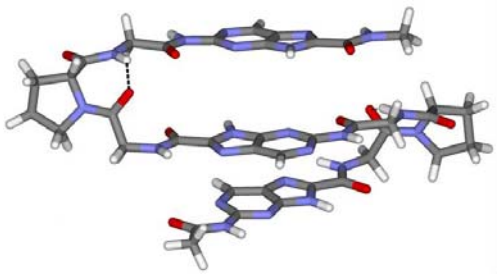

Figure 4-6. Folded structure predicted (by computation) for ε-purinyl amino acids linked with Gly-^{D}Pro-Gly.

Amide Functionality at the C(8) Position

Using the C(8)-CN and -CO_2Me derivatives as amide precursors appeared as a promising synthetic strategy to both elaborate the core and work toward ε-purinyl amino acid structures. Conversion of the methyl esters to carboxylic acid intermediates (C(8)-CO_2H) was attempted first, in hopes that the acid could be used conventionally in amide bond forming reactions (by direct coupling reactions or initial conversion of the acid to an activated ester or acid chloride). Carboxylic acid functionality on the C(8) position of the purine is reported only once in the literature, however, and is reported to be very unstable.[63]

For the initial studies, to eliminate the possibility of side reactions at C(2) or C(6), compound **2.10c** containing a dimethylamino group at both positions was used as the starting methyl ester. The C(8) carboxylate **4.1** was formed initially from **2.10c** by heating it to 100 °C in a sealed tube with 10% aqueous sodium hydroxide and methanol (Figure 4-7). It was then discovered that a synthetic step in the sequence could be saved by reacting the C(8) cyano derivative **2-10b** under the same conditions to form **4.1** directly. When **4.1** was isolated as its sodium salt it proved stable and could be left on the benchtop under air and ambient light indefinitely (consistent with the literature observation for a related compound).[63] Once acidified, **4.1** rapidly decarboxylated to yield the C(8)-H compound **2.10** (monitored by TLC and ^{1}H NMR). The reactivity of the carboxylic acid of **4.1** required that it be used immediately after work-up and that it be kept cold thoughout this process. With care, the free acid of **4.1** was then heated with thionyl chloride to form the C(8) acid chloride **4.2**. Compound **4.2** was quickly placed in THF with Et_3N and butylamine (a reactive primary amine that would produce a soluble amide product); a complex mixture of products was obtained from the reaction that included a

23% yield of the desired amide **4.3** (Figure 4-7). This shows that even with the lability of the acid, some was converted to the acid chloride and further to the desired product **4.3**.

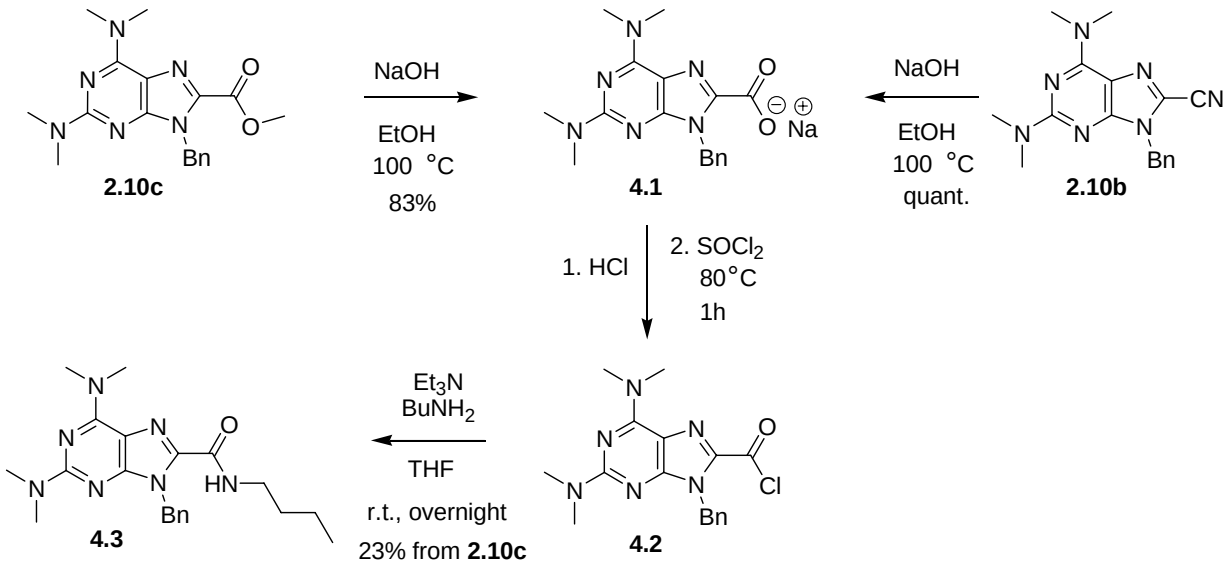

Figure 4-7. C(8) amide formation via an acid chloride.

Successful, albeit low-yielding formation of the C(8) amide **4.3** inspired attempt at the formation of a purinyl dimer by using the acid chloride **4.2** and a purine bearing a C(2) primary amine. This reaction resulted in a complex mixture of inseparable products (Figure 4-8). The low yield of **4.3** and the complex product mixture of the reaction in figure 4-8 are most likely a result of slow reaction of the relatively weakly nucleophilic C(2) amino group coupled with apparently rapid decarboxylation of the **4.1** carboxylic acid (or decomposition of **4.2**) under the reaction conditions.

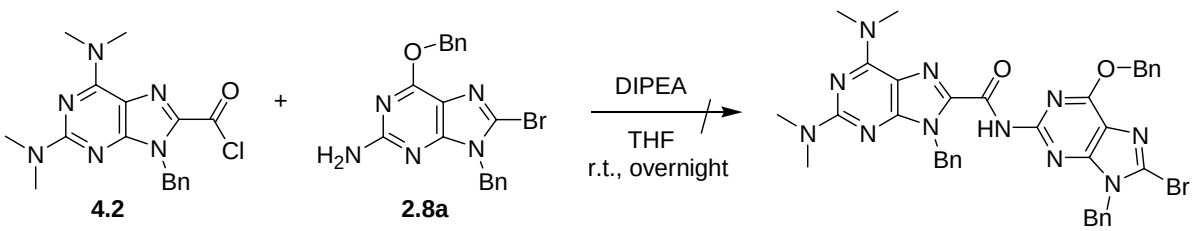

Figure 4-8. Unsuccessful coupling reaction to synthesize a purine dimer via the acid chloride.

The use of conventional peptide coupling conditions directly from the acid **4.1** (e.g., DCC/DMAP) were next attempted; this approach eliminates the activation step and was found to improve the product yield dramatically. By this strategy, C(8) amide derivatives **4.3** and **4.5**–**4.7** were formed (Figure 4-9). Compound **4.3** was formed to compare product yields between amide formation via the acid chloride and DCC/DMAP coupling. This showed that product yields almost doubled (23 → 42%) by using DCC/DMAP coupling. Products **4.5** and **4.6** were formed using the methyl ester protected amino acids of glycine and 5-aminovaleric acid. The methylesters of these compounds can potentially be deprotected and further coupled to form oligomeric species. The formation of **4.7** shows that C(8) coupling with aliphatic amines can be performed in the presence a free primary amine on the C(2) position (**4.4** to **4.7**) since the latter is considerably less nucleophilic.

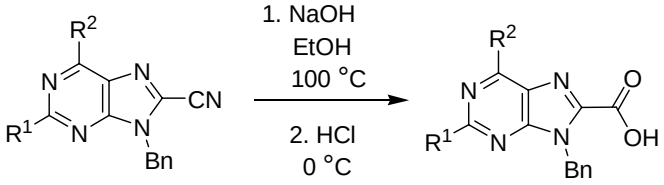

2.10b $R^1 = N(Me)_2$, $R^2 = N(Me)_2$
2.12b $R^1 = N(Me)_2$, $R^2 = NH_2$

4.1 $R^1 = N(Me)_2$, $R^2 = N(Me)_2$
4.4 $R^1 = N(Me)_2$, $R^2 = NH_2$

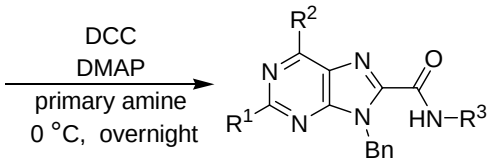

4.3	$R^1 = N(Me)_2$, $R^2 = N(Me)_2$, $R^3 = (CH_2)_3CH_3$	42% from **2.10b**
4.5	$R^1 = N(Me)_2$, $R^2 = N(Me)_2$, $R^3 = CH_2CO_2CH_3$	82% from **2.10b**
4.6	$R^1 = N(Me)_2$, $R^2 = N(Me)_2$, $R^3 = (CH_2)_4CO_2CH_3$	45% from **2.10b**
4.7	$R^1 = N(Me)_2$, $R^2 = NH_2$, $R^3 = CH_2CO_2CH_3$	51% from **2.12b**

Figure 4-9. C(8) amide formation using the DCC/DMAP conditions.

Extension of the DCC/DMAP conditions to purinyl dimer formation resulted in none of the desired product, however, and instead a large percentage of C(8)-H derivative **2.10** was

recovered from the reaction (Figure 4-10). This suggests that the acid or in situ generated activated ester of **4.1** decomposes prior to nucleophilic attack by the N(2) primary amine of **2.8a**. Of note, very few C(8)-amido purines have been reported in the literature.[112,113] The C(8)-amido purines reported in this thesis appear to be the first formed through conventional amide chemistry using acid precursors.

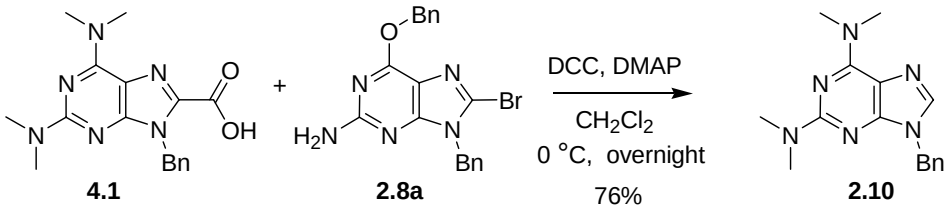

Figure 4-10. Coupling reaction to form a purinyl dimer using DCC/DMAP.

Crystal Structure of the C(8)-Amide Purine 4.7

Molecular Level Structure

Single crystals suitable for X-ray diffraction, perfomed by Dr. Khalil Abboud, could be grown by slow evaporation of a methanol/methylene chloride solution of **4.7** over one week. The X-ray structure of **4.7** (Figure 4-10a) reveals the dimethylamino substituent, defined by atoms N(11), C(12), and C(13), to be planar at N(11) and with the purine core. The sum of the N(11) bond angles is 359.91°, consistent with sp^2 hybridization at nitrogen. Nearly identical geometries were observed in the crystal structures of **2.7b**, **2.12b**, and **2.10c**.

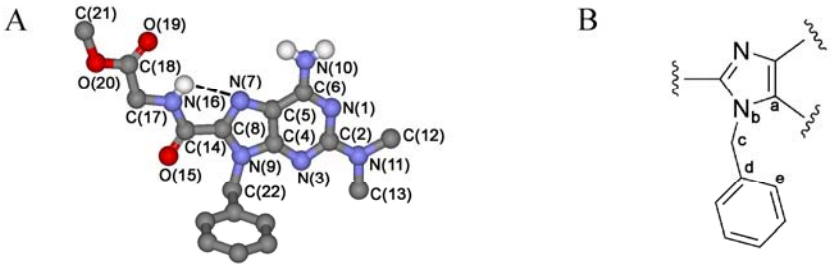

Figure 4-11. Single molecule from the crystal structure of **4.7**.

The N(9) benzyl substituent geometry can again be defined by torsion angles α (defined by a-b-c-d) = 88.79° and β (defined by b-c-d-e) = 76.96° for **4-7** (Figure 4-10b). The values show that as in **2.7b**, **2.12b**, and **2.12c** the benzyl group extends nearly perpendicular to the plane of the purine core (α), while angle β remains sensitive to the intermolecular interactions involving the phenyl group. The crystal structure also confirms the expected positioning of the amide substituent with respect to the purine core; namely, planar and with the –NH group on the same side as N(7) (N(16)•••N(7) = 2.74 Å). This preference is predicted by computation (vide supra) and speaks to the ability to control local conformation through favorable intramolecular electrostatic (e.g., hydrogen-bonding) interactions in these heterocyclic amide systems.

Crystal Packing for Compound 4.7

The crystal packing for compound **4.7** reveals extended π-stacking where the C(8) amide moiety of one molecule is extended over the pyrimidine ring of a neighboring purine core (Figure 4-11a). The distance between the least squares planes defined by N(1), N(3), N(7), and N(9) is equal to 3.35 Å. Intermolecular hydrogen bonding is also observed between the amide carbonyl oxygen O(15) and the N(10) hydrogen of an adjacent purine (N(15)•••N(10) = 2.97 Å (Figure 4-11b). That simple dipolar π-stacking is not observed, but extended intermolecularly H-bonded chains are, reemphasizes how simple changes in functionality can influence supramolecular ordering. Particularly interesting from the standpoint of optoelectronic applications (e.g., second-order nonlinear optics) is how intermolecular hydrogen bonding confers polar ordering to the molecules of **4.7** within one-dimensional rows (Figure 4-11b). The distance between these one-dimensional rows is 3.35 Å (benzyl groups pointing toward each other) and 3.52 Å (benzyl groups pointing away from each other).

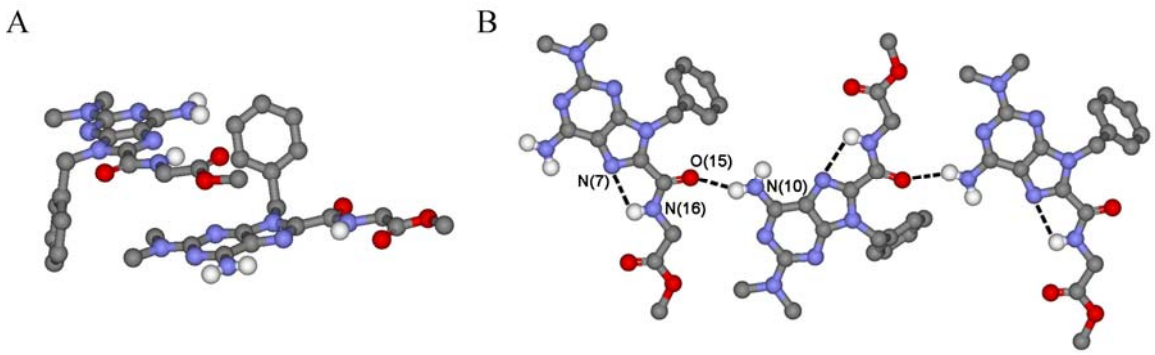

Figure 4-12. Dominant noncovalent interactions found in the crystal structure of **4.7**. A) π-stacking. B) Inter- and intramolecular hydrogen bonding.

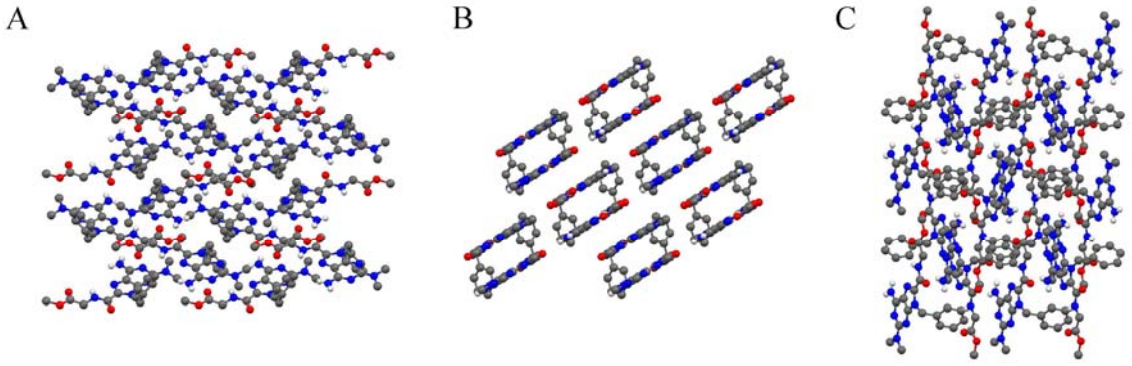

Figure 4-13. The crystal packing of **4.7** along its crystallographic axes. A) Axis *a*. B) Axis *b*. C) Axis *c*.

Photophysical Data for the C(8)-Amide Derivatives

Absorption and fluorescence emission measurements were taken for C(8) amide compounds **4.3** and **4.5**. Many of the photophysical trends reported in Chapter 3, seen with the nitriles and esters, are also observed with these compounds.

Table 4-1. Photophysical data for compounds **4.3** and **4.5** in 1,4-dioxane.[a]

Purine	λ_{max}, abs/nm	log ε /M^{-1} cm^{-1}	λ_{max},[b] em/nm	$\Delta\lambda_{max}$, em-abs/nm	Φ_F [c]
2.10b	345	4.3	392	38	0.96
2.10c	344	4.3	392	58	1
4.3	332	4.2	392	60	1
4.5	336	4.3	397	61	1

[a]All measurements performed at room temperature. [b]All experiments were performed using optical densities ≤ 0.1 at the excitation wavelength (λ_{ex} = 360 nm). [c]Fluorescence quantum yields are relative to the quantum yield of quinine sulfate in 0.5 M H_2SO_4 (Φ_F = 0.546).

Photophysical comparisons for compounds **4.3** and **4.5** are made using compounds **2.10b** and **2.10c**, the C(8)-CN and -COOMe purines, respectively, that have the same C(2) and C(6) donors as **4.3** and **4.5** (Tables 4-1–4-4).

Table 4-2. Photophysical data for compounds **4.3** and **4.5** in methylene chloride.[a]

Purine	λ_{max}, abs/nm	log ε /M^{-1} cm^{-1}	λ_{max}, em/nm	$\Delta\lambda_{max}$,[b] em-abs/nm	Φ_F [c]	τ_F/ns
2.10b	348	4.4	388	40	0.20	7.6±1.1
2.10c	348	4.3	409	61	0.90	2.7±0.3
4.3	338	4.2	402	64	0.87	1.9±0.3
4.5	343	4.3	407	64	0.91	1.6±0.4

[a]All measurements performed at room temperature. [b]All experiments were performed using optical densities ≤ 0.1 at the excitation wavelength (λ_{ex} = 360 nm). [c]Fluorescence quantum yields are relative to the quantum yield of quinine sulfate in 0.5 M H_2SO_4 (Φ_F = 0.546).

The absorption maxima appear to be weakly solvent dependent, vary linearly with concentration, and the molar extinction coefficients remain high. The emitting $^1(\pi\pi^* L_a)$ absorption band is found to be blue-shifted for **4.3** and **4.5** when it is compared to **2.10b** and **2.10c**.

Table 4-3. Photophysical data for compounds **4.3** and **4.5** in acetonitrile.[a]

Purine	λ_{max}, abs/nm	log ε /M^{-1} cm^{-1}	λ_{max},[b] em/nm	$\Delta\lambda_{max}$, em-abs/nm	Φ_F [c]
2.10b	344	4.3	394	50	0.26
2.10c	347	4.3	415	68	0.86
4.3	333	4.2	405	72	1
4.5	336	4.3	409	73	1

[a]All measurements performed at room temperature. [b]All experiments were performed using optical densities ≤ 0.1 at the excitation wavelength (λ_{ex} = 360 nm). [c]Fluorescence quantum yields are relative to the quantum yield of quinine sulfate in 0.5 M H_2SO_4 (Φ_F = 0.546).

This could be due to electron donation from the amide nitrogen to the amide carbonyl interfering with conjugation between C(8) and the amide carbonyl. The emission maximum for compound **4.3** is red shifted from 392 nm to 424 nm in solvents of increasing polarity, 1,4-dioxane and methanol, respectively. These values are comparable to the values observed for methyl ester compound **2.10c**.

Table 4-4. Photophysical data for compounds **4.3** and **4.5** in methanol.[a]

Purine	λ_{max}, abs/nm	log ε /M^{-1} cm^{-1}	λ_{max},[b] em/nm	$\Delta\lambda_{max}$, em-abs/nm	Φ_F [c]
2.10b	342	4.4	403	61	0.032
2.10c	347	4.2	432	85	0.66
4.3	335	4.2	424	89	0.89
4.5	340	4.2	429	89	0.90

[a]All measurements performed at room temperature. [b]All experiments were performed using optical densities ≤ 0.1 at the excitation wavelength (λ_{ex} = 360 nm). [c]Fluorescence quantum yields are relative to the quantum yield of quinine sulfate in 0.5 M H_2SO_4 (Φ_F = 0.546).

Stokes shifts also increase with increasing solvent polarity and the range between Stokes shifts for the lowest and highest polarity solvents are 29 nm for **4.3** and 28 nm for **4.5**; these values show that the solvent sensitivity for these compounds is similar to **2.10c** (27 nm Stokes shift). Of greater interest, the quantum yield values remain close to unity in spite of increases in solvent polarity, and are even higher for **4.3** (Φ_F = 0.89) and **4.5** (Φ_F = 0.90) than **2.10c** (Φ_F = 0.66) in methanol.

C(8)-Amide Photostability

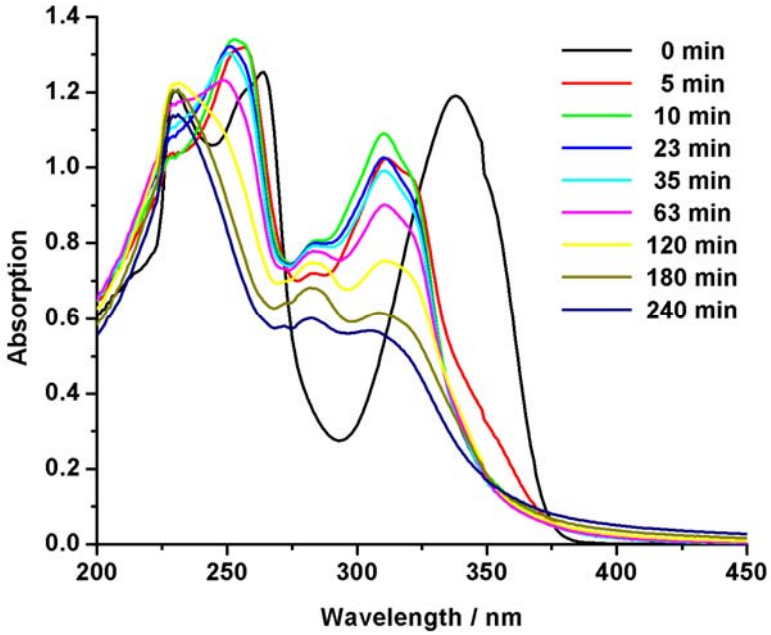

Figure 4-14. Changes observed in the absorption spectrum of a 60 μM solution of **4.3** in methylene chloride after exposure to 254 nm ultraviolet light at varying time intervals.

When a 60 μM solution of **4.3** in methylene chloride was exposed to 254 nm light from a hand-held UV lamp for varying time intervals, the absorption spectra exhibited more dramatic changes (Figure 4-14) than were observed under similar conditions for compounds **2.14b** and **2.14c** (Figures 3-15 and 3-16). The $^1(\pi\pi^*\ L_a)$ absorption band at 334 nm is completely deteriorated within 5 min of exposure and a new band appears at 306 nm. After 10 min this new band begins to lose absorption intensity. The $^1(\pi\pi^*\ L_b)$ absorption band progressively blue shifts and loses intensity over the 240 min of UV exposure.

Theoretical Data

Again, both semiempirical and high-level DFT (B3LYP/6-31++G**) calculations have been used to shed light on the electronic nature of the C(8) amide derivatives and their absorption properties.

Table 4-5. Electronic Structure Data for the D-A Purine Amide Derivatives Compared to the Corresponding Nitriles and Esters.[a]

Purine[b]	μ_g	HOMO calcd (eV)	LUMO calcd (eV)	ΔE calcd (eV)	ΔE optical[c] (eV)	λ_{max} L_a calcd (nm, [eV]), f [d]	λ_{max} L_a CH_2Cl_2 (nm)
2-AP-CONHMe[e]	0.78	–6.16	–1.84	4.32	N.D.[f]	326, 0.53	N.D.[f]
2.6c-Me	5.19	–6.24	–2.04	4.20	3.4	331, 0.58	328
2.6b-Me	5.45	–6.52	–2.27	4.25	3.5	328, 0.57	326
4.3-Me	3.36	–5.36	–1.25	4.11	3.3	344, 0.57	338
2.10c-Me	2.81	–5.40	–1.48	3.92	3.2	354, 0.61	348
2.10b-Me	5.52	–5.64	–1.60	4.04	3.3	344, 0.62	348
4.7-Me	2.88	–5.47	–1.33	4.14	N.D.[f]	339, 0.57	N.D.[f]
2.12c-Me	3.16	–5.53	–1.56	3.97	3.2	348, 0.61	338
2.12b-Me	5.66	–5.75	–1.68	4.07	3.4	339, 0.61	336

[a] See the Experimental (Chapter 2)section for computational details. [b] All benzyl groups have been replaced by methyl groups for the calculations. [c] Calculated as the end-absorption of the lowest energy transition in the UV-vis spectrum. [d] All correspond to one-electron HOMO (S_0) → LUMO (S_1) transitions. [e] One imaginary frequency was identified for this structure indicating a transition state. The frequency is associated with rotation around the amide methyl group based on analysis of the coordinate files.[f] Not determined.

Ground state geometries, dipoles, and orbital energies have been obtained for **4.3-Me**, **4.7-Me**, and the parent 2-AP derivative bearing a CONHMe group in the C(8) position (Me on N(9)), **2-AP-CONHMe** (structure not shown). In all cases, the amide torsion angle used for the starting structures was that found in the Figure 4-11 X-ray structure. Summarized in Table 4-5 are the dipole and orbital energy data obtained from the DFT calculations. Complementary orbital density plots of the HOMO and LUMO levels (Molden v. 4.6) to show graphically the electronic nature of the ground state are shown in Figure 4-15.

The HOMO consists of delocalized p orbitals on the purine plane, with the greatest density in the N9-C4-C5-C6 region consistent with the nitriles and esters. Localized p_z orbitals are seen on the exocyclic donor heteroatoms and the acceptor functionality; the degree of charge separation in the HOMO is similar to that of the esters. Interestingly, some orbital density is noted on the amide nitrogen atom that is likely related to interaction with N(7). The LUMO is again concentrated on the acceptor portion, C(8) and the amide. The density on the C(2) donor group diminishes quite dramatically in the LUMO; the C(6) donor orbital coefficient is only slightly affected. In general the amides have slightly higher HOMO energies than the esters, but more significantly increased (~0.2 eV) LUMO energies (resulting in overall larger HOMO-LUMO gaps). The LUMO energy may be affected by the intramolecular H-bonding interaction between the amide and N(7). ZINDO/S CI semi-empirical calculations, as before, reveal that the lowest energy transition is associated with promotion of an electron from the HOMO to the LUMO in all cases. Although the experimental data is limited, the energy of the long wavelength transition correlates well with λ_{max} in CH_2Cl_2. Based on the plots in Figure 4-15, the transition mainly involves transfer of charge from the amino group on C(2) (and the pyrimidine ring) to the C(8) acceptor group.

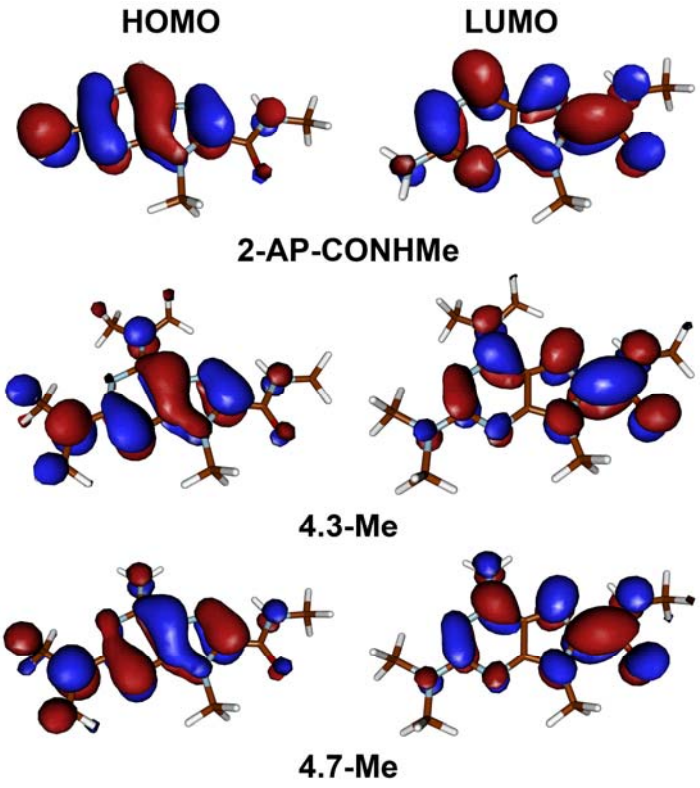

Figure 4-15. Orbital density plots for D-A purinyl amide derivatives calculated from the B3LYP/6-31++G** optimized geometries (using Molden v. 4.6).

Amide Functionalization and Boc protection of the Primary Amine Donors

Amide Formation at C(2) of the Purine Core

Discussed in the introduction, also worth exploring is functionalization of the $-NH_2$ group on C(2) or C(6); we focused initially on acylation at this position due to its relevance to generating oligopeptide architectures. A simple acylation reaction was explored by adding benzoyl chloride to compound **2.7** (Figure 4-16). The C(2) amine was found to quickly react with this relatively active acid chloride to produce amide **4.8** in reasonable yield. This result is consistent with any number of similar reactions from the literature that show acylation of 2-aminopurine derivatives with acid chlorides[114,115] and acetic anhydride.[116]

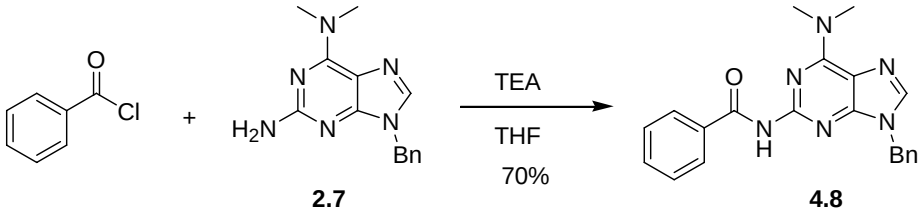

Figure 4-16. Amide formation on the C(2) amine via an acid chloride.

Milder coupling reagents were explored for C(2) amide formation to obviate HCl generation associated with the use of acid chlorides that could lead to epimerization of α-amino acid sequences that might later be introduced. Reactions using DCC/DMAP in methylene chloride or EDCI/HOBt/DMAP in DMF proved unsuccessful for coupling compound **2.7** with an aliphatic carboxylic acid, butyric acid. An alternative peptide coupling condition, HOAt/EDCI/amine base in DMF, has been found to successfully couple deactivated amines and would be worth trying in the future.[117] If no mild coupling conditions are successful for C(2) amide formation, an acid chloride can be generated from the Fmoc-protected glycine to react with the C(2) amine. Once the amide on C(2) is formed, milder reagents can be used to form subsequent peptide bonds.[117]

Boc Protection of the C(2) and C(6) Primary Amines

Along the same lines, employment of the purines described thus far as amino acid building blocks requires some investigation of their protection and deprotection chemistry. This was initially investigated using the conventional Boc protecting group. The C(2) and C(6) primary amines on the C(8)-H (not shown) and the C(8)-Br purines could be successfully protected with Boc groups under mild conditions (Figure 4-17). The reaction conditions do require four equivalents of $(Boc)_2O$ (and a catalytic amount of DMAP in THF) since the reagent reacts twice with each primary amine (a surprising result given steric considerations). Similar observations have been reported for purines[118] and confirmed here by MS and ^1H NMR (absence of amide –

NH peak). That the reactions shown in figure 4-17 work, while the ones shown in figures 4-8 and 4-10 fail, further implicates the relatively unstable C(8) carboxylic acid function as the source of the previous difficulties. Unfortunately, the $(Boc)_2O$ reaction (same reaction conditions) could not be extended to the D-A purines **2.7b** and **2.7c**, no desired product was obtained and the D-A purines appeared to decompose.

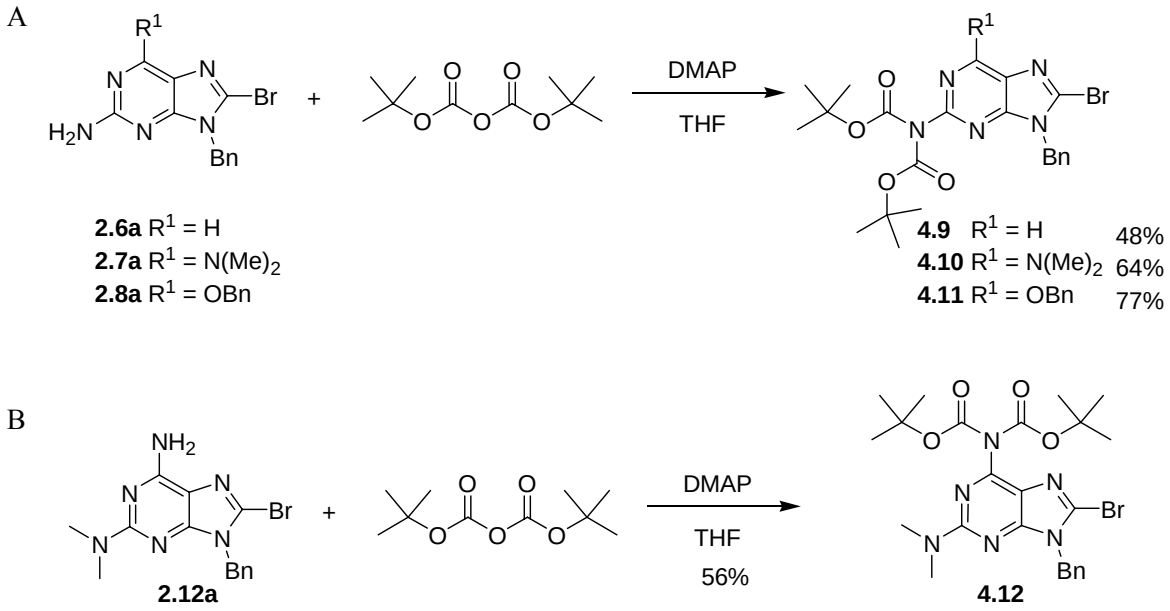

Figure 4-17. Boc protection of primary amines on the purine core. A) On the C(2) amine. B) On the C(6) amine.

Urea Formation on the C(2) Amine: Building Blocks for Self-assembled Structures

Early in this thesis, reactivity at the C(2) amino group was evaluated through reaction with isocyanate electrophiles in work aimed at expanding the hydrogen-bonding abilities of the purinyl building blocks. The general design is shown in Figure 4-18. Formation of an intramolecular hydrogen bond between the urea hydrogen and purine N(3) exposes a hydrogen bond donor-acceptor-donor-acceptor face capable of dimer formation by four hydrogen bonds. Since its conception, self-complementary quadruply hydrogen bonded complexes from urea-functionalized 2,6-diaminopurines have been explored and published by the Castellano Group.[119]

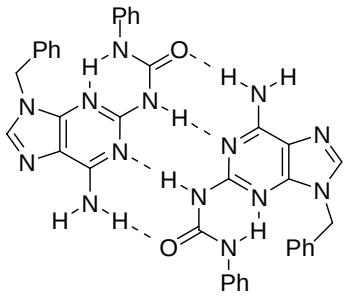

Figure 4-18. General design of self-complementary quadruply hydrogen bonded dimers based on purines.

To initiate this work, the author explored the general reactivity of **2.5**, **2.6**, and **2.7** toward isocyanates (Figure 4-19). Each purine bears only one reactive amino group (unlike what is required for dimerization as shown in Figure 4-18) to simplify the studies.

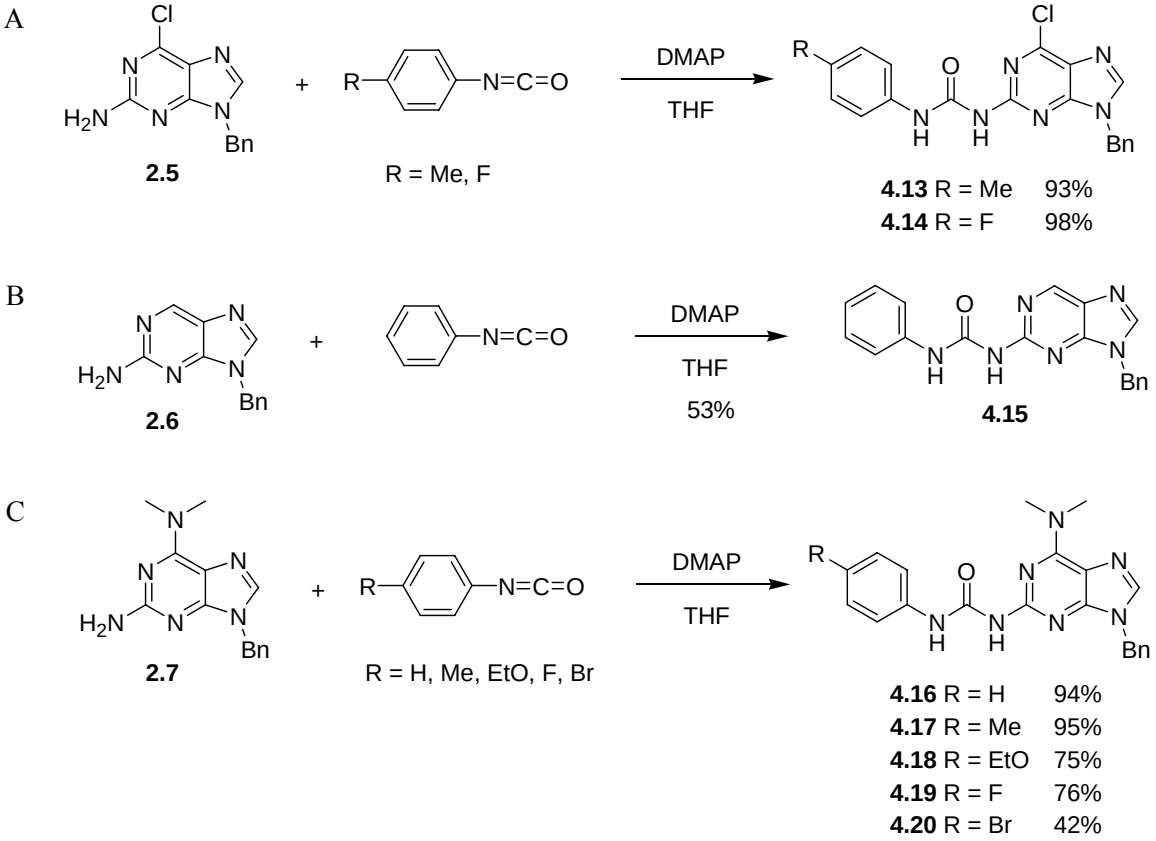

Figure 4-19. Urea formation using the C(2) primary amine.

The purinyl urea compounds were formed smoothly upon treating 2-aminopurine derivatives with aryl isocyanate derivatives in pyridine/DMAP. Most of the reactions gave reasonable to good product yields. Urea compounds formed from compound **2.5** can in theory be treated with methanolic ammonia (that converts C(6)-Cl to C(6)-NH_2) to produce self-complementary hydrogen bonded dimers (Figure 4-18), while the ureas formed from compounds **2.6** and **2.7** served as model compounds for ^{1}H NMR chemical shift comparison. The solubility of ureas **4.13**–**4.20** did, however, prove to be quite low in solvents that were critical for examination of their hydrogen bonding properties, like chloroform. Alkyl ureas were envisioned as an easy alternative to increase solubility, however, no reaction was found to occur between the purine C(2) amine and alkyl isocyanates under the reaction conditions shown in figure 4-19. Efforts in the Castellano Group have since circumvented these reactivity issues through elevated temperatures and direct deprotonation of the amine.

Critical Crystal Structure of Ureidopurine 4-16

Single crystals of **4.16** suitable for X-ray analysis, perfomed by Dr. Khalil Abboud, could be grown by slow evaporation (two weeks) from pyridine. The structure of the compound as determined in the solid state by X-ray crystallography is shown in figure 4-20.[119] It critically reveals that intramolecular hydrogen bonding between the urea hydrogen on N(12) with N(3) (N(12)•••N(3) = 2.74 Å) is accessible through a planar arrangement (despite the bulky N(9) benzyl substituent). There is also a near edge-to-face relationship between the aromatic substituents with the angle between the least squares planes on the aromatic rings equal to 86.3° and the closest carbon-carbon distance equal to 3.67 Å. The dimethylamino substituent, defined by atoms N(19), C(20), and C(21), is largely planar but slightly twisted (~ 9°) around the C(6)-N(19) bond. Consistent with the solid-state data for **4-16**, the chemical shift of its urea H^b proton in $CDCl_3$ (~ 5 mM) is significantly deshielded to 11.4 ppm (relative to TMS); H^a appears at ~ 7.2

ppm. This conformation is identical to the one adopted by C(6)-amino (rather than dimethylamino) derivatives upon dimer formation in solution and the solid state.

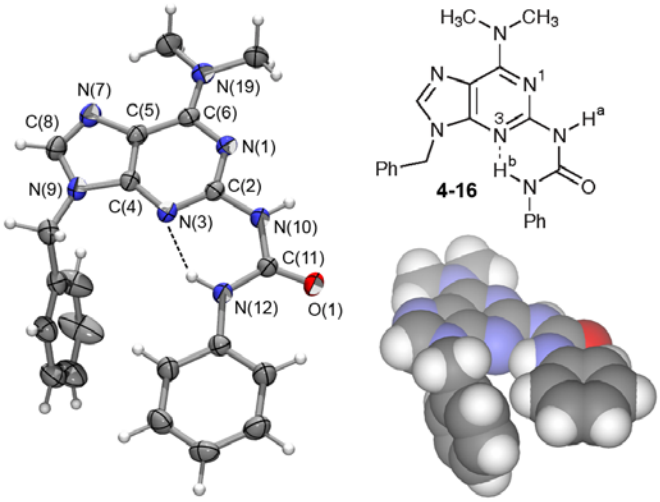

Figure 4-20. Intramolecular hydrogen bonding of **4-16** in the solid state (ellipsoids drawn at the 50% probability level). The side view of a CPK representation shows the extent of contact achievable for the two phenyl rings in the N(3) H-bonded conformer.

Conclusion and Future Directions

In conclusion, donor-acceptor (D-A) purines have been prepared, many of which have unity or near unity quantum yields in organic solution. Many of these compounds, especially the C(8)-COOMe purines, expressed more sensitivity to their solvent environment than 2-aminopurine and other nucleobase analogues used for biological studies. Future work will include making and studying the photophysical properties of N(9) sugar functionalized derivatives of **2.6b** and **2.6c** along with new D-A compounds (Figure 4-21) that are water soluble and have the ability to base pair with natural nucleobases.

X-ray crystal structures revealed that simple changes in the functionality of C(2), C(6), and C(8) dramatically changed the π-stacking and hydrogen bonding of the purines in the solid state. Future work in this area will include making luminescent purine derivatives and evaluating their supramolecular properties. Some examples are shown in figures 4-21 and 4-22a,b.

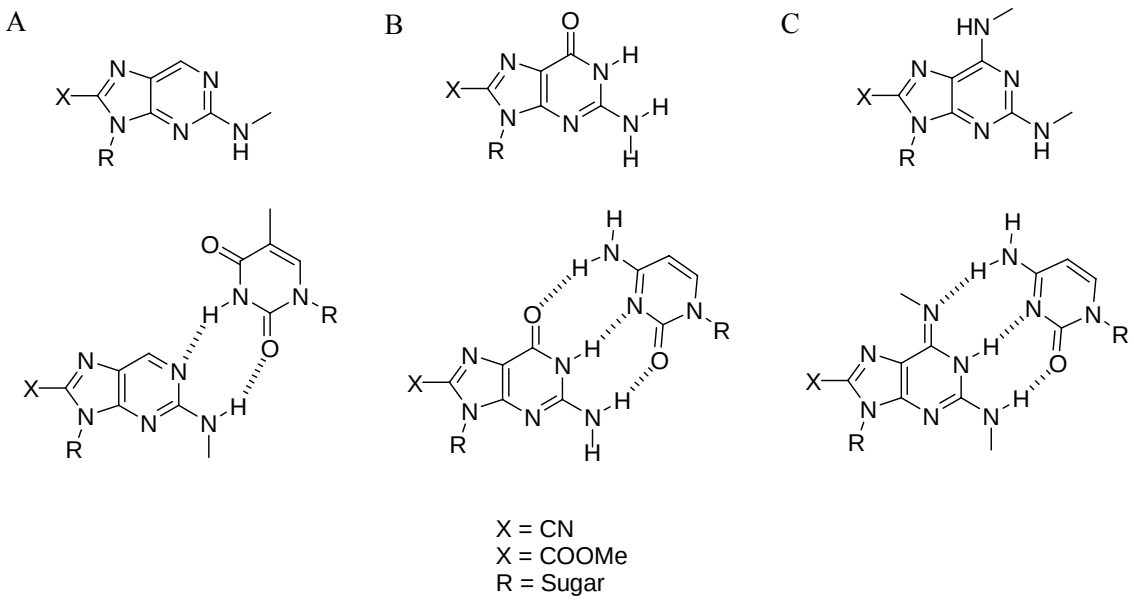

Figure 4-21. Design of donor-acceptor purines to be prepared for future photophysical studies.

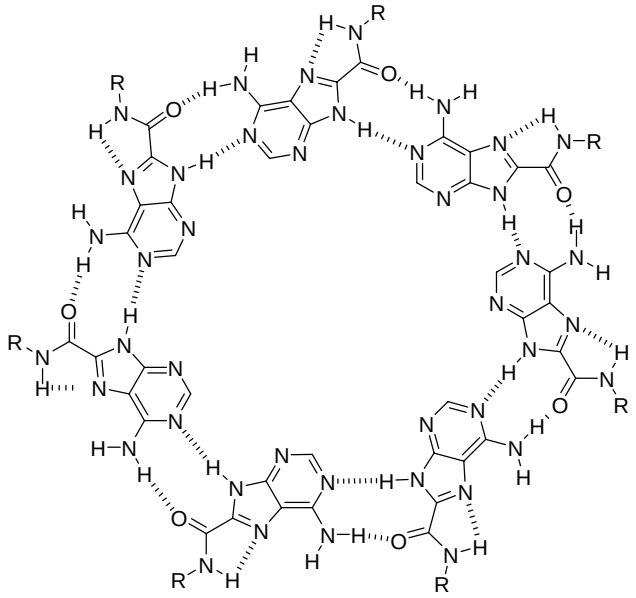

Figure 4-22. Potential supramolecular structure of an C(8)-amide adenine analogue.

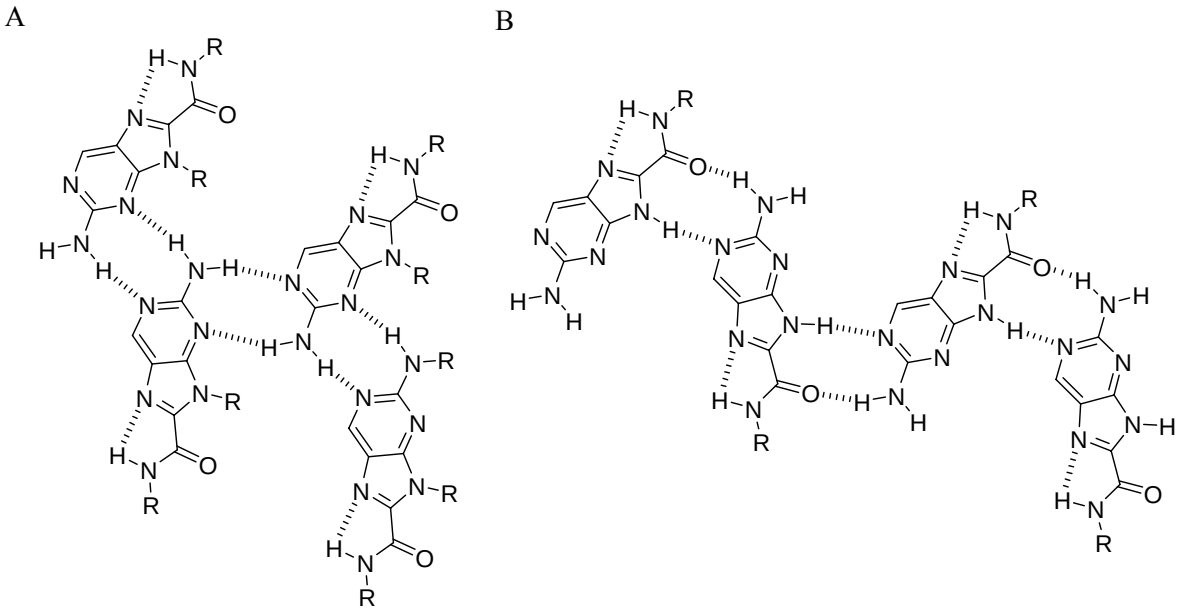

Figure 4-23. Potential supramolecular structure of C(8)-amide 2-aminopurine derivatives.

Figure 4-22 shows a C(8)-amide functionalized adenine forming a seven-membered ring directed by hydrogen bonding interactions. Figure 4-23a,b shows C(8)-amide functionalized 2-aminopurine forming two different ribbon structures directed by the N(9) functionality. When N(9) is functionalized, hydrogen bonding can potentially direct the formation of the structure presented in figure 4-23a, and then a much different ribbon (Figure 4-23b) can be envisioned when N(9) is hydrogen.

Compound **2.7b** was found to emit light when incorporated (using a spin casting technique) into an OLED device. Work will continue with device exploration using the D-A purines as the emissive layer. The performance of the C(8)-COOMe and C(8)-amide derivatives will be investigated. Vapor deposited films of the D-A compounds will also be tested in devices.

Successful C(8)-amide functionalization of the D-A purines opens the potential for future work involving the development of homo- and hetero-oligopeptides discussed at the beginning of

this chapter. Synthetic strategies will be continued on progression toward C(2)-amide functionalization and oligopeptide formation.

Experimental Section

Synthesis of Compounds

General Method A *(Boc protection of C(2) or C(6) primary amine).* $(Boc)_2O$ (4 equiv), DMAP (0.1 equiv), and a purine containing a primary amine were dissolved in dry THF (50 mL). The solution was stirred overnight, concentrated under reduced pressure, and the desired product was obtained by flash chromatography (40% EtOH/hexanes).

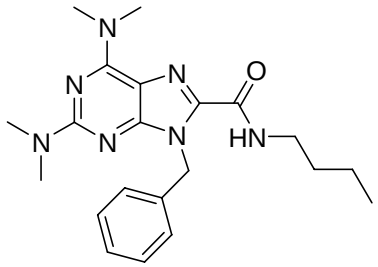

2,6-Bis(dimethylamino)-8-butylamide-9-benzyl purine (4.3). Compound **2.10b** (0.10 g, 0.31 mmol) was heated overnight at 100 °C with EtOH (25 mL) and 10% aqueous NaOH (25 mL). The ethanol was then removed under reduced pressure and the solution, once cooled to 0 °C, was acidified to a pH of 2. The solution was then extracted with cold ethyl acetate (100 mL x 5). The combined organic layers were dried with magnesium sulfate and concentrated under reduced pressure with the solution kept below 20 °C at all times. The white solid that resulted was dried under high vacuum for 15 min. The solid was then dissolved in cold, dry CH_2Cl_2 and added to butylamine (0.013 g, 0.18 mmol) in dry CH_2Cl_2 (150 mL) at 0 °C. DCC (0.040 g, 0.19 mmol) and DMAP (0.024 g, 0.19 mmol) were then added and the reaction was stirred at room temperature overnight. The reaction was filtered, the solvent was removed under reduced pressure, and the crude solid was purified by column chromatography (40%, EtOAc/hexanes) to yield a white solid (0.052 g, 42% from **2.10b**): m.p. 112–114 °C. ^{1}H NMR (300 MHz, DMSO-

d_6) δ 0.88 (t, 3H, J = 7.2 Hz), 1.27 (m, 2H), 1.47 (m, 2H), 3.11 (s, 6H), 3.38 (q, 2H, J = 7.2), 3.45 (bs, 6H), 5.65 (s, 2H), 7.29 (m, 5H), 8.46 (t, 1H, J = 7.2 Hz). ^{13}C NMR (75 MHz, DMSO-d_6) δ 13.67, 19.56, 31.29, 36.78, 38.18, 45.88, 111.98, 127.22, 127.66, 128.25, 136.44. 138.06, 149.96, 154.20, 154.49, 159.00, 159.15. HRMS calcd for $C_{21}H_{30}N_7O$ $[M+H]^+$: 396.2512, found: 396.2506.

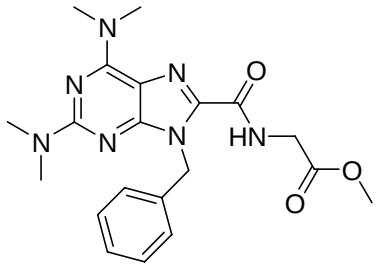

2,6-Bis(dimethylamino)-8-carbonyl-amino-acetic acid methyl ester-9-benzylpurine (4.5). Compound **2.10b** (0.10 g, 0.31 mmol) was heated overnight at 100 °C with EtOH (25 mL) and 10% aqueous NaOH (25 mL). The ethanol was then removed under reduced pressure and the solution once cooled to 0 °C was acidified to a pH of 2. The solution was then extracted with cold ethyl acetate (100 mL x 5). The combined organic layers were dried with magnesium sulfate and concentrated under reduced pressure with the solution kept below 20 °C at all times. The white solid that resulted was dried under high vacuum for 15 min. The solid was then dissolved in cold, dry CH_2Cl_2 and added to glycine methylester HCl (0.037 g, 0.29 mmol) in dry CH_2Cl_2 (150 mL) at 0 °C. DCC (0.067 g, 0.32 mmol) and DMAP (0.08 g, 0.7 mmol) were then added and the reaction was stirred at room temperature overnight. The reaction was filtered, the solvent was removed under reduced pressure, and the crude solid was purified by column chromatography (40%, EtOAc/hexanes) to yield a white solid (0.10 g, 82% from **2.10b**): m.p. 133–135 °C. ^{1}H NMR (300 MHz, $CDCl_3$) δ 3.30 (s, 6H), 3.46 (bs, 6H), 3.78 (s, 3H), 4.19 (d, 2H, J = 5.6 Hz), 5.75 (s, 2H), 7.23 (m, 3H), 7.46 (m, 2H), 7.75 (t, 1H, J = 5.6 Hz). ^{13}C NMR (75 MHz, $CDCl_3$) δ 37.30, 38.27, 40.83, 46.72, 52.38, 113.27, 127.30, 128.23, 128.40, 135.40,

138.00, 155.13, 159.55, 170.23. HRMS calcd for $C_{20}H_{26}N_7O_3$ $[M+H]^+$: 412.2097, found: 412.2088.

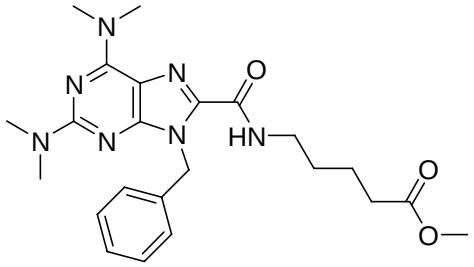

2,6-Bis(dimethylamino)-8-pentanoic amide methyl ester-9-benzyl purine (4.6).

Compound **2.10b** (0.10 g, 0.31 mmol) was heated overnight at 100 °C with EtOH (25 mL) and 10% aqueous NaOH (25 mL). The ethanol was then removed under reduced pressure and the solution once cooled to 0 °C was acidified to a pH of 2. The solution was then extracted with cold ethyl acetate (100 mL x 5). The combined organic layers were dried with magnesium sulfate and concentrated under reduced pressure with the solution kept below 20 °C at all times. The white solid that resulted was dried under high vacuum for 15 min. The solid was then dissolved in cold, dry CH_2Cl_2 and added to methyl 5-aminovalurate (0.049 g, 0.29 mmol) in dry CH_2Cl_2 (150 mL) at 0 °C. DCC (0.067 g, 0.32 mmol) and DMAP (0.08 g, 0.65 mmol) were then added and the reaction was stirred at room temperature overnight. The reaction was filtered, the solvent was removed under reduced pressure, and the crude solid was purified by column chromatography (40 %, EtOAc/hexanes) to yield a white solid (0.063g, 45% from **2.10b**): m.p. 85–86 °C. ^{1}H NMR (300 MHz, $CDCl_3$) δ 1.70 (m, 4H), 2.37 (t, 2H, J = 6.9 Hz), 3.21 (s, 6H), 3.41 (q, 2H, J = 6.6 Hz), 3.47 (s, 6H), 3.68 (s, 3H), 5.81 (s, 2H), 7.24 (m, 3H), 7.37 (t, 1H, J = 6.3 Hz), 7.51 (m, 2H). ^{13}C NMR (75 MHz, DMSO-d_6) δ 21.78, 28.53, 32.85, 36.75, 38.02, 45.87, 51.11, 111.98, 127.16, 127.65, 128.20, 136.34, 138.00, 154.18, 154.47, 159.04, 159.13, 173.20. HRMS calcd for $C_{23}H_{31}N_7O_3$ $[M+H]^+$: 454.2561, found: 454.2597.

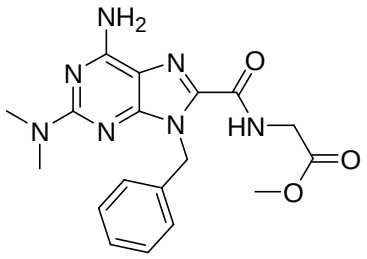

[(6-Amino-9-benzyl-2-dimethylamino-9*H*-purine-8-carbonyl)-amino]-acetic acid methyl ester (4.7). Compound **2.12b** (0.10 g, 0.34 mmol) was heated overnight at 100 °C with EtOH (25 mL) and 10% aqueous NaOH (25 mL). The ethanol was then removed under reduced pressure and the solution once cooled to 0 °C was acidified to a pH of 2. The cold acidified solution was then extracted with cold ethyl acetate (100 mL x 5). The combined organic layers were dried with magnesium sulfate and concentrated under reduced pressure with the solution kept below 20 °C at all times. The white solid that resulted was dried under high vacuum for 15 min. The solid was then dissolved in cold, dry CH_2Cl_2 and added to glycine methylester HCl (0.040 g, 0.32 mmol) in dry CH_2Cl_2 (150 mL) at 0 °C. DCC (0.079 g, 0.38 mmol) and DMAP (0.09 g, 0.77 mmol) were then added and the reaction was stirred at room temperature overnight. The reaction was filtered, the solvent was removed under reduced pressure, and the crude solid was purified by column chromatography (40%, EtOAc/hexanes) to yield a white solid (0.066 g, 51% from **2.12b**): m.p. 170–171 °C. ^{1}H NMR (300 MHz, DMSO-d_6) δ 3.11 (s, 6H), 3.65 (s, 3H), 4.04 (d, 2H, J = 6.3 Hz), 5.62 (s, 2H), 6.97 (s, 2H), 7.29 (m, 5H), 8.55 (t, 1H, J = 6.3 Hz). ^{13}C NMR (75 MHz, DMSO-d_6) δ 36.91, 40.63, 46.04, 51.80, 111.79, 127.27, 127.74, 128.28, 136.77, 137.80, 153.23, 156.32, 159.40, 160.19, 160.19, 169.93. HRMS calcd for $C_{18}H_{21}N_7O_3$ $[M+H]^+$: 384.1779, found: 384.1788.

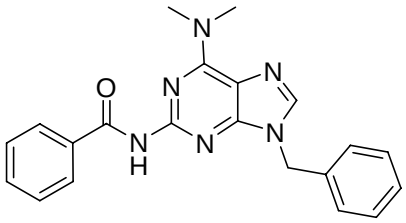

N-(9-Benzyl-6-dimethylamino-purin-2-yl)-benzamide (4.8). Benzoyl chloride (0.12 g, 0.82 mmol) was added dropwise to a solution of compound **2.7** (0.20 g, 0.75 mmol) and triethylamine (0.75 g, 0.75 mmol) in dry THF (100 mL). The reaction was stirred at rt for 2 h, was concentrated under reduced pressure, and purified by flash chromatography (40% EtOAC/ Hexanes) to yield an off-white foamy solid (0.19 g, 70%): m.p. 55–60 ° C. ^{1}H NMR (300 MHz, DMSO-d_6) δ 3.35 (s, 6H), 5.33 (s, 2H), 7.23 (m, 5H), 7.47 (m, 3H), 7.90 (d, 2H), 8.16 (s, 1H), 10.40 (s, 1H). ^{13}C NMR (75 MHz, DMSO-d_6) δ 37.59, 45.86, 116.57, 127.44, 127.61, 127.91, 128.10, 128.59, 131.38, 135.06, 137.16, 139.23, 151.39, 152.36, 154.26, 165.76. $C_{21}H_{20}N_6O$ $[M+H]^+$: 373.1771, found: 373.1801.

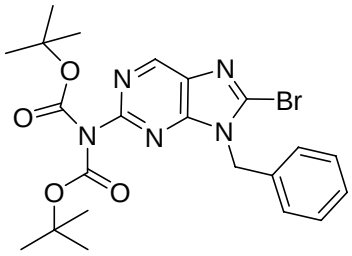

2-Di-tert-butoxycarbonylamine-8-bromo-9-benzylpurine (4.9). Compound **2.6a** (0.21 g, 0.66 mmol) was reacted under the conditions of general method **A** to yield a white solid (0.16 g, 48%). ^{1}H NMR (300 MHz, DMSO-d_6) δ 1.31 (s, 18H), 5.50 (s, 2H), 7.20 (m, 2H), 7.32 (m, 3H), 9.19 (s, 1H). ^{13}C NMR (75 MHz, DMSO-d_6) δ 28.0, 47.6, 83.6, 127.6, 128.8, 129.5, 132.9, 135.9, 136.9, 148.7, 151.0, 152.8, 153.8. HRMS calculated for $C_{22}H_{27}BrN_5O_4$ $[M+H]^+$: 504.1241, found: 504.1241.

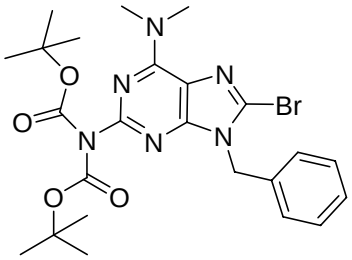

2-Di-tert-butoxycarbonlyamine-6-dimethylamino-8-bromo-9-benzylpurine (4.10).

Compound **2.7a** (0.20 g, 0.58 mmol) was reacted under the conditions of general method **A** to yield a white solid (0.35 g, 64%). ^{1}H NMR (300 MHz, $CHCl_3$) δ 1.41 (s, 18H), 3.45 (bs, 6H), 5.35 (s, 2H), 7.28 (m, 5H). ^{13}C NMR (75 MHz, $CHCl_3$) δ 28.1, 38.6, 47.5, 82.8, 119.1, 125.1, 127.9, 128.2, 128.9, 135.7, 151.5, 152.7, 153.3, 154.4. HRMS calculated for $C_{24}H_{32}BrN_6O_4$ $[M+H]^+$: 548.1692, found: 548.1701.

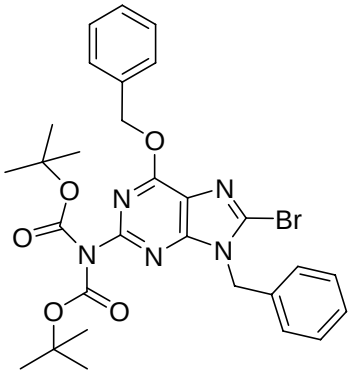

2-Di-tert-butoxycarbonylamine-6-benzyloxy-8-bromo-9-benzylpurine (4.11).

Compound **2.8a** (0.38 g, 0.93 mmol) was reacted under the conditions of general method **A** to yield a white solid (0.44 g, 77%). ^{1}H NMR (300 MHz, DMSO-d_6) δ 1.32 (s, 18H), 5.44 (s, 2H), 5.60 (s, 2H), 7.38 (m, 10H). ^{13}C NMR (75 MHz, DMSO-d_6) δ 27.1, 27.3, 47.2, 68.4, 82.9, 119.2, 126.9, 128.0, 128.4, 128.5, 128.8, 131.7, 135.3, 135.7, 150.1, 153.8, 159.0. HRMS calculated for $C_{28}H_{32}BrN_5O_5$ $[M+H]^+$: 610.1660, found: 610.1660.

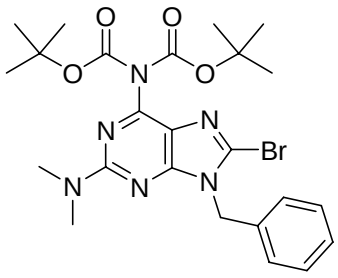

2-Di-tert-butoxycarbonlyamine-6-dimethylamino-8-bromo-9-benzylpurine (4.12). Compound **2.12a** (0.20 g, 0.58 mmol) was reacted under the conditions of general method **A** to yield a white solid (0.31 g, 56%). ^{1}H NMR (300 MHz, DMSO-d_6) δ 1.38 (s, 18H), 3.13 (s, 6H), 5.32 (s, 2H), 7.33 (m, 5H). ^{13}C NMR (75 MHz, DMSO-d_6) δ 27.9, 47.3, 83.8, 120.4, 127.9, 128.0, 128.6, 129.0, 129.5, 136.5, 148.9, 150.6, 156.3, 159.2. HRMS calculated for $C_{24}H_{32}BrN_6O_4$ $[M+H]^+$: 547.1663, found: 547.1701.

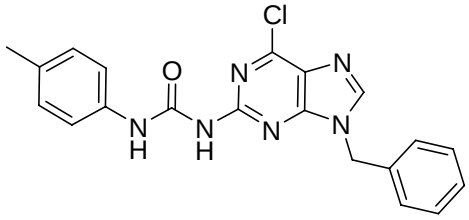

1-(9-Benzyl-6-chloro-purin-2-yl)-3-*p*-tolyl-urea (4.13). Compound **2.5** (0.10 g, 0.39 mmol) and *p*-tolylisocyanate (0.077 g, 0.58 mmol) were dissolved in dry pyridine and stirred at rt. The reaction was monitored by TLC until complete (no longer than 24 h). The pyridine was removed under reduced pressure and the crude product was purified by recrystallization in EtOH to yield a white solid (0.14 g, 93%): m.p. 204–205 °C. ^{1}H NMR (300 MHz, DMSO-d_6) δ 2.25 (s, 3H), 5.55 (s, 2H), 7.09 (m, 2H), 7.29 (m, 7H), 8.62 (s, 1H), 10.34 (s, 1H), 10.68 (s, 1H). ^{13}C NMR (75 MHz, DMSO-d_6) δ 20.3, 46.9, 119.4, 126.4, 127.0, 127.9, 128.3, 128.8, 129.2, 132.0, 135.7, 135.8, 146.1, 149.8, 150.8, 152.8. HRMS calcd for $C_{19}H_{16}N_6O$ $[M+H]^+$: 393.1225, found: 393.1261.

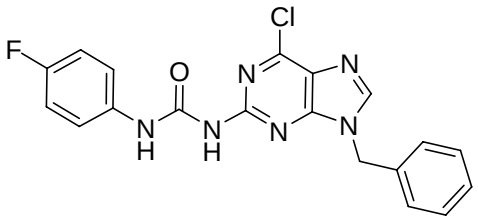

1-(9-Benzyl-6-chloro-purin-2-yl)-3-(4-fluoro-phenyl)-urea (4.14). Compound **2.5** (0.10 g, 0.39 mmol) and 4-fluorophenylisocyanate (0.42 g, 3.1 mmol) were dissolved in dry pyridine (7 mL) and stirred at rt. The reaction was monitored by TLC until complete (no longer than 24 h). The pyridine was removed under reduced pressure and the crude product was purified from recrystallization in EtOH to yield a white solid (0.150 g, 98%). ^{1}H NMR (300 MHz, DMSO-d_6) δ 5.54 (s, 1H), 7.16 (m, 2H), 7.35 (m, 7H), 8.60 (s, 1H), 10.34 (s, 1H), 10.69 (s, 1H). ^{13}C NMR (75 MHz, DMSO-d_6) δ 46.9, 115.2, 115.5, 121.2, 126.5, 127.1, 127.9, 128.8, 134.6, 135.8, 146.2, 149.8, 150.9, 152.0, 152.8. HRMS calcd for $C_{19}H_{15}N_6O$ $[M+H]^+$: 397.0980, found: 397.0992.

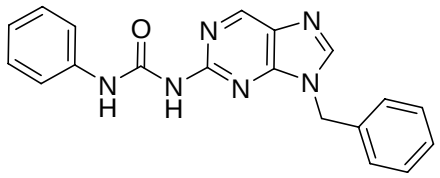

1-(9-Benzyl-9H-purin-2-yl)-3-phenyl-urea (4.15). Compound **2.6** (0.10 g, 0.44 mmol) and phenylisocyanate (0.85 g, 7.1 mmol) were dissolved in dry pyridine (7 mL) and stirred at rt. The reaction was monitored by TLC until complete (no longer than 24 h). The pyridine was removed under reduced pressure and the crude product was purified from recrystallization in EtOH to yield a white solid (0.081 g, 53%): m.p. 260–261 °C. ^{1}H NMR (300 MHz, DMSO-d_6) δ 5.51 (s, 2H), 7.04 (m, 3H), 7.33 (m, 7H), 7.47 (m, 2H), 8.57 (s, 1H), 9.04 (s, 1H), 10.13 (s, 1H), 11.36 (s, 1H). ^{13}C NMR (75 MHz, DMSO-d_6) δ 46.2, 119.3, 122.9, 127.2, 127.9, 128.3, 128.8, 129.4, 136.2, 138.5, 146.0, 148.7, 151.4, 151.7, 153.6. HRMS calcd for $C_{19}H_{17}N_6O$ $[M+H]^+$: 345.1464, found: 345.1471.

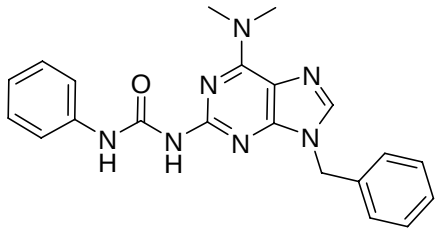

1-(9-Benzyl-6-dimethylamino-purin-2-yl)-3-phenyl-urea (4.16). Compound **2.7** (0.10 g, 0.37 mmol) and phenylisocyanate (0.65 mL, 6.0 mmol) were dissolved in dry pyridine (7 mL) and stirred at rt. The reaction was monitored by TLC until complete (no longer than 24 h). The pyridine was removed under reduced pressure and the crude product was purified from recrystallization in EtOH to yield a white solid (0.137 g, 94%): m.p. 234–236 °C. ^{1}H NMR (300 MHz, DMSO-d_6) δ 3.62 (bs, 6H), 5.40 (s, 2H), 7.28 (m, 10H), 8.13 (s, 1H), 9.41 (s, 1H), 11.45 (s, 1H). ^{13}C NMR (75 MHz, DMSO-d_6) δ 46.1, 60.0, 115.46, 119.17, 122.7, 126.8, 126.9, 127.6, 128.7, 128.8, 136.8, 138.7, 138.9, 151.8, 153.0, 154.1. HRMS calculated for $C_{21}H_{22}N_7O$ $[M+H]^+$: 388.1886, found: 388.1921.

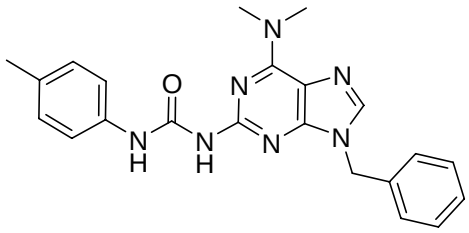

1-(9-Benzyl-6-dimethyl amino-purin-2-yl)-3-*p*-tolyl-urea (4.17). Compound **2.7** (0.10 g, 0.37 mmol) and *p*-tolylisocyanate (0.10 g, 0.75 mmol) were dissolved in dry pyridine and stirred at rt. The reaction was monitored by TLC until complete (no longer than 24 h). The pyridine was removed under reduced pressure and the crude product was purified from recrystallization in EtOH to yield a white solid (0.14 g, 95%): m.p. 204–205 °C. ^{1}H NMR (300 MHz, DMSO-d_6) δ 2.25 (s, 3H), 3.42 (bs, 6H), 5.41 (s, 2H), 7.07 (m, 2H), 7.27 (m, 7H), 8.14 (s, 1H), 9.34 (s, 1H), 11.38 (s, 1H). ^{13}C NMR (75 MHz, DMSO-d_6) δ 21.0, 46.9, 116.2, 119.9,

127.6, 128.4, 129.4, 129.9, 132.3, 136.8, 137.5, 139.6, 151.0, 152.5, 153.7, 154.8. HRMS calcd for $C_{22}H_{24}N_7O$ $[M+H]^+$: 402.2042, found: 402.2061.

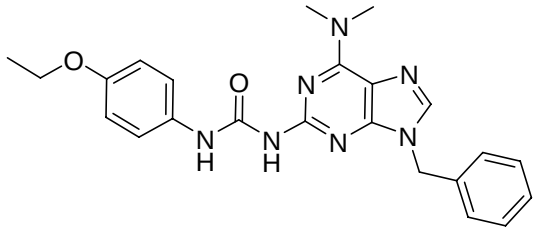

1-(9-Benzyl-6-dimethylamino-purin-2-yl)-3-(4-ethoxy-phenyl)-urea (4.18). Compound **2.7** (0.10 g, 0.37 mmol) and 4-ethoxyphenylisocyanate (0.091 g, 0.56 mmol) were dissolved in dry pyridine and stirred at rt. The reaction was monitored by TLC until complete (no longer than 24 h). The pyridine was removed under reduced pressure and the crude product was purified from recrystallization in EtOH to yield a white solid (0.12 g, 75%). ^{1}H NMR (300 MHz, $CHCl_3$) δ 1.38 (t, 3H, *J* = 6.8 Hz), 3.48 (bs, 6H), 3.98 (q, 2H, *J* = 6.8 Hz), 5.27 (s, 2H), 6.82 (m, 2H), 7.24 (m, 8H), 7.59 (s, 1H), 11.18 (s, 1H). ^{13}C NMR (75 MHz, $CHCl_3$) δ 15.1, 47.4, 63.9, 115.1, 121.9, 127.6, 128.6, 129.3. HRMS calcd for $C_{23}H_{26}N_7O_2$ $[M+H]^+$: 432.2142, found: 432.2164.

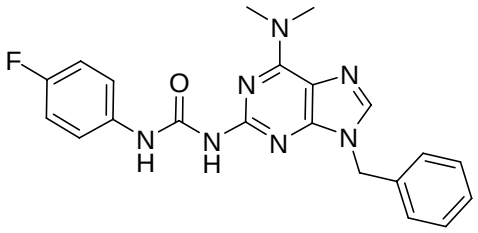

1-(9-Benzyl-6-dimethylamino-purin-2-yl)-3-(4-fluoro-phenyl)-urea (4.19). Compound **2.7** (0.10 g, 0.37 mmol) and 4-fluorophenylisocyanate (0.10 g, 0.75 mmol) were dissolved in dry pyridine (7 mL) and stirred at rt. The reaction was monitored by TLC until complete (no longer than 24 h). The pyridine was removed under reduced pressure and the crude product was purified from recrystallization in EtOH to yield a white solid (0.064 g, 42%). ^{1}H NMR (300 MHz, DMSO-d_6) δ 3.45 (bs, 6H), 5.42 (s, 2H), 7.14 (m, 2H), 7.33 (m, 7H), 8.14 (s, 1H), 9.45 (s,

1H), 11.46 (s, 1H). ^{13}C NMR (75 MHz, DMSO-d_6) δ 46.1, 115.1, 115.42, 120.9, 121.0, 126.8, 127.6, 128.7, 135.0, 136.8, 138.9, 150.2, 151.9, 152.9, 154.1. HRMS calcd for $C_{21}H_{21}FN_7O$ $[M+H]^+$: 406.1792, found: 406.1789.

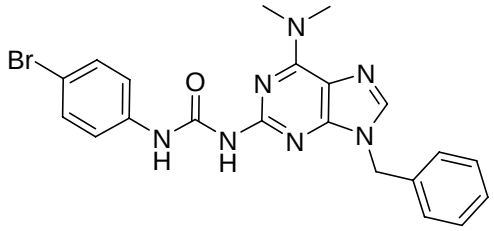

1-(9-Benzyl-6-dimethylamino-purin-2-yl)-3-(4-bromo-phenyl)-urea (4.20). Compound **2.7** (0.10 g, 0.37 mmol) and 4-bromophenylisocyanate (0.11 g, 0.56 mmol) were dissolved in dry pyridine and stirred at rt. The reaction was monitored by TLC until complete (no longer than 24 h). The pyridine was removed under reduced pressure and the crude product was purified from recrystallization in EtOH to yield a white solid (0.13 g, 76%). ^{1}H NMR (300 MHz, DMSO-d_6) δ 3.42 (bs, 6H), 5.43 (s, 2H), 7.30 (m, 9H), 7.15 (s, 1H), 9.53 (s, 1H), 11.54 (s, 1H). ^{13}C NMR (75 MHz, DMSO-d_6) δ 46.1, 114.1, 115.5, 121.1, 126.7, 127.6, 128.7, 131.5, 136.8, 138.03, 139.0, 150.2, 151.7, 152.8, 154.1. HRMS calcd for $C_{22}H_{24}N_7O$ $[M+H]^+$: 466.0985, found: 466.0978.

X-ray Crystallography

General. Data were collected at 173 K on a Siemens SMART PLATFORM equipped with a CCD area detector and a graphite monochromator utilizing MoK_α radiation (λ = 0.71073 Å). Cell parameters were refined using up to 8192 reflections. A full sphere of data (1850 frames) was collected using the ω-scan method (0.3° frame width). The first 50 frames were re-measured at the end of data collection to monitor instrument and crystal stability (maximum correction on I was < 1 %). Absorption corrections by integration were applied based on measured indexed crystal faces. The structure was solved by the Direct Methods in *SHELXTL6,* and refined using full-matrix least squares. The non-H atoms were treated anisotropically,

whereas the hydrogen atoms were calculated in ideal positions and were riding on their respective carbon atoms.

Compound 4.7. The NH_2 protons were obtained from a Difference Fourier map and refined without any constraints. A total of 268 parameters were refined in the final cycle of refinement using 3472 reflections with $I > 2\sigma(I)$ to yield R_1 and wR_2 of 4.42% and 11.01%, respectively. Refinement was done using F^2.

Compound 4.16. A total of 272 parameters were refined in the final cycle of refinement using 3194 reflections with $I > 2\sigma(I)$ to yield R_1 and wR_2 of 3.74% and 9.66%, respectively. Refinement was done using F^2.

APPENDIX A
[1]H NMR SPECTRA OF SELECTED PURINES

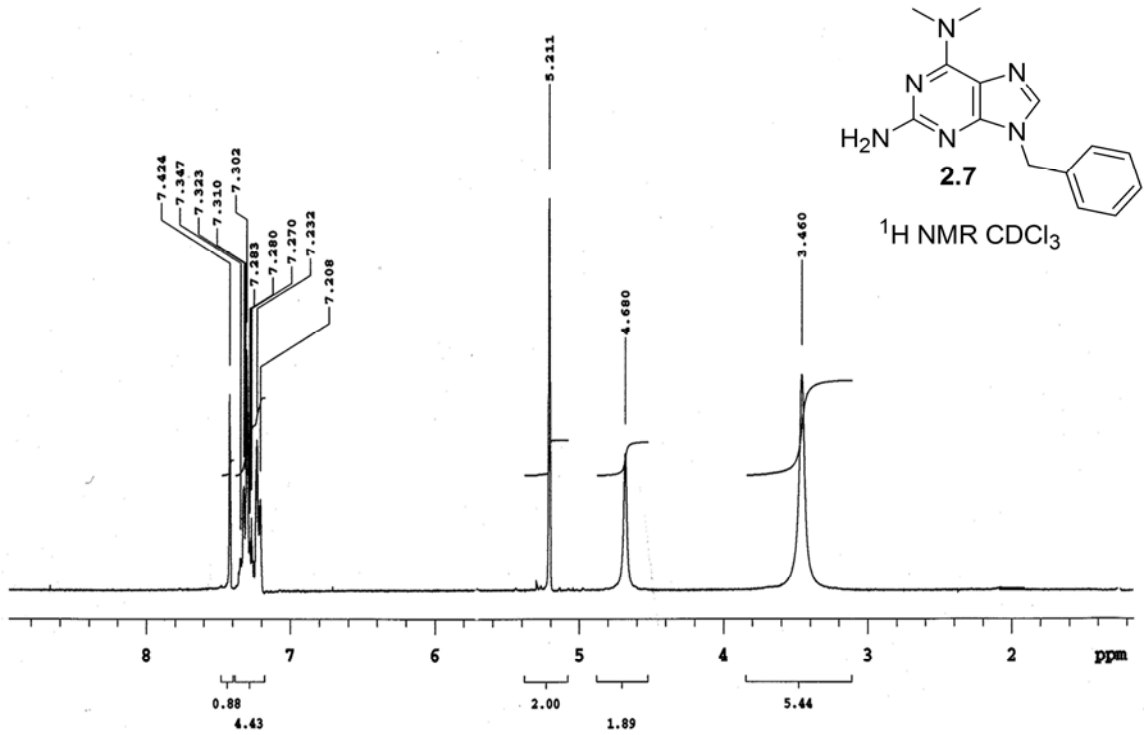

Figure A-1. [1]H NMR of **2.7** in $CHCl_3$.

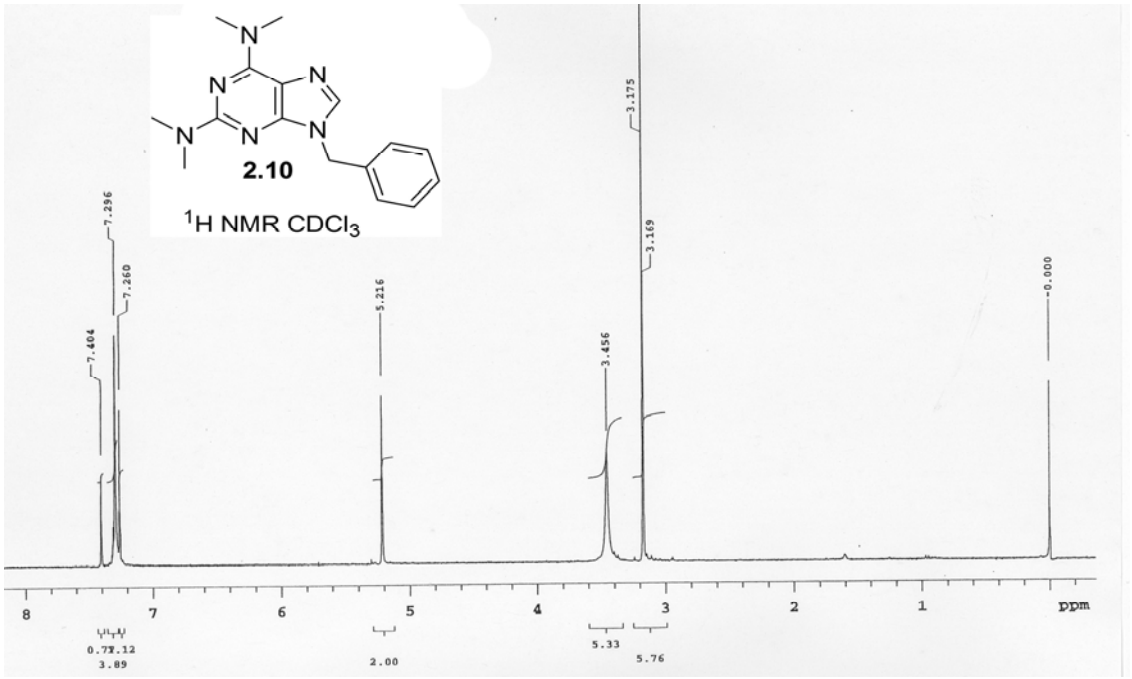

Figure A-2. [1]H NMR of **2.10** in $CHCl_3$.

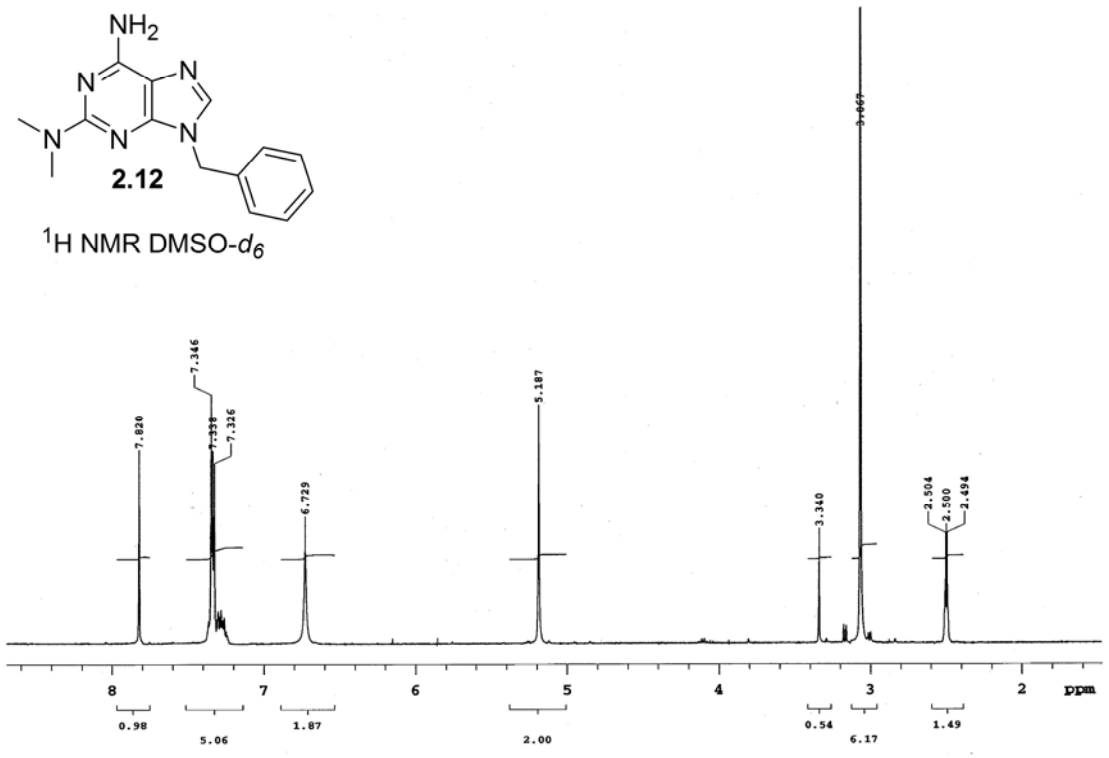

Figure A-3. ^{1}H NMR of **2.12** in DMSO-d_6.

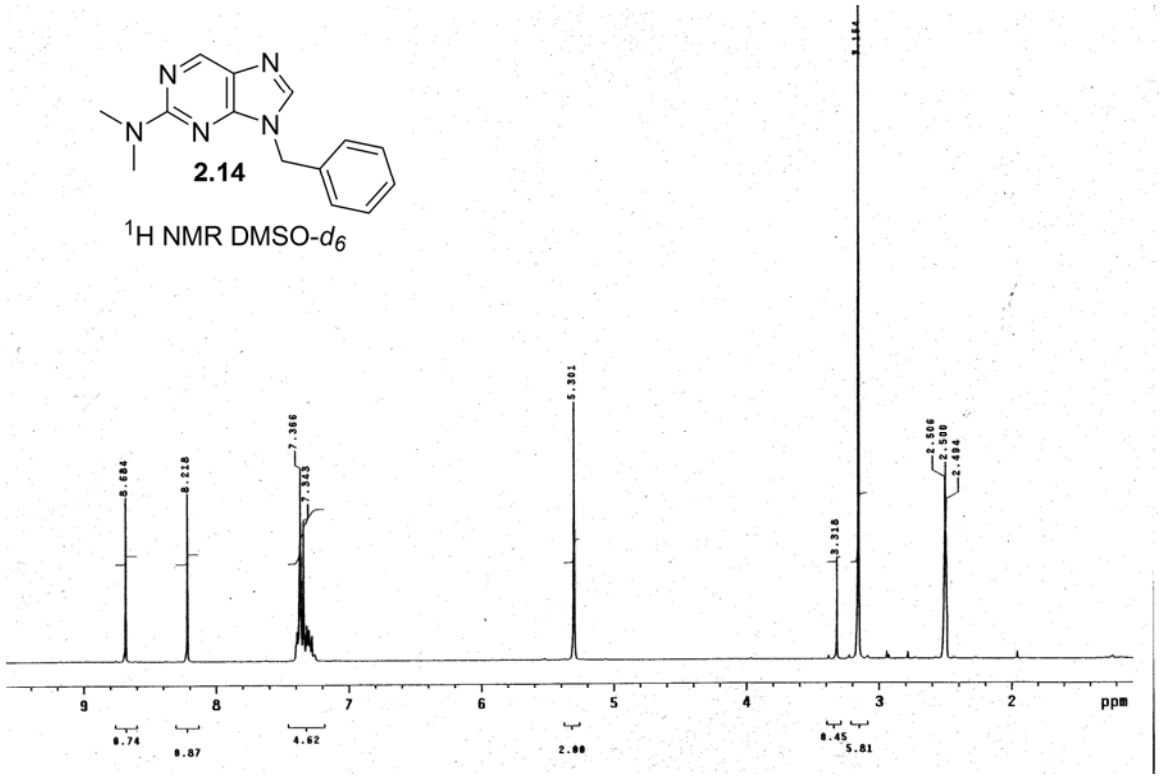

Figure A-4. ^{1}H NMR of **2.14** in DMSO-d_6.

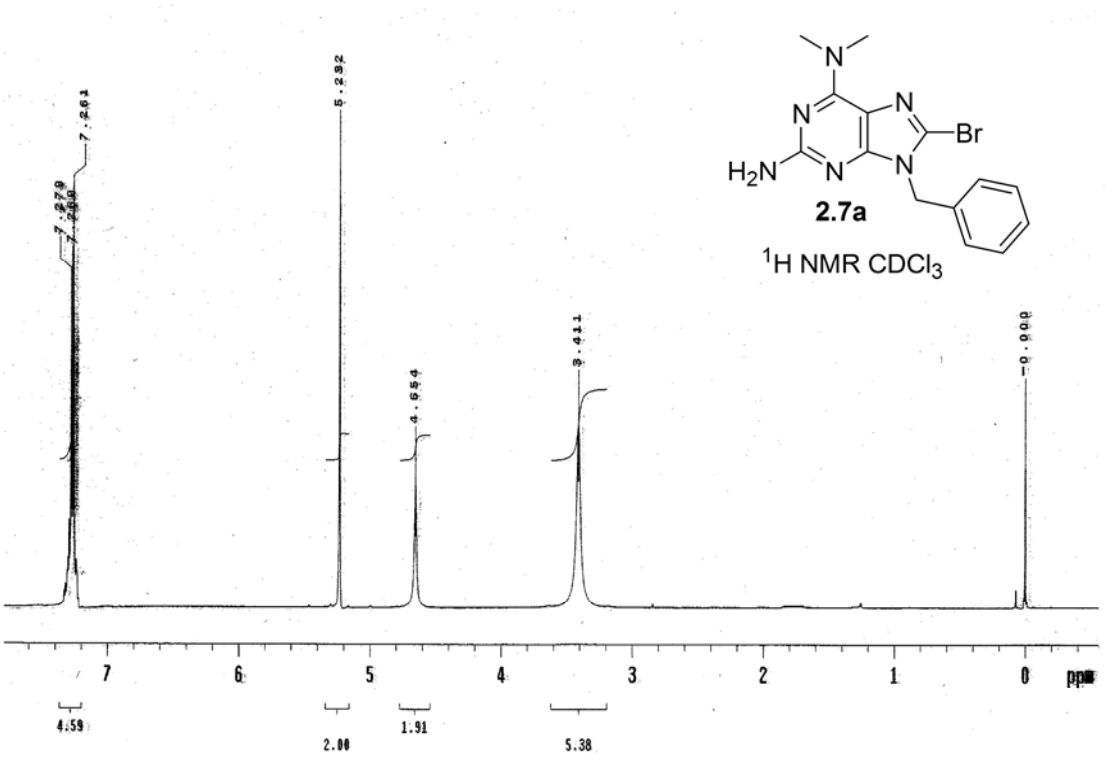

Figure A-5. ^{1}H NMR of **2.7a** in $CHCl_3$.

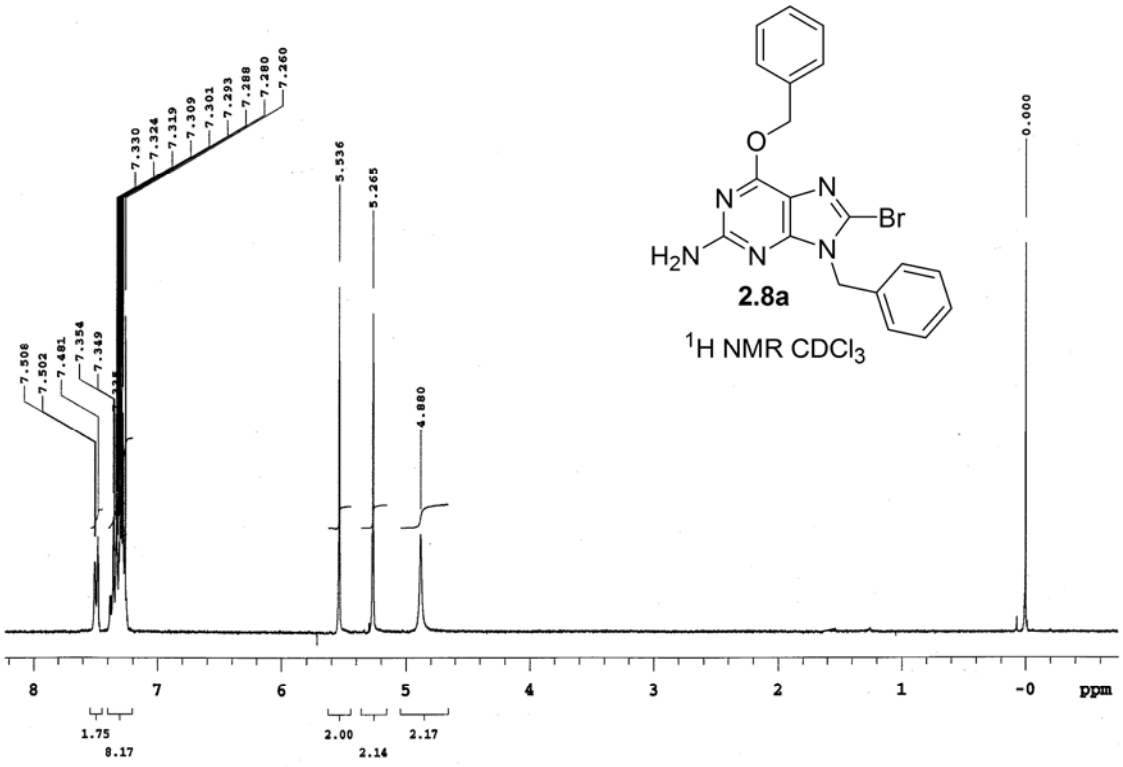

Figure A-6. ^{1}H NMR of **2.8a** in $CHCl_3$.

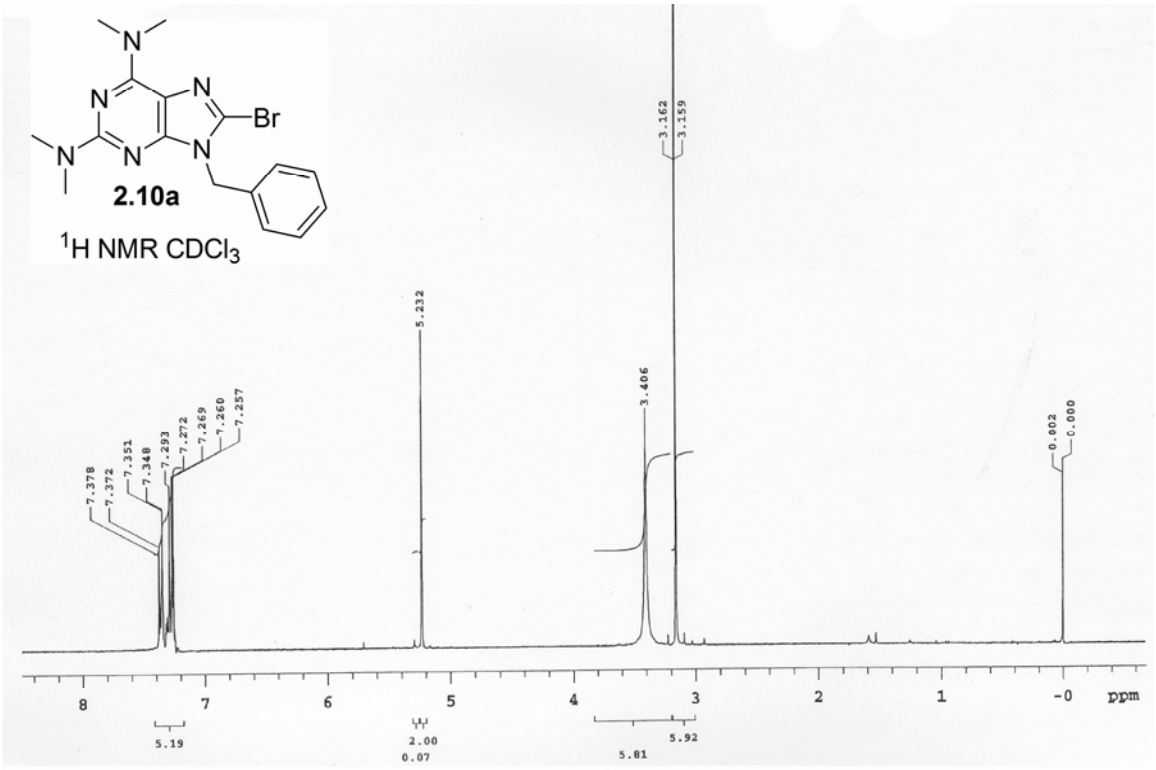

Figure A-7. ^{1}H NMR of **2.10a** in $CHCl_3$.

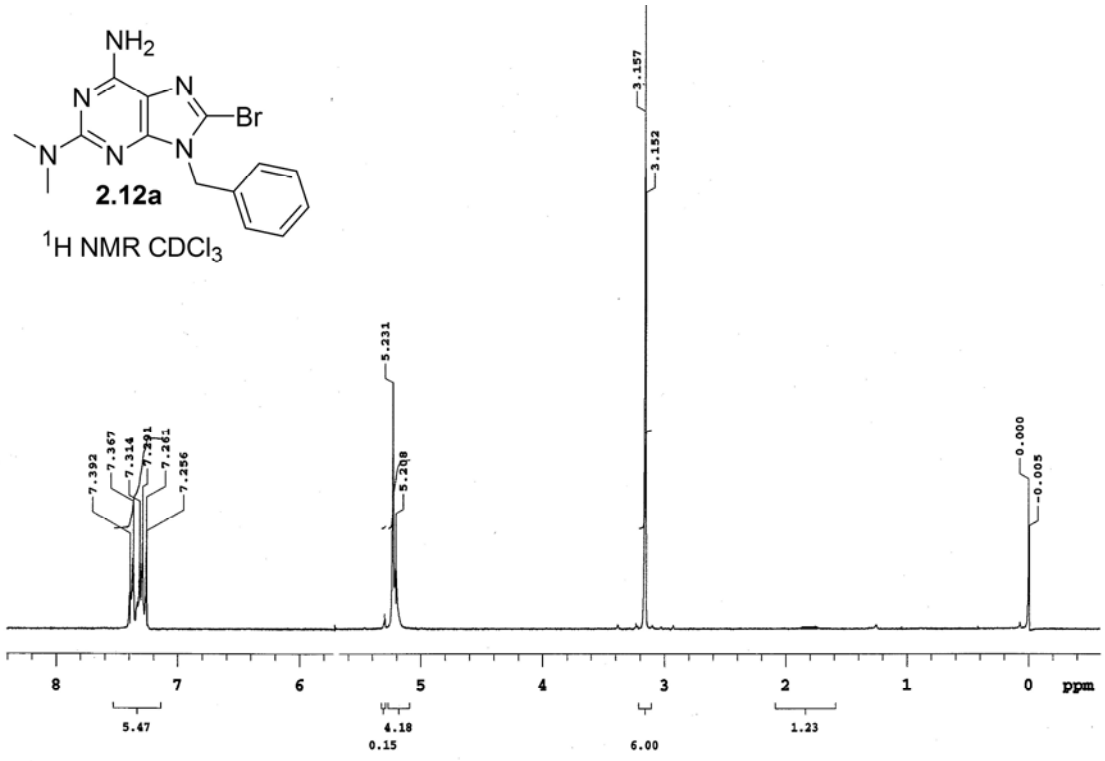

Figure A-8. ^{1}H NMR of **2.12a** in $CHCl_3$.

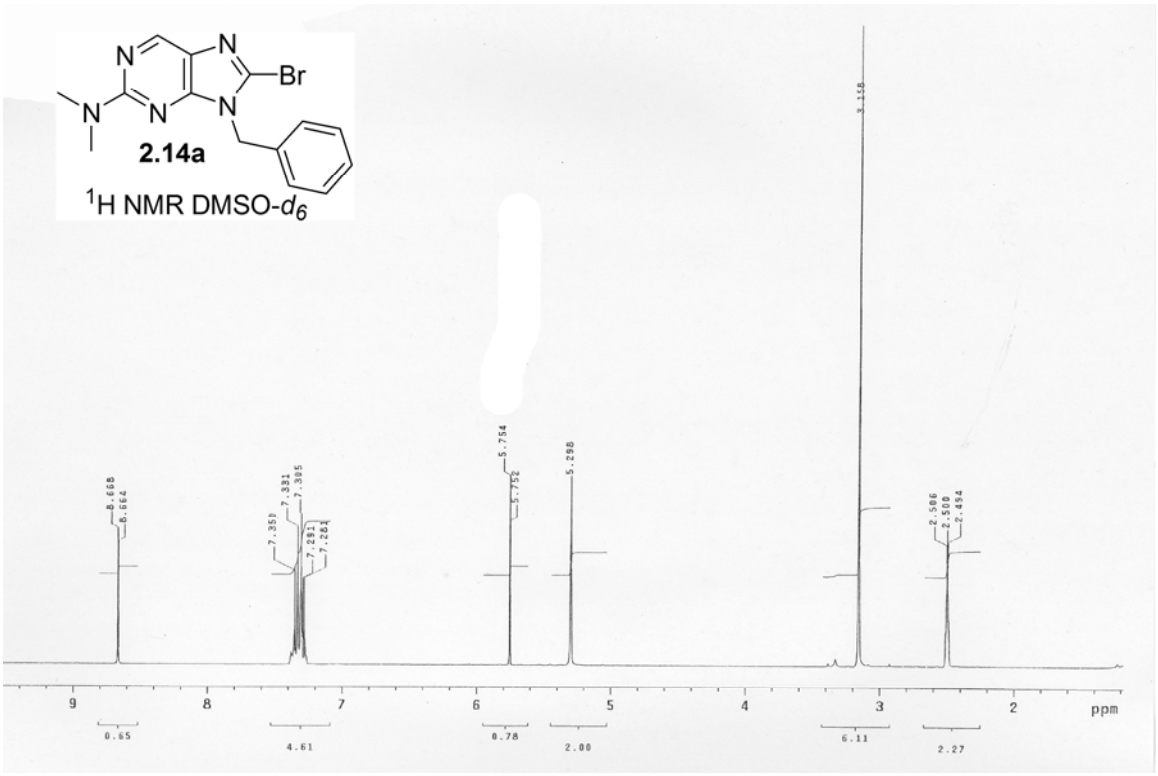

Figure A-9. ^{1}H NMR of **2.14a** in DMSO-d_6.

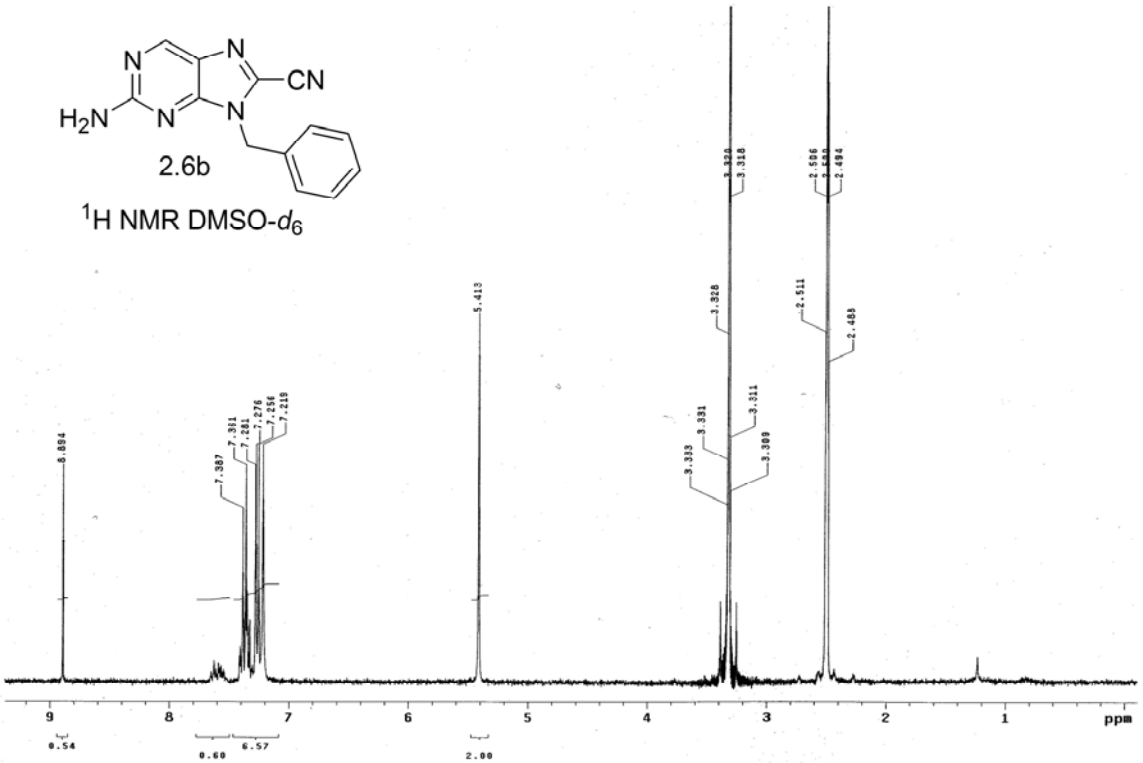

Figure A-10. ^{1}H NMR of **2.6b** in DMSO-d_6.

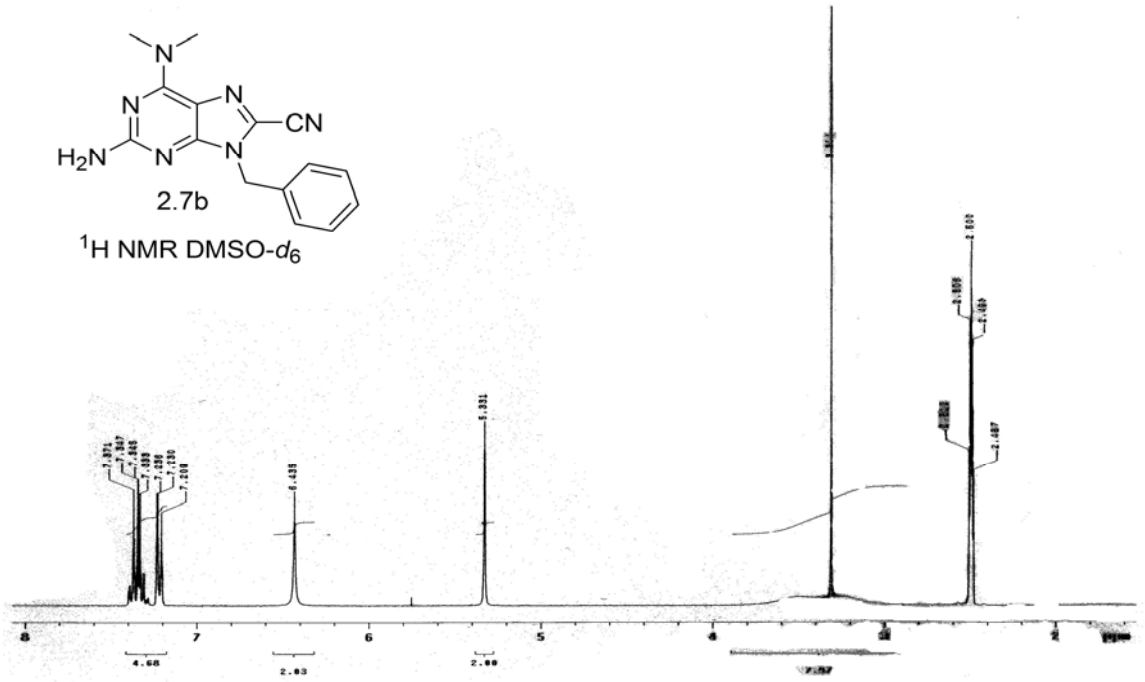

Figure A-11. ^{1}H NMR of **2.7b** in DMSO-d_6.

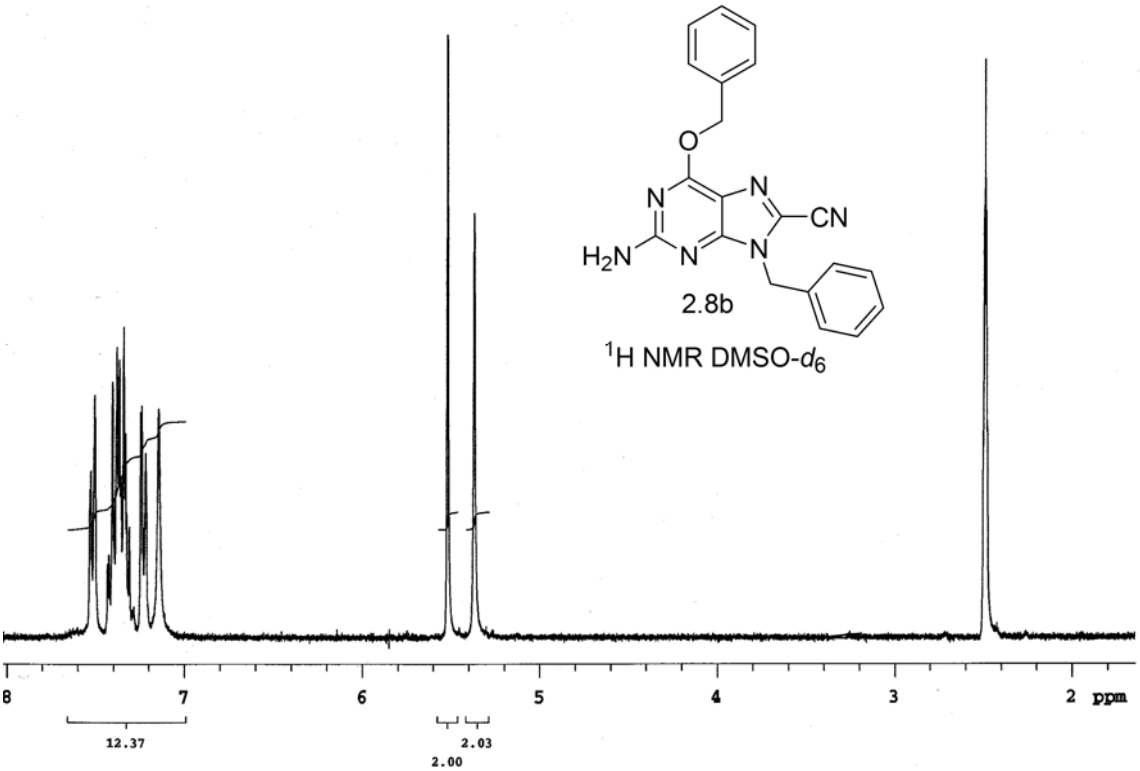

Figure A-12. ^{1}H NMR of **2.8** in DMSO-d_6.

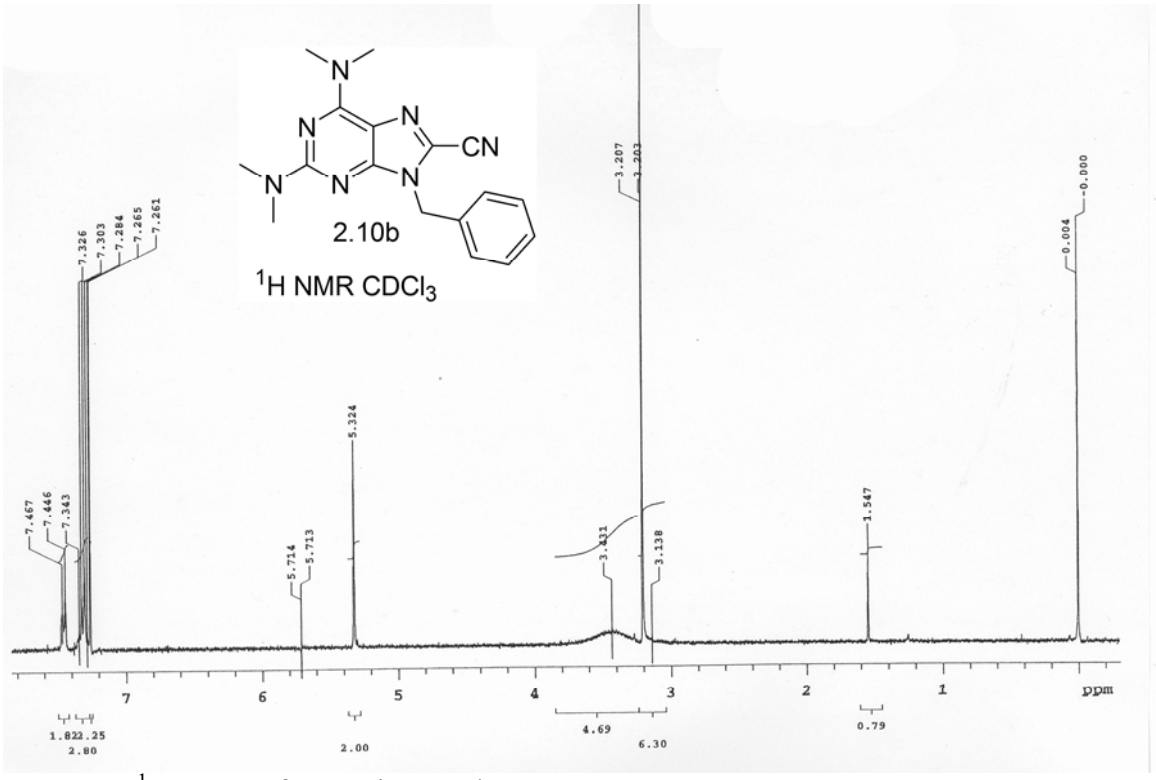

Figure A-13. ^{1}H NMR of **2.10b** in $CHCl_3$.

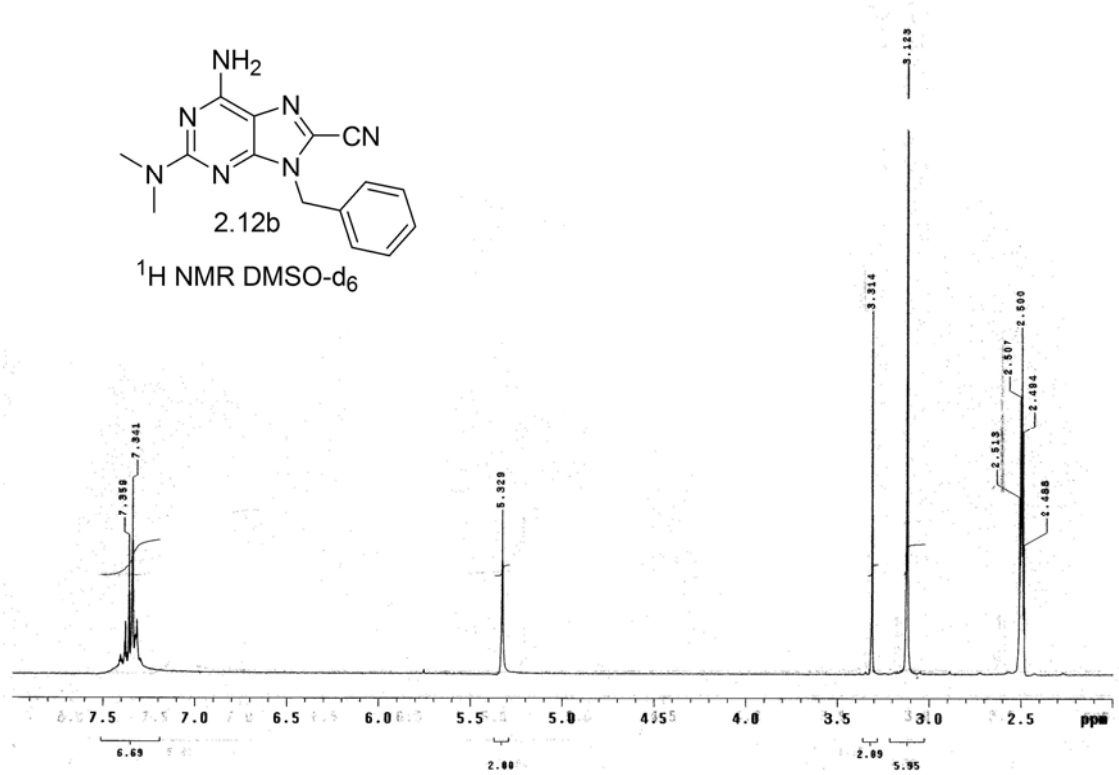

Figure A-14. 1H NMR of 2.12b in DMSO-d6.

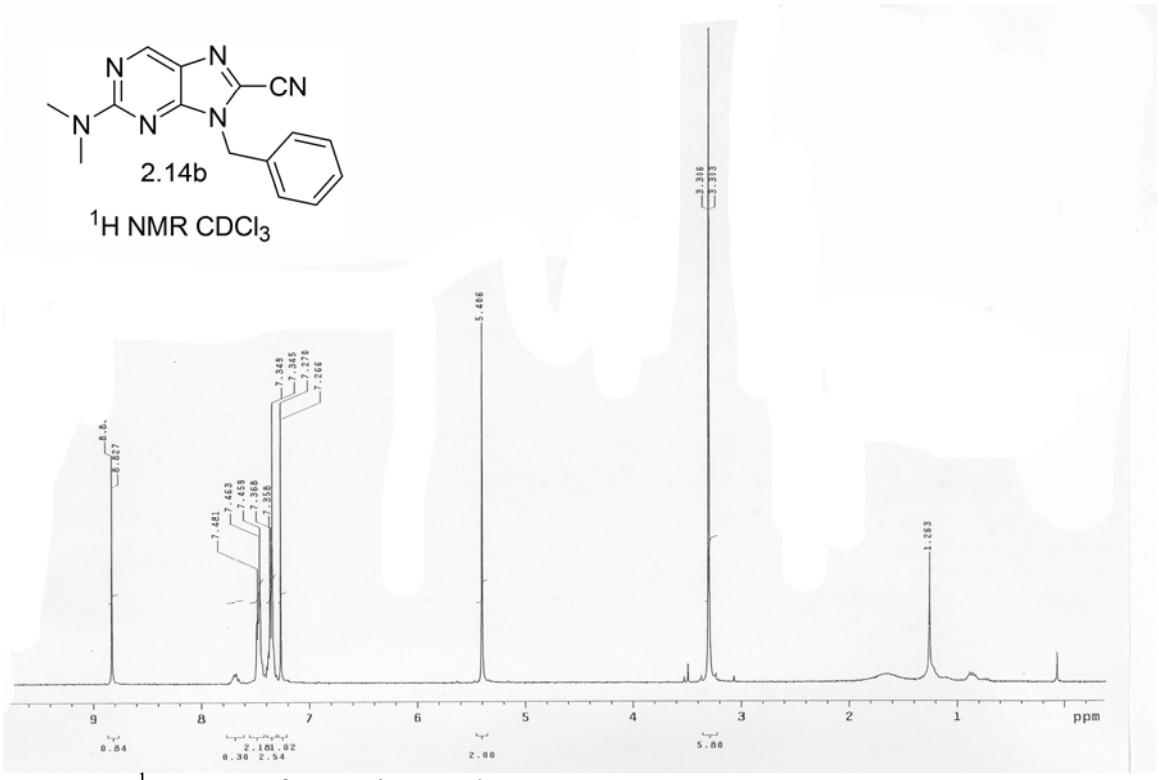

Figure A-15. ^{1}H NMR of **2.14b** in $CHCl_3$.

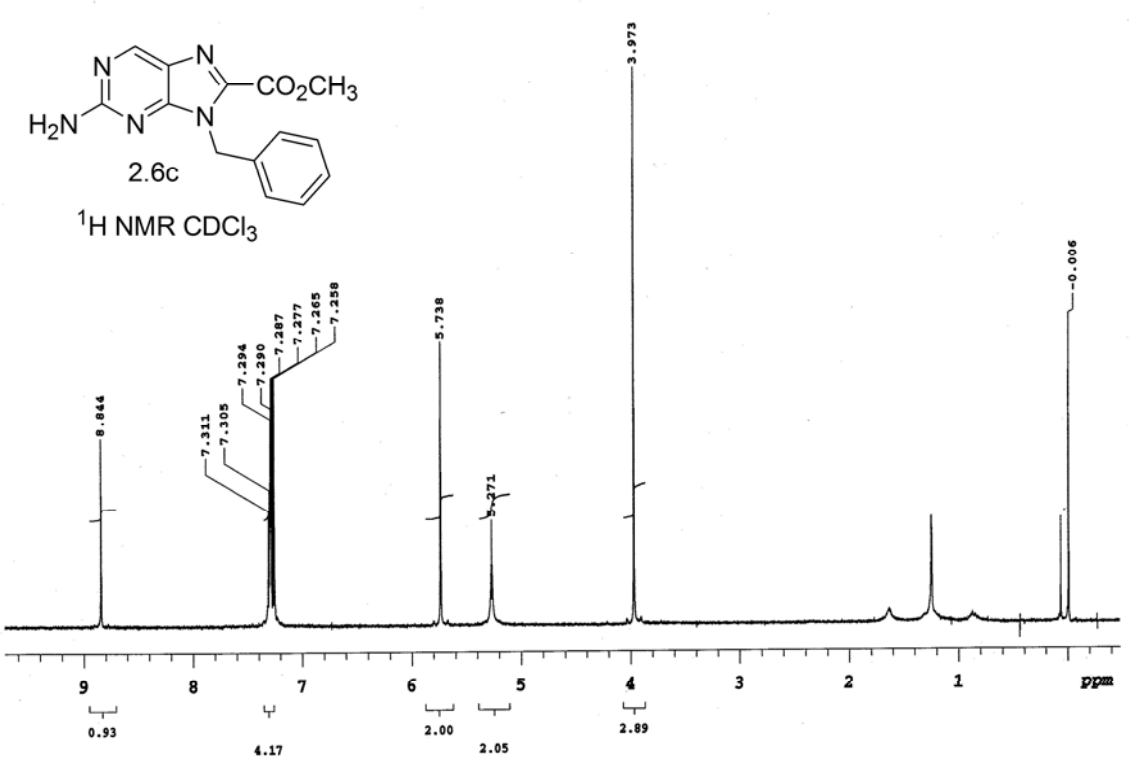

Figure A-16. ^{1}H NMR of **2.6c** in $CHCl_3$.

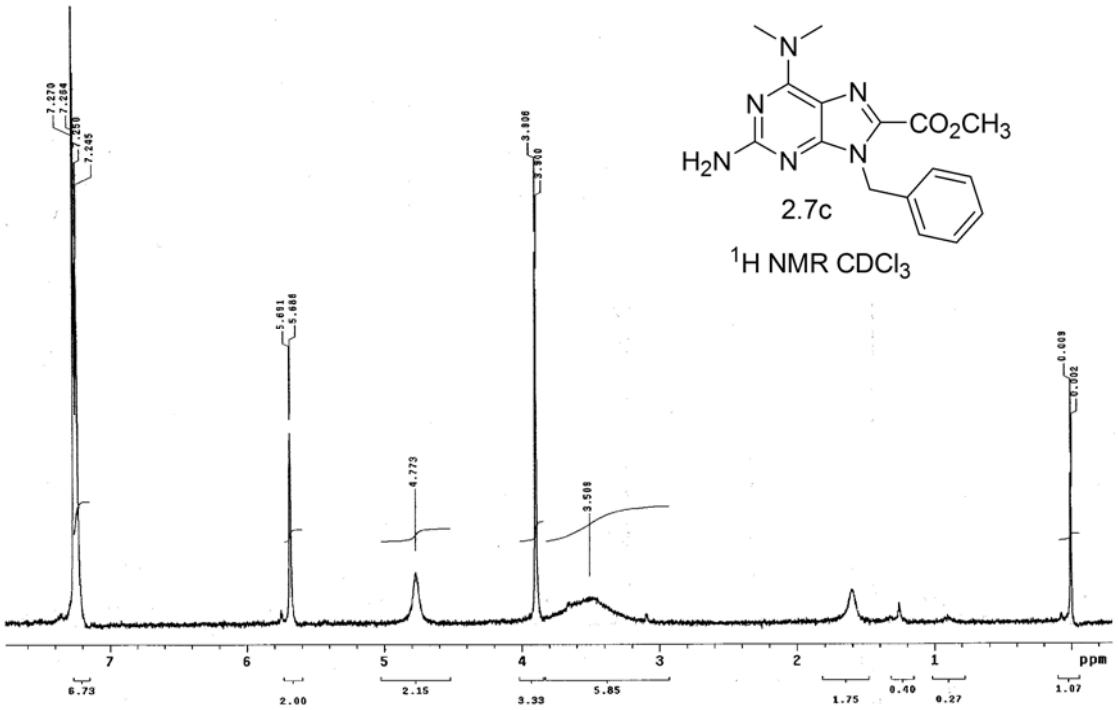

Figure A-17. ^{1}H NMR of **2.7c** in $CHCl_3$.

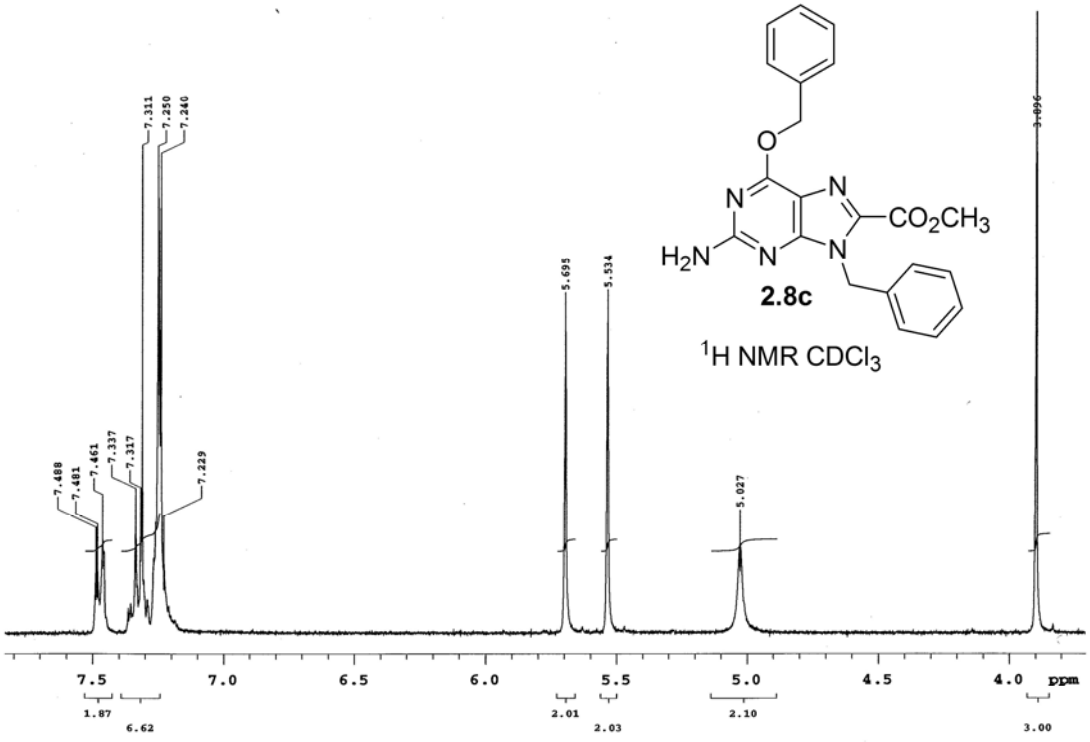

Figure A-18. ^{1}H NMR of **2.8** in $CHCl_3$.

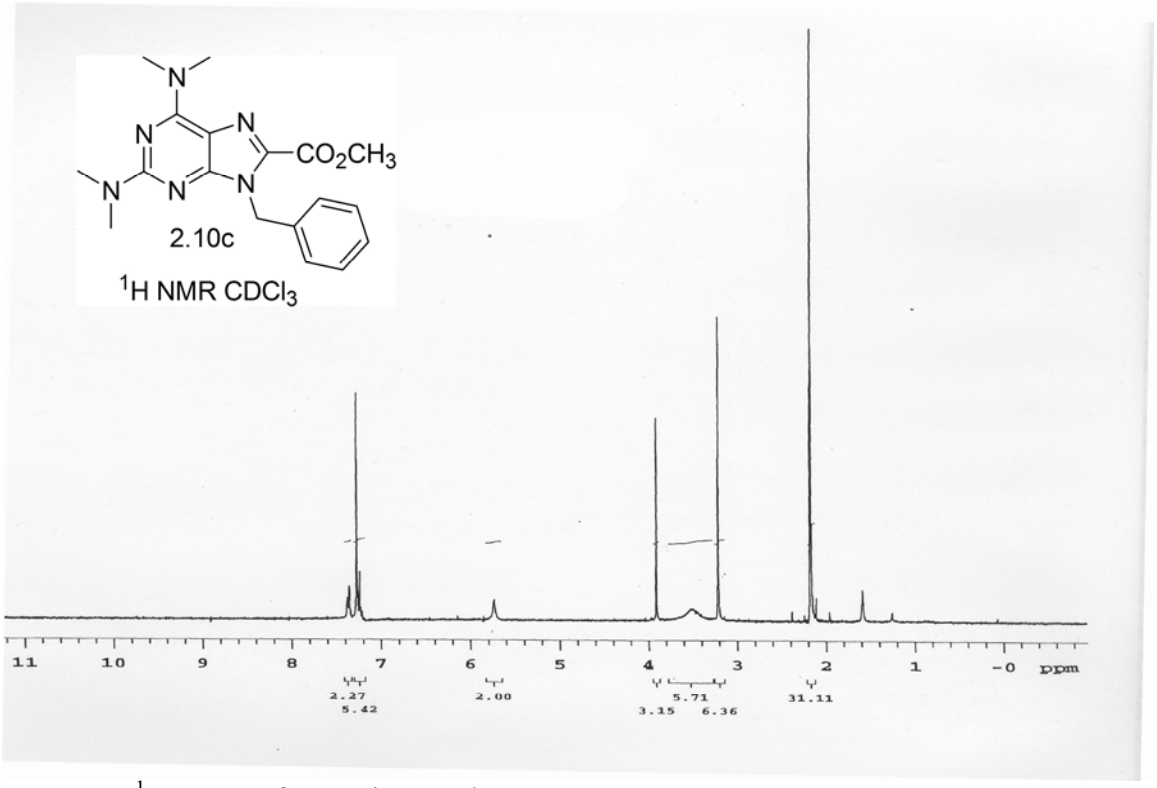

Figure A-19. ^{1}H NMR of **2.10c** in $CHCl_3$.

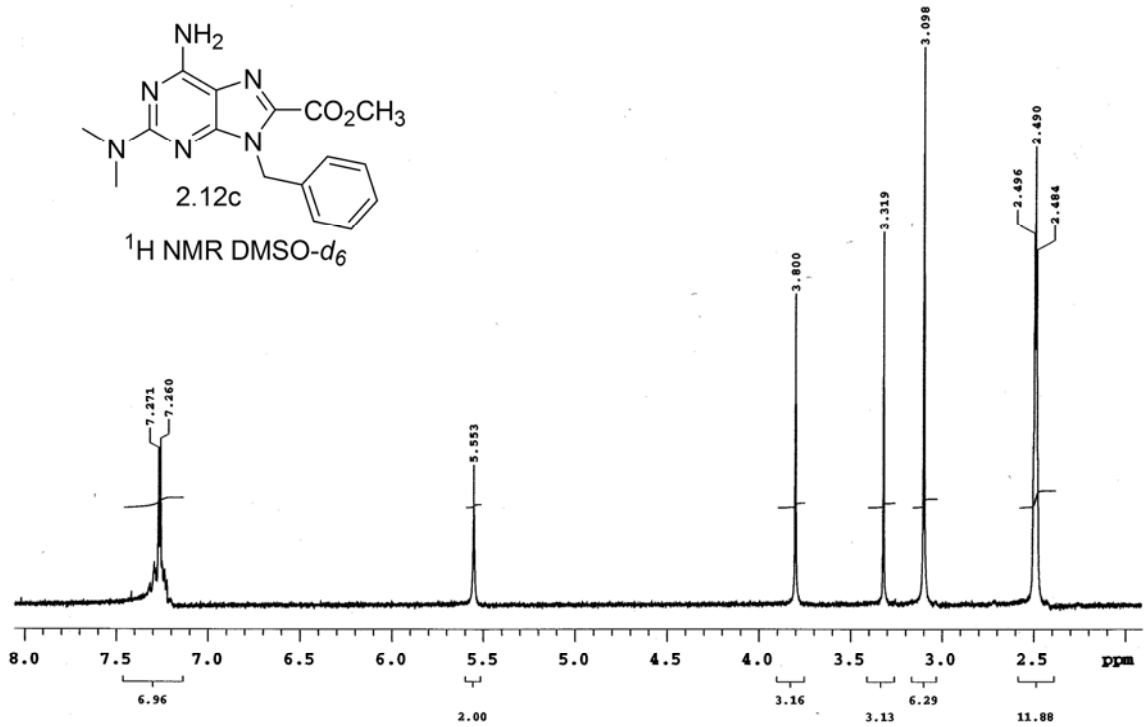

Figure A-20. ^{1}H NMR of **2.12c** in DMSO-d_6.

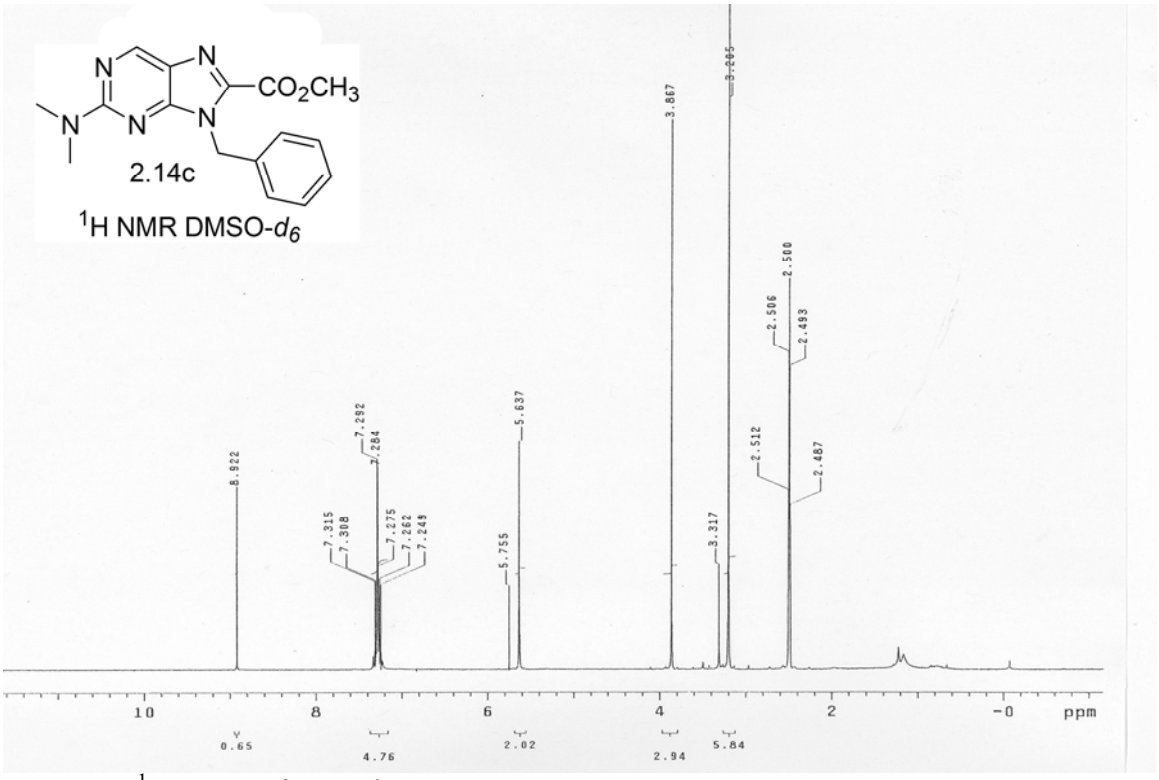

Figure A-21. ^{1}H NMR of **2.14c** in DMSO-d_6.

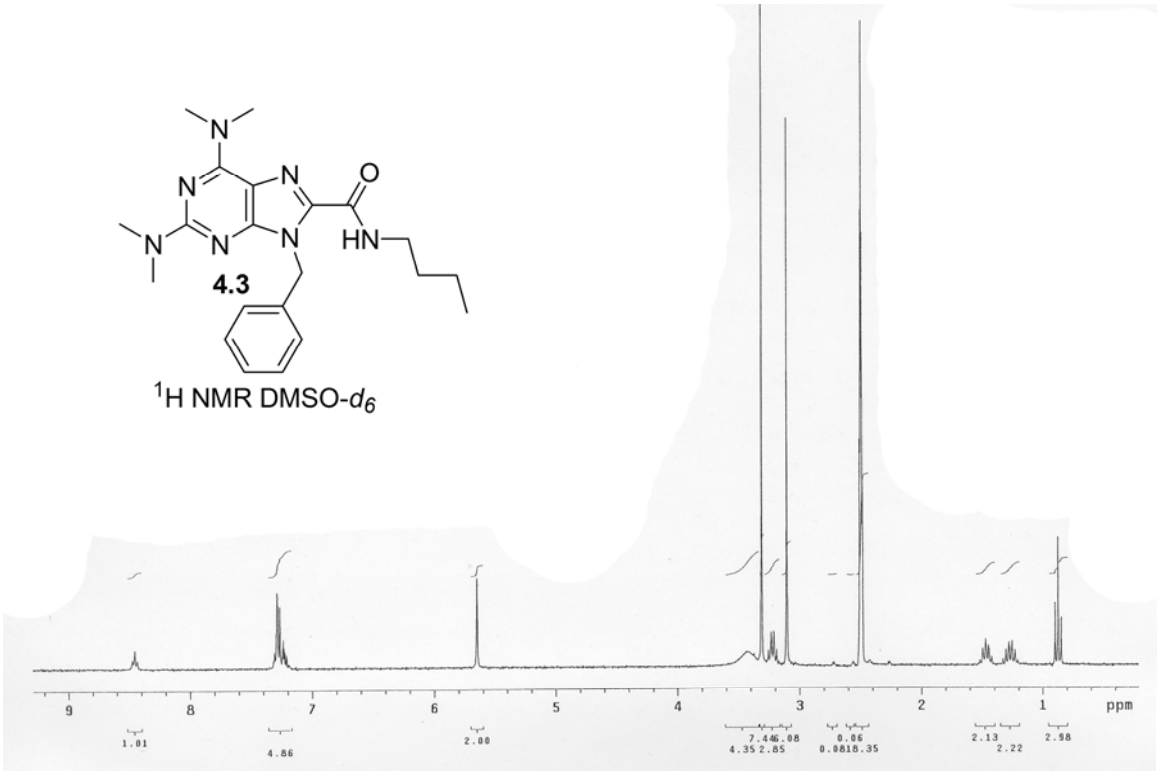

Figure A-22. ^{1}H NMR of **4.3** in DMSO-d_6.

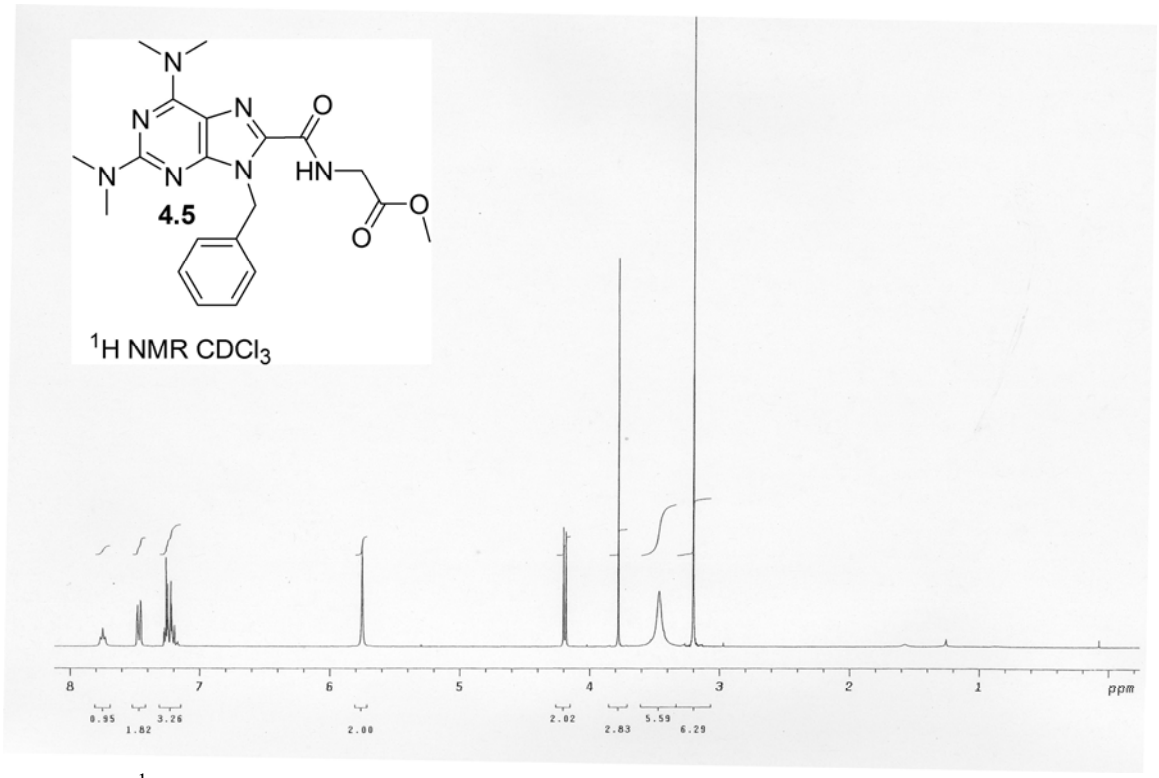

Figure A-23. ^{1}H NMR of **4.5** in $CHCl_3$.

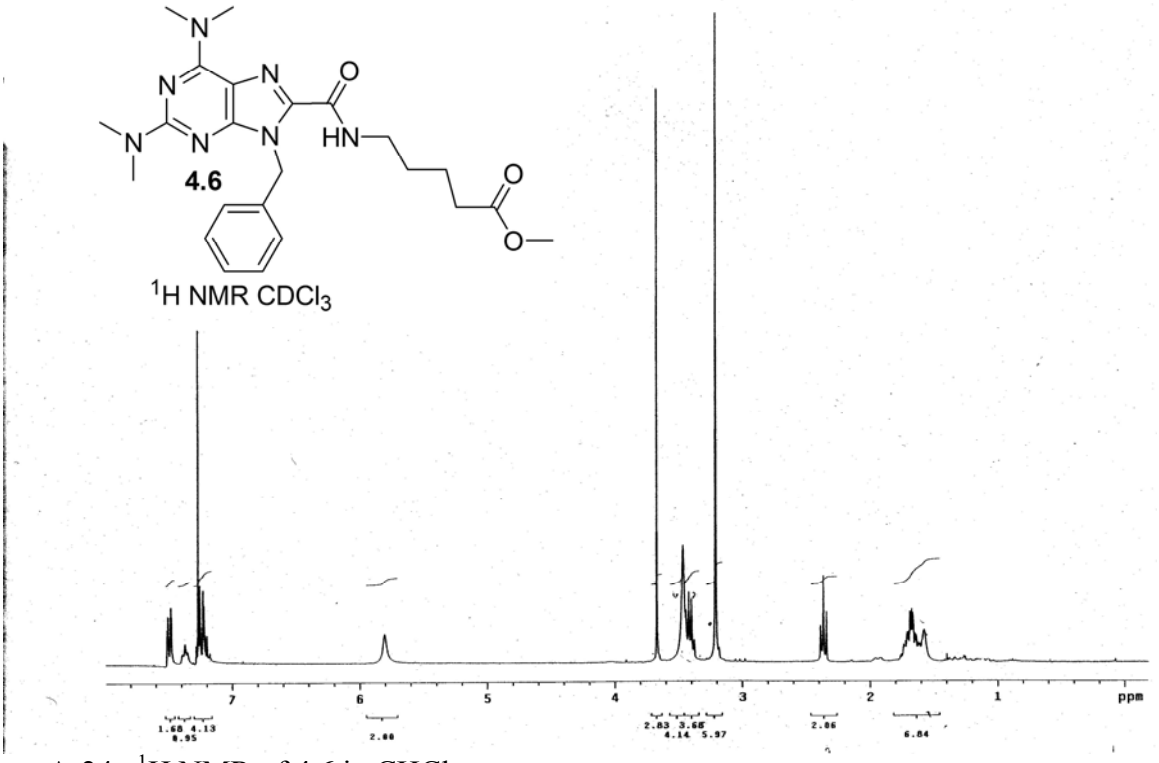

Figure A-24. ^{1}H NMR of **4.6** in $CHCl_3$.

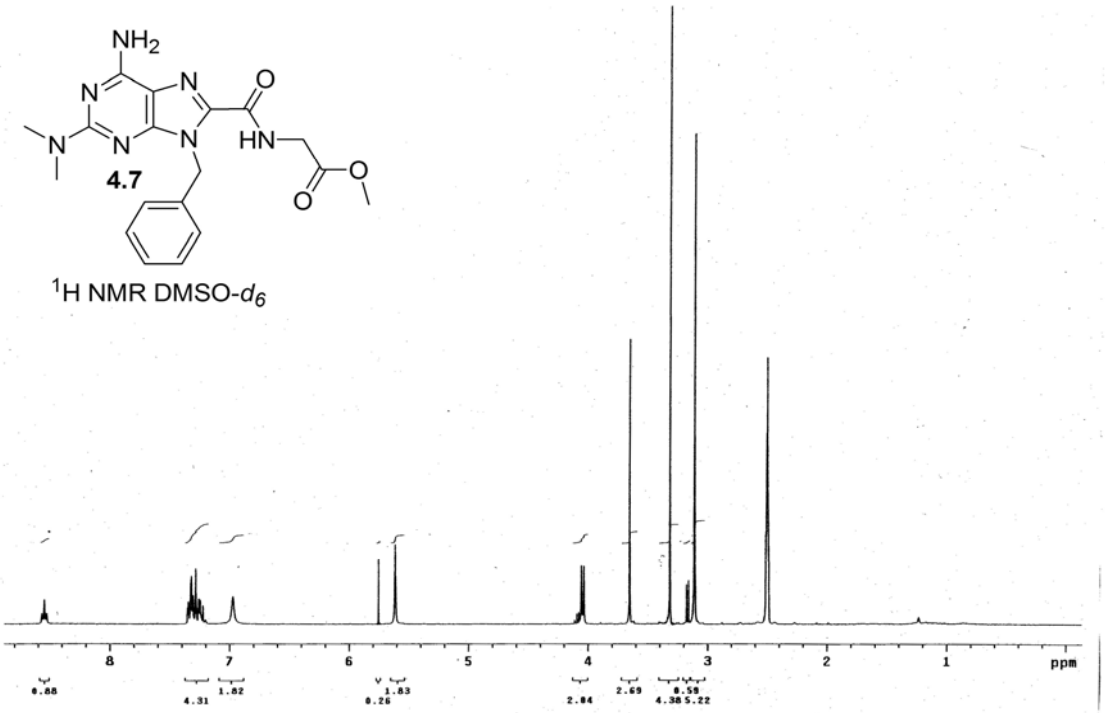

Figure A-25. ^{1}H NMR of **4.7** in DMSO-d_6.

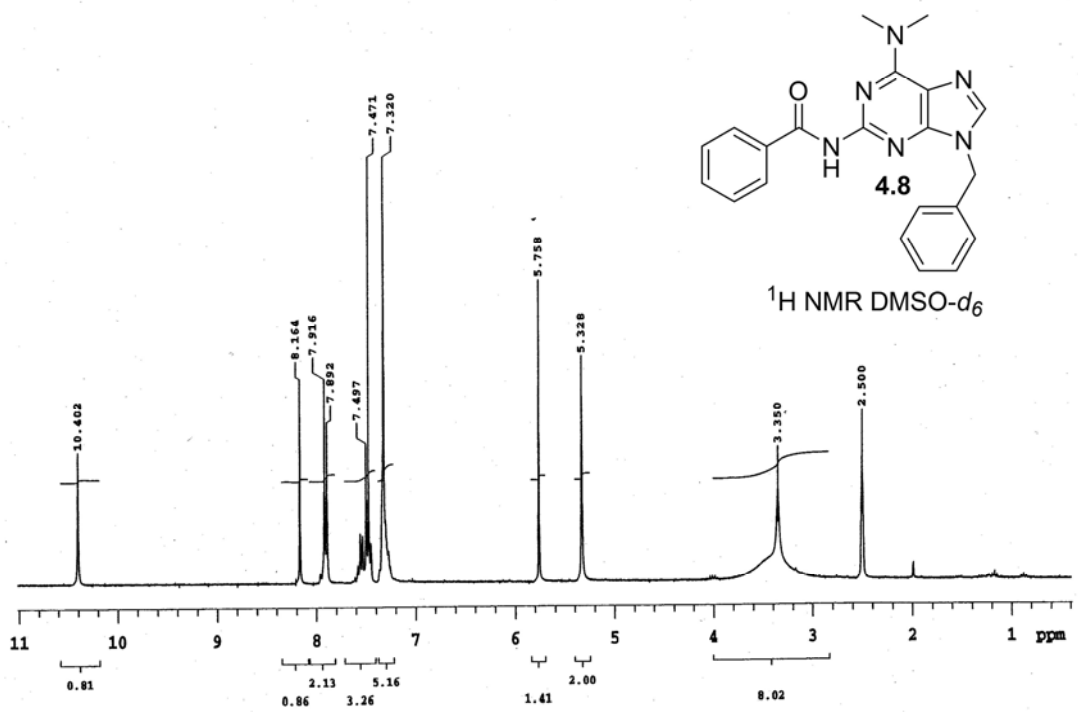

Figure A-26. ^{1}H NMR of **4.8** in DMSO-d_6.

APPENDIX B
X-RAY CRYSTAL STRUCTURE DATA

Table B-1. Crystal Structure Parameters.

Parameters	**2.7b**	**2.12b**	**2.12c**	**4.7**	**4.16**
Empirical formula	$C_{15}H_{15}N_7$	$C_{15}H_{15}N_7$	$C_{16}H_{18}N_6O_2$	$C_{18}H_{21}N_7O_3$	$C_{21}H_{21}N_7O$
Formula weight	293.34	293.34	326.36	383.42	387.45
Temperature K	173(2)	173(2)	173(2)	173(2)	173(2)
Wavelength Å	0.71073	0.71073	0.71073	0.71073	0.71073
Crystal system	Triclinic	Monoclinic	Triclinic	Monoclinic	Monoclinic
Space group	P-1	$P2_1/n$	P-1	$P2_1/n$	P2(1)/n
Unit cell dimensions	a=8.5576(6)Å α=79.739(1)° b=9.1964(7)Å β=74.878(1)° c=10.2811(7)Å γ=65.164(1)°	a=10.0863(8)Å α=0° b=8.6914(7)Å β=98.137(2)° c=16.9812(14)Å γ=90°	A=6.4306(13)Å α=84.052(4)° b=10.050(2)Å β=84.765(3)° c=11.980(2)Å γ=88.383(4)°	a=10.6415(8)Å α=90° b=13.5541(10)Å β= 107.01(1)° c=13.0430(9)Å γ=90°	a=9.0629(6)Å α=90° b=19.8629(1Å β=106.862(1)° c=11.3182(7)Å γ=90°
Volume $Å^3$	706.68(9)	1473.7(2)	766.7(3)	1799.0(2)	1949.9(2)
Z	2	4	2	4	4
Density (calculated) Mg/m^3	1.379	1.322	1.414	1.416	1.320
Absorption coefficient mm^{-1}	0.090	0.087	0.099	0.101	0.087
F(000)	308	616	344	808	816
Crystal size mm^3	0.19 x 0.18 x 0.15	0.21 x 0.19 x 0.15	0.13 x 0.09 x 0.07	0.32 x 0.08 x 0.06	0.19 x 0.18 x 0.17
Theta range for data collection	2.06 to 27.49°	2.22 to 27.50°	1.72 to 27.50°	2.18 to 27.49°.	2.05 to 27.49°
Index ranges	$-11\le h\le 9$, $-11\le k\le 8$, $-13\le l\le 12$	$-13\le h\le 13$, $-10\le k\le 11$, $-10\le l\le 21$	$-8\le h\le 8$, $-7\le k\le 13$, $-13\le l\le 15$	$-13\le h\le 13$, $-15\le k\le 17$, $-16\le l\le 16$	$-11\le h\le 10$, $-25\le k\le 20$, $-14\le l\le 14$
Reflections collected	4656	9095	5277	12006	12603

Table B-1. Continued					
Independent reflections	3099 [R(int) = 0.0258]	3304 [R(int) = 0.0615]	3445 [R(int) = 0.0248]	4125 [R(int) = 0.0418]	4406 [R(int) = 0.0337]
Completeness to theta = 27.49°	95.4 %	97.6 %	97.7 %	99.7 %	98.5 %
Absorption correction	Integration	Integration	Integration	Integration	Integration
Max. and min. transmission	0.9894 and 0.9819	0.9895 and 0.9803	0.9931 and 0.9873	0.9941 and 0.9756	0.9943 and 0.9800
Refinement method	Full-matrix least-squares on F^2	Full-matrix least-squares on F^2	Full-matrix least-squares on F^2	Full-matrix least-squares on F^2	Full-matrix least-squares on F^2
Data / restraints / parameters	3099 / 0 / 208	3304 / 0 / 207	3445 / 0 / 227	4125 / 0 / 268	4406 / 0 / 272
Goodness-of-fit on F^2	1.032	1.048	1.029	1.064	1.063
Final R indices [I>2sigma(I)]	R1 = 0.0383, wR2 = 0.1027 [2624]	R1 = 0.0475, wR2 = 0.1200 [2770]	R1 = 0.0392, wR2 = 0.0982 [2572]	R1 = 0.0442, wR2 = 0.1101 [3472]	R1 = 0.0374, wR2 = 0.0966 [3194]
R indices (all data)	R1 = 0.0450, wR2 = 0.1065	R1 = 0.0569, wR2 = 0.1269	R1 = 0.0550, wR2 = 0.1046	R1 = 0.0545, wR2 = 0.1162	R1 = 0.0572, wR2 = 0.1038
Largest diff. peak and hole e.Å^{-3}	0.229 and -0.266	0.275 and -0.228	0.200 and -0.228	0.304 and -0.206	0.185 and -0.176

LIST OF REFERENCES

(1) Jones, M. *Organic Chemistry*; second ed.; W. W. Norton & Compny, Inc: New York, 2000.

(2) Lakowicz, J. R. *Principles of Fluorescence Spectroscopy*; Third ed.; Springer Science+Buisness Media: New York, 2006.

(3) Dawson, W. R.; Windsor, M. W. *J. Phys. Chem.* **1968**, *72*, 3251-&.

(4) Meier, H. *Angew. Chem. Int. Ed.* **2005**, *44*, 2482-2506.

(5) Wolff, J. J.; Wortmann, R. In *Advances in Physical Organic Chemistry, Vol 32* 1999, p 121-217.

(6) Dimitrakopoulos, C. D.; Malenfant, P. R. L. *Adv. Mater.* **2002**, *14*, 99-+.

(7) Friend, R. H.; Gymer, R. W.; Holmes, A. B.; Burroughes, J. H.; Marks, R. N.; Taliani, C.; Bradley, D. D. C.; Dos Santos, D. A.; Bredas, J. L.; Logdlund, M.; Salaneck, W. R. *Nature* **1999**, *397*, 121-128.

(8) Hoeben, F. J. M.; Jonkheijm, P.; Meijer, E. W.; Schenning, A. *Chem. Rev.* **2005**, *105*, 1491-1546.

(9) Meijer, E. W.; Schenning, A. *Nature* **2002**, *419*, 353-354.

(10) Krueger, A. T.; Lu, H. G.; Lee, A. H. F.; Kool, E. T. *Acc. Chem. Res.* **2007**, *40*, 141-150.

(11) Sivakova, S.; Rowan, S. J. *Chem. Soc. Rev.* **2005**, *34*, 9-21.

(12) Brunsveld, L.; Folmer, B. J. B.; Meijer, E. W.; Sijbesma, R. P. *Chem. Rev.* **2001**, *101*, 4071-4097.

(13) Sijbesma, R. P.; Meijer, E. W. *Chem. Commun.* **2003**, 5-16.

(14) Bosman, A. W.; Brunsveld, L.; Folmer, B. J. B.; Sijbesma, R. P.; Meijer, E. W. *Macromol. Symp.* **2003**, *201*, 143-154.

(15) Sijbesma, R. P.; Beijer, F. H.; Brunsveld, L.; Folmer, B. J. B.; Hirschberg, J.; Lange, R. F. M.; Lowe, J. K. L.; Meijer, E. W. *Science* **1997**, *278*, 1601-1604.

(16) Beijer, F. H.; Sijbesma, R. P.; Kooijman, H.; Spek, A. L.; Meijer, E. W. *J. Am. Chem. Soc.* **1998**, *120*, 6761-6769.

(17) Beijer, F. H.; Kooijman, H.; Spek, A. L.; Sijbesma, R. P.; Meijer, E. W. *Angew. Chem. Int. Ed.* **1998**, *37*, 75-78.

(18) Söntjens, S. H. M.; Sijbesma, R. P.; van Genderen, M. H. P.; Meijer, E. W. *J. Am. Chem. Soc.* **2000**, *122*, 7487-7493.

(19) Ward, D. C.; Reich, E.; Stryer, L. *J. Biol. Chem.* **1969**, *244*, 1228-1237.

(20) Rist, M. J.; Marino, J. P. *Curr. Org. Chem.* **2002**, *6*, 775-793.

(21) Wan, C. Z.; Fiebig, T.; Schiemann, O.; Barton, J. K.; Zewail, A. H. *Proc. Natl. Acad. Sci. U. S. A.* **2000**, *97*, 14052-14055.

(22) Kelley, S. O.; Barton, J. K. *Science* **1999**, *283*, 375-381.

(23) Xu, D. G.; Nordlund, T. M. *Biophys. J.* **2000**, *78*, 1042-1058.

(24) Martí, A. A.; Jockusch, S.; Li, Z.; Ju, J.; Turro, N. J. *Nucleic Acids Res.* **2006**, *34*, e50.

(25) Kawai, M.; Lee, M. J.; Evans, K. O.; Nordlund, T. M. *J. Fluoresc.* **2001**, *11*, 23-32.

(26) Rachofsky, E. L.; Osman, R.; Ross, J. B. A. *Biochemistry* **2001**, *40*, 946-956.

(27) Jean, J. M.; Hall, K. B. *Proc. Natl. Acad. Sci. U. S. A.* **2001**, *98*, 37-41.

(28) Gaied, N. B.; Glasser, N.; Ramalanjaona, N.; Beltz, H.; Wolff, P.; Marquet, R.; Burger, A.; Mély, Y. *Nucleic Acids Res.* **2005**, *33*, 1031-1039.

(29) Secrist, J. A.; Weber, G.; Leonard, N. J.; Barrio, J. R. *Biochemistry* **1972**, *11*, 3499-&.

(30) Secrist, J. A.; Barrio, J. R.; Leonard, N. J. *Science* **1972**, *175*, 646-&.

(31) Scopes, D. I. C.; Barrio, J. R.; Leonard, N. J. *Science* **1977**, *195*, 296-298.

(32) Firth, A. G.; Fairlamb, I. J. S.; Darley, K.; Baumann, C. G. *Tetrahedron Lett.* **2006**, *47*, 3529-3533.

(33) Greco, N. J.; Tor, Y. *Tetrahedron* **2007**, *63*, 3515-3527.

(34) Strässler, C.; Davis, N. E.; Kool, E. T. *Helv. Chim. Acta* **1999**, *82*, 2160-2171.

(35) Ren, R. X. F.; Chaudhuri, N. C.; Paris, P. L.; Rumney, S.; Kool, E. T. *J. Am. Chem. Soc.* **1996**, *118*, 7671-7678.

(36) Kool, E. T. *Acc. Chem. Res.* **2002**, *35*, 936-943.

(37) Wilson, J. N.; Kool, E. T. *Org. Biomol. Chem.* **2006**, *4*, 4265-4274.

(38) Kim, S. J.; Kool, E. T. *J. Am. Chem. Soc.* **2006**, *128*, 6164-6171.

(39) Giorgi, T.; Grepioni, F.; Manet, I.; Mariani, P.; Masiero, S.; Mezzina, E.; Pieraccini, S.; Saturni, L.; Spada, G. P.; Gottarelli, G. *Chem. Eur. J.* **2002**, *8*, 2143-2152.

(40) Maruccio, G.; Visconti, P.; Arima, V.; D'Amico, S.; Blasco, A.; D'Amone, E.; Cingolani, R.; Rinaldi, R.; Masiero, S.; Giorgi, T.; Gottarelli, G. *Nano Letters* **2003**, *3*, 479-483.

(41) Gellert, M.; Lipsett, M. N.; Davies, D. R. *Proc. Natl. Acad. Sci. U. S. A.* **1962**, *48*, 2013-&.

(42) Davis, J. T. *Angew. Chem. Int. Ed.* **2004**, *43*, 668-698.

(43) Wong, A.; Ida, R.; Spindler, L.; Wu, G. *J. Am. Chem. Soc.* **2005**, *127*, 6990-6998.

(44) Cai, M.; Marlow, A. L.; Fettinger, J. C.; Fabris, D.; Haverlock, T. J.; Moyer, B. A.; Davis, J. T. *Angew. Chem. Int. Ed.* **2000**, *39*, 1283-+.

(45) Otero, R.; Schock, M.; Molina, L. M.; Laegsgaard, E.; Stensgaard, I.; Hammer, B.; Besenbacher, F. *Angew. Chem. Int. Ed.* **2005**, *44*, 2270-2275.

(46) Igi, M.; Hayashi, T.; Eur. Pat.,: EP 543095, 1993.

(47) Holý, A.; Günter, J.; Dvoráková, H.; Masojídková, M.; Andrei, G.; Snoeck, R.; Balzarini, J.; De Clercq, E. *J. Med. Chem.* **1999**, *42*, 2064-2086.

(48) Wasserfallen, D.; Kastler, M.; Pisula, W.; Hofer, W. A.; Fogel, Y.; Wang, Z. H.; Mullen, K. *J. Am. Chem. Soc.* **2006**, *128*, 1334-1339.

(49) Liu, F.; Dalhus, B.; Gundersen, L.-L.; Rise, F. *Acta Chem. Scand.* **1999**, *53*, 269-279.

(50) Kelley, J. L.; Linn, J. A.; Selway, J. W. T. *J. Med. Chem.* **1989**, *32*, 218-224.

(51) Linn, J. A.; McLean, E. W.; Kelley, J. L. *J. Chem. Soc., Chem. Commun.* **1994**, 913-914.

(52) Francom, P.; Janeba, Z.; Shibuya, S.; Robins, M. J. *J. Org. Chem.* **2002**, *67*, 6788-6796.

(53) Kurimoto, A.; Ogino, T.; Ichii, S.; Isobe, Y.; Tobe, M.; Ogita, H.; Takaku, H.; Sajiki, H.; Hirota, K.; Kawakami, H. *Bioorg. Med. Chem.* **2003**, *11*, 5501-5508.

(54) Ellis, G. P.; Romneyalexander, T. M. *Chem. Rev.* **1987**, *87*, 779-794.

(55) Matsuda, A.; Nomoto, Y.; Ueda, T. *Chem. Pharm. Bull.* **1979**, *27*, 183-192.

(56) Ho, C. Y.; Kukla, M. J. *Bioorg. Med. Chem. Lett.* **1991**, *1*, 531-534.

(57) Tanji, K.; Higashino, T. *Heterocycles* **1990**, *30*, 435-440.

(58) Nair, V.; Purdy, D. F. *Tetrahedron* **1991**, *47*, 365-382.

(59) Gundersen, L. L. *Acta Chem. Scand.* **1996**, *50*, 58-63.

(60) Marcantonio, K. M.; Frey, L. F.; Liu, Y.; Chen, Y.; Strine, J.; Phenix, B.; Wallace, D. J.; Chen, C. Y. *Org. Lett.* **2004**, *6*, 3723-3725.

(61) Sundermeier, M.; Mutyala, S.; Zapf, A.; Spannenberg, A.; Beller, M. *J. Organomet. Chem.* **2003**, *684*, 50-55.

(62) Chidambaram, R. *Tetrahedron Lett.* **2004**, *45*, 1441-1444.

(63) Kato, T.; Arakawa, E.; Ogawa, S.; Suzumura, Y. *Chem. Pharm. Bull.* **1986**, *34*, 3635-3643.

(64) Neely, R. K.; Magennis, S. W.; Parsons, S.; Jones, A. C. *ChemPhysChem* **2007**, *8*, 1095-1102.

(65) Lynch, D. E. M., I. *Acta Crystallogr., Sect. C* **2003**, *59*, 53-56.

(66) Harnden, M. R. J., R.L.; Slawin, A.M.Z.; Williams, D.J. *Nucleosides & Nucleotides* **1992**, *9*, 499.

(67) Moonen, N. N. P.; Gist, R.; Boudon, C.; Gisselbrecht, J.-P.; Seiler, P.; Kawai, T.; Kishioka, A.; Gross, M.; Irie, M.; Diederich, F. *Org. Biomol. Chem.* **2003**, *1*, 2032-2034.

(68) Moonen, N. N. P.; Pomerantz, W. C.; Gist, R.; Boudon, C.; Gisselbrecht, J. P.; Kawai, T.; Kishioka, A.; Gross, M.; Irie, M.; Diederich, F. *Chem. Eur. J.* **2005**, *11*, 3325-3341.

(69) Meyer, E. A.; Castellano, R. K.; Diederich, F. *Angew. Chem. Int. Ed.* **2003**, *42*, 1210-1250.

(70) Würthner, F.; Yao, S. *Angew. Chem. Int. Ed.* **2000**, *39*, 1978-1981.

(71) Würthner, F.; Yao, S.; Debaerdemaeker, T.; Wortmann, R. *J. Am. Chem. Soc.* **2002**, *124*, 9431-9447.

(72) Wortmann, R.; Rösch, U.; Redi-Abshiro, M.; Würthner, F. *Angew. Chem. Int. Ed.* **2003**, *42*, 2080-2083.

(73) Yao, S.; Beginn, U.; Gress, T.; Lysetska, M.; Würthner, F. *J. Am. Chem. Soc.* **2004**, *126*, 8336-8348.

(74) Matsuda, A.; Shinozaki, M.; Suzuki, M.; Watanabe, K.; Miyasaka, T. *Synthesis* **1986**, 385-386.

(75) Gerster, J. F.; Robins, R. K.; Jones, J. W. *J. Org. Chem.* **1963**, *28*, 945-&.

(76) Hayakawa, H.; Haraguchi, K.; Tanaka, H.; Miyasaka, T. *Chem. Pharm. Bull.* **1987**, *35*, 72-79.

(77) Congdanh, N.; Beaucourt, J. P.; Pichat, L. *Tetrahedron Lett.* **1979**, 2385-2388.

(78) Mitschke, U.; Bauerle, P. *J. Mater. Chem.* **2000**, *10*, 1471-1507.

(79) Tainaka, K.; Tanaka, K.; Ikeda, S.; Nishiza, K.-i.; Unzai, T.; Fujiwara, Y.; Saito, I.; Okamoto, A. *J. Am. Chem. Soc.* **2007**, *129*, 4776-4784.

(80) Lu, Z. K.; Lord, S. J.; Wang, H.; Moerner, W. E.; Twieg, R. J. *J. Org. Chem.* **2006**, *71*, 9651-9657.

(81) Mason, S. F. *J. Chem. Soc.* **1954**, 2071-2081.

(82) Smagowicz, J.; Wierzchowski, K. L. *Journal of Luminescence* **1974**, *8*, 210-232.

(83) Sharon, E.; Lévesque, S. A.; Munkonda, M. N.; Sévigny, J.; Ecke, D.; Reiser, G.; Fischer, B. *ChemBioChem* **2006**, *7*, 1361-1374.

(84) Wilhelmsson, L. M.; Sandin, P.; Holmén, A.; Albinsson, B.; Lincoln, P.; Nordén, B. *J. Phys. Chem. B* **2003**, *107*, 9094-9101.

(85) Lin, W.; Li, H.; Ming, X.; Seela, F. *Org. Biomol. Chem.* **2005**, *3*, 1714-1718.

(86) Serrano-Andrés, L.; Merchán, M.; Borin, A. C. *Proc. Natl. Acad. Sci. U. S. A.* **2006**, *103*, 8691-8696.

(87) Drobnik, J.; Augenstein, L. *Photochemistry and Photobiology* **1966**, *5*, 83-97.

(88) Drobnik, J.; Augenstein, L. *Photochemistry and Photobiology* **1966**, *5*, 13-30.

(89) Kyogoku, Y.; Lord, R. C.; Rich, A. *Proc. Natl. Acad. Sci. U. S. A.* **1967**, *57*, 250-257.

(90) Holmén, A.; Nordén, B.; Albinsson, B. *J. Am. Chem. Soc.* **1997**, *119*, 3114-3121.

(91) Albinsson, B. *J. Am. Chem. Soc.* **1997**, *119*, 6369-6375.

(92) Suppan, P. G., N *Solvatochromism*; The Royal Society of Chemistry: Cambridge, 1997.

(93) http://www.speckanalytical.co.uk/products/Tips/bps.html

(94) Ryazanova, O. A.; Zozulya, V. N.; Voloshin, I. M.; Karachevtsev, V. A.; Makitruk, V. L.; Stepanian, S. G. *Spectrochim. Acta, Part A* **2004**, *60*, 2005-2011.

(95) Cui, Y. Z.; Fang, Q.; Huang, Z. L.; Xue, G.; Xu, G. B.; Yu, W. T. *J. Mater. Chem.* **2004**, *14*, 2443-2449.

(96) Sumalekshmy, S.; Gopidas, K. R. *J. Phys. Chem. B* **2004**, *108*, 3705-3712.

(97) Weber, G.; Farris, F. J. *Biochemistry* **1979**, *18*, 3075-3078.

(98) Wolak, M. A.; Jang, B. B.; Palilis, L. C.; Kafafi, Z. H. *J. Phys. Chem. B* **2004**, *108*, 5492-5499.

(99) Frisch, M. J. T., G. W.; Schlegel, H. B.; Scuseria, G. E.; Robb, M. A.; Cheeseman, J. R.; Montgomery, Jr., J. A.; Vreven, T.; Kudin, K. N.; Burant, J. C.; Millam, J. M.; Iyengar, S. S.; Tomasi, J.; Barone, V.; Mennucci, B.; Cossi, M.; Scalmani, G.; Rega, N.; Petersson, G. A.; Nakatsuji, H.; Hada, M.; Ehara, M.; Toyota, K.; Fukuda, R.; Hasegawa, J.; Ishida, M.; Nakajima, T.; Honda, Y.; Kitao, O.; Nakai, H.; Klene, M.; Li, X.; Knox, J. E.; Hratchian, H. P.; Cross, J. B.; Bakken, V.; Adamo, C.; Jaramillo, J.; Gomperts, R.; Stratmann, R. E.; Yazyev, O.; Austin, A. J.; Cammi, R.; Pomelli, C.; Ochterski, J. W.; Ayala, P. Y.; Morokuma, K.; Voth, G. A.; Salvador, P.; Dannenberg, J. J.; Zakrzewski, V. G.; Dapprich, S.; Daniels, A. D.; Strain, M. C.; Farkas, O.; Malick, D. K.; Rabuck, A. D.; Raghavachari, K.; Foresman, J. B.; Ortiz, J. V.; Cui, Q.; Baboul, A. G.; Clifford, S.; Cioslowski, J.; Stefanov, B. B.; Liu, G.; Liashenko, A.; Piskorz, P.; Komaromi, I.; Martin, R. L.; Fox, D. J.; Keith, T.; Al-Laham, M. A.; Peng, C. Y.; Nanayakkara, A.; Challacombe, M.; Gill, P. M. W.; Johnson, B.; Chen, W.; Wong, M. W.; Gonzalez, C.; and Pople, J. A.; Gaussian, Inc.: 2004.

(100) Schaftenaar, G. N., J. H. *J. Comput. -Aided Mol. Design* **2000**, *14*, 123-134.

(101) Rachofsky, E. L.; Ross, J. B. A.; Krauss, M.; Osman, R. *J. Phys. Chem. A* **2001**, *105*, 190-197.

(102) Ridley, J. Z., M.C. *Theor. Chim. Acta* **1976**, *42*, 223-236.

(103) Yu, M. X.; Chang, L. C.; Lin, C. H.; Duan, J. P.; Wu, F. I.; Chen, I. C.; Cheng, C. H. *Adv. Funct. Mater.* **2007**, *17*, 369-378.

(104) Shen, J. Y.; Yang, X. L.; Huang, T. H.; Lin, J. T.; Ke, T. H.; Chen, L. Y.; Wu, C. C.; Yeh, M. C. P. *Adv. Funct. Mater.* **2007**, *17*, 983-995.

(105) Liu, Q. D.; Lu, J. P.; Ding, J. F.; Day, M.; Tao, Y.; Barrios, P.; Stupak, J.; Chan, K.; Li, J. J.; Chi, Y. *Adv. Funct. Mater.* **2007**, *17*, 1028-1036.

(106) Perun, S.; Sobolewski, A. L.; Domcke, W. *Mol. Phys.* **2006**, *104*, 1113-1121.

(107) Huc, I. *Eur. J. Org. Chem.* **2004**, 17-29.

(108) Jiang, H.; Leger, J. M.; Huc, I. *J. Am. Chem. Soc.* **2003**, *125*, 3448-3449.

(109) Ernst, J. T.; Becerril, J.; Park, H. S.; Yin, H.; Hamilton, A. D. *Angew. Chem. Int. Ed.* **2003**, *42*, 535.

(110) Dervan, P. B. *Bioorg. Med. Chem.* **2001**, *9*, 2215-2235.

(111) Hill, D. J.; Mio, M. J.; Prince, R. B.; Hughes, T. S.; Moore, J. S. *Chem. Rev.* **2001**, *101*, 3893-4011.

(112) Garcia-Sosa, A. T.; Firth-Clark, S.; Mancera, R. L. *J. Chem Inf. Model.* **2005**, *45*, 624-633.

(113) Tu, C.; Keane, C.; Eaton, B. *Nucleosides & Nucleotides* **1997**, *16*, 227-237.

(114) Chou, S. H.; Flynn, P.; Reid, B. *Biochemistry* **1989**, *28*, 2422-2435.

(115) McLaughlin, L. W.; Piel, N.; Hellmann, T. *Synthesis* **1985**, 322-323.

(116) Moroder, H.; Kreutz, C.; Lang, K.; Serganov, A.; Micura, R. *J. Am. Chem. Soc.* **2006**, *128*, 9909-9918.

(117) Sewald, N. J., H. *Peptides: Chemistry and Biology*; Wiley-VCH: Weinheim, 2002.

(118) Dey, S.; Garner, P. *J. Org. Chem.* **2000**, *65*, 7697-7699.

(119) Martin, A. M.; Butler, R. S.; Ghiviriga, I.; Giessert, R. E.; Abboud, K. A.; Castellano, R. K. *Chem. Commun.* **2006**, 4413-4415.

BIOGRAPHICAL SKETCH

Roslyn Susanne Butler was born in 1978 in Elizabethtown, KY. After growing up in South Central Kentucky, she graduated in 2001 with a B.S. in chemistry from Western Kentucky University, where she worked in the lab of Prof. Robert Holman. During her undergraduate education she also briefly worked in the lab of Prof. Spiro Alexandratos at the University of Tennessee, and as a park ranger at Mammoth Cave National Park. After working on her M.S. in organic chemistry for a year at Western Kentucky University, she then moved to Gainesville, FL in 2002 to pursue her Ph.D. in organic chemistry at the University of Florida under the guidance of Prof. Ronald K. Castellano. In August 2007 she will join the teaching faculty at Marian High School in Mishawaka, IN to teach chemistry and biology.